ACS OMEGA

http://pubs.acs.org/journal/acsodf
Review

MXene: A Roadmap to Sustainable Energy Management, Synthesis Routes, Stabilization, and Economic Assessment

Mumtahina Mim, Khairul Habib,* Sazratul Nayeem Farabi, Syed Awais Ali,* Md Abu Zaed, Mohammad Younas, and Saidur Rahman

Cite This: *ACS Omega* 2024, 9, 32350−32393

ABSTRACT: MXenes with their wide range of tunability and good surface chemistry provide unique and distinctive characteristics offering potential employment in various aspects of energy management applications. These high-performance materials have attracted considerable attention in recent decades due to their outstanding characteristics. In the literature, most of the work is related to specific methods for the preparation of MXenes. In this Review, we present a detailed discussion on the synthesis of MXenes through different etching routes involving acids, such as hydrochloric acid, hydrofluoric acid, and lithium fluoride, and non-acidic alkaline solution, electrochemical, and molten salt methods. Furthermore, a concise overview of the different structural, optical, electronic, and magnetic properties of MXenes is provided corresponding to their role in supporting high thermal, chemical, mechanical, environmental, and electrochemical stability. Additionally, the role of MXenes in maintaining the thermal management performance of photovoltaic thermal systems (PV/T), wearable light heaters, solar water desalination, batteries, and supercapacitors is also briefly discussed. A techno-economic and life cycle analysis of MXenes is provided to analyze their sustainability, scalability, and commercialization to facilitate a comprehensive array of energy management systems. Lastly, the technology readiness level of MXenes is defined, and future recommendations for MXenes are provided for their further utilization in niche applications. The present work strives to link the chemistry of MXenes to process economics for energy management applications.

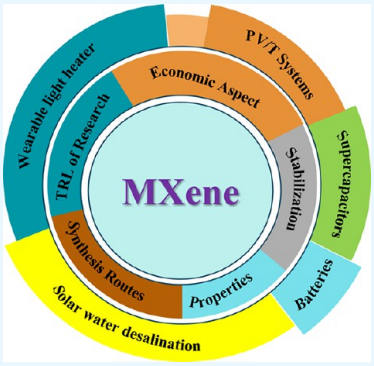

1. INTRODUCTION

The synthesis and development of advanced nanomaterials have garnered significant attention in recent years due to the unique properties and potential applications of these materials across various energy management systems. Nanomaterials undoubtedly play a vital role in heat transfer and thermal management applications. A variety of materials, including metallic, nonmetallic, organic, and carbon-based nanomaterials, are employed in different energy management applications.[1,2] However, these materials often fall short of meeting the escalating demands at higher performance levels. Consequently, there is significant global interest in discovering and developing advanced materials that can achieve superior performance and efficiency at a higher level. This focus on innovative nanomaterials aims to address the limitations of current technologies and pave the way for more efficient and sustainable energy solutions.[3,4] Recently, the use two-dimensional (2D) layered nanomaterials has attracted many researchers due to their excellent structural, optical, electronic, magnetic, and electrochemical properties. Apart from the extremely examined 2D layered structure graphene, phosphorene, and transition metal dichalcogenides (TMDs), 2D-layered titanium carbide powders (Ti_3C_2) have demonstrated exceptionally advanced structural, magnetic, and electronic features, making their utilization highly favorable for numerous energy management systems.[5] The MXenes ($M_{n+1}X_nT_x$), in which M represents scandium (Sc), vanadium(V), chromium (Cr), titanium (Ti), zirconium (Zr), molybdenum (Mo), niobium (Nb), hafnium (Hf), or tantalum (Ta), X represents nitrogen (N) or carbon (C), and T corresponds to −OH, −O, and −F, can be synthesized by selective etching of aluminum (Al), cadmium (Cd), silicon (Si), phosphorus (P), sulfur (S), galium (Ga), arsenic (As), germanium (Ge), indium (In), tin (Sn), titanium (Ti), or lead (Pb) elemental layers from 3-fold metal nitrides and carbides (MAX phase). To date, the successful synthesis of MXene encompasses over 30 distinct configurations, with predictions indicating the potential realization of more than 100 stoichiometric compositions of MXenes.[6,7] In general, $M_{n+1}AX_n$ (MAX) phases serve as the initial compounds, with the formation of MXenes achieved through the selective etching of the A layer as illustrated in Figure 1a and b.[8] MXene could be applied in a wide range of applications due to its graphene-like morphology and the additional characteristics of a high number

Received: May 23, 2024
Revised: June 22, 2024
Accepted: June 27, 2024
Published: July 18, 2024

https://doi.org/10.1021/acsomega.4c04849
ACS Omega 2024, 9, 32350−32393

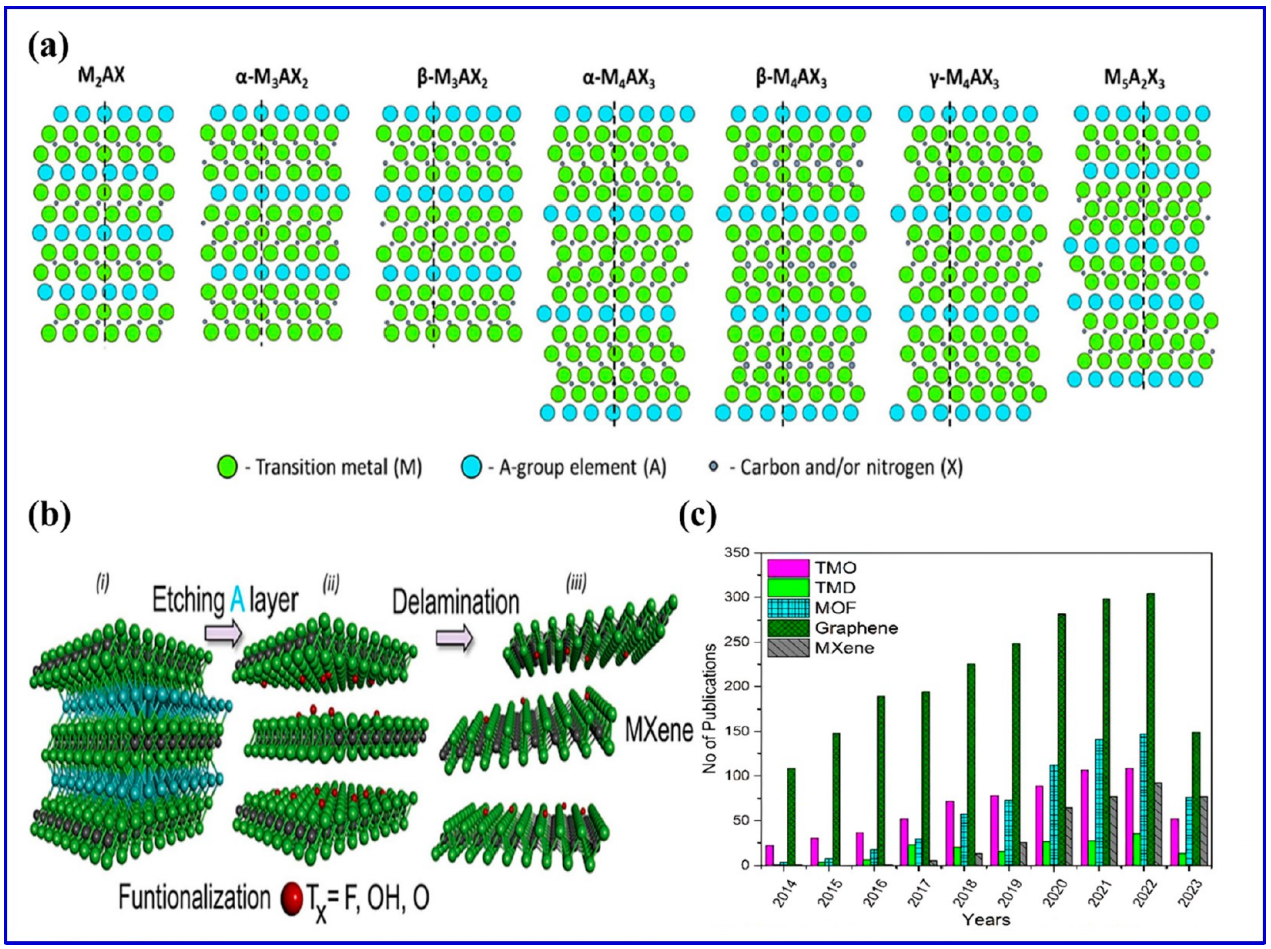

Figure 1. (a) Crystal structures of various MAX phases (M_2AX, α-M_3AX_2, β-M_3AX_2, α-M_4AX_3, β-M_4AX_3, and γ-M_4AX_3) and hybrid $M_5A_2X_3$ phases. (b) Illustration of (i) the etching of "A" layers to produce (ii) the accordion-like structure of MXenes and (iii) delamination of the MXenes to produce single- to few-layered MXenes. Adapted from ref 21. Copyright 2023 Elsevier. (c) Yearly number of publications on different 2D materials. Adopted from ref 22. Copyright 2024 Elsevier.

of active sites, large surface area, large interlayer spacing, high thermal stability, and high thermal/electrical conductivity, along with higher sorption/reduction capacity and more negative zeta potential.[9,10]

The synthesis of high-quality MXenes from their respective MAX phases is subject to various factors, involving the careful consideration of suitable precursors, etching agents, synthesis conditions, and the intricacies of the intercalation process.[11] MXene could be synthesized from a variety of techniques such as etching involving acids like hydrofluoric (HF), hydrochloric acid (HCl), and lithium fluoride (LiF) and through acid-free methods involving alkaline solution, electrochemical reactions, and molten salts.[8] Table 1 shows a brief description of the advantages and disadvantages of each category of MXene synthesis by linking their etching conditions, surface terminations, and applications. An immense amount of data is available covering the comprehensive review of MXene and its wide range of applications in different energy management applications. MXenes, due to their distinctive properties, have been reviewed by several researchers for different energy management applications. Figure 1c shows the yearly data on the increasing number of publications, showing an increasing trend of "MXene" publications in the research community. For instance, Li et al.[12] discussed the surface chemistry of MXenes across different energy management devices and provided guidelines for the utilization of MXenes' surface terminations to control the properties and improve the performance of batteries and supercapacitors. Xiong et al.[13] presented the progress in the process design and fabrication of MXene-based films for different battery thermal management applications. Lim et al.[14] discussed the strategies for the synthesis and rational design of MXenes and their hybrid composites for catalytic energy conversion and storage applications. Wang et al.[15] reviewed the fabrication approaches of (0D, 1D, 2D, and 3D) MXene materials, with a special focus on their challenges and opportunities for their effective thermal utilization. Other notable studies by Zhang et al.,[16] Das et al.,[17] Tan et al.,[18] Zaed et al.,[19] and Shaharudin et al.[20] that cover in-detail discussions on the synthesis strategies of MXene-based nanostructures from commercial and low-cost precursors and their their economic footprint for effective thermal utilization are worthwhile references to develop a basic understanding of individual topics. However, there very limited discussion is provided on synthesis strategies of MXene discussing the advantages and disadvantages of each method, including scalability, cost-effectiveness, and environmental impact. Additionally, the discussion on the economic analysis of MXene through linking its production with thermal management and economic assessments, including their market demand,

https://doi.org/10.1021/acsomega.4c04849
ACS Omega 2024, 9, 32350−32393

Table 1

etching technique	MXene	precursor	etching conditions: etchants	etching conditions: temperature (°C)	etching conditions: time (h)	surface group	pros and cons	application	ref
acid-based etching	$Ti_3C_2T_x$	Ti_3AlC_2	48% HF, 37% HCl	35	24	OH, O	**pros:**		81
	V_4C_3	V_4AlC_3	40% HF	55	96	OH, O, F	•exfoliation from the original MAX phase is obvious and layers are clearly separated.		82
	$Zr_3C_2T_x$	$Zr_3Al_3C_5$	HF	RT	60	F	•this method requires less temperature for the execution compared to other methods		83
	$W_{4/3}CT_x$	$(W_{2/3}Sc_{1/3})_2AlC$	HF	RT	30	F	•as a substrate, it is more suitable and is relatively intact in the lamellar structure	atomic lamination	84
	Nb_2CT_x	Nb_2AlC	HF	RT	90	F, O	**cons:**	Li-ion battery	85
	$Hf_3C_2T_x$	$Hf_3[Al(Si)]_4C_6$	HF	RT	60	F	•it has the limitation of applying in etching methods as it is a harmful substance		32
	$V_4C_3T_x$	V4AlC3	HF		165	V, C	•despite having a lower temperature requirement, this method takes a long time to process	hydrogen evolution reaction	86
	Mo_2ScC_2	Mo2ScAlC2	HF	50	16	Mo	•this type of etching method is cost-consuming, difficult to control and in some extent unmanageable		87
	$W_{1.33}C$	$(W_{2/3}Sc_{1/3})_2AlC$	HF	RT	35	W, C, O			88
	Ti_2C	Ti_2AlC	50% HF	RT	2	OH, F			89
	Ta_4C_3	Ta_4AlC_3	50% HF	RT	72	Ta, O, C, F			89
	TiNbC	Ti_3AlCN	50% HF	RT	18	Ti, Nb, C, F, O			89
	$(V_{0.5}, Cr_{0.5})_3C_2$	$(V_{0.5},Cr_{0.5})_3AlC_2$	50% HF	RT	69	V, Cr, C, F, O			89
	Ti_3CN_x	$(Ti_{0.5},Nb_{0.5})_2AlC$	50% HF	RT	28	OH, F			89
	Ta_4C_3	Ta_4AlC_3	HF	RT	72	Ta, C, O		theranostic (biomedical)	90
	$V_4C_3T_x$	V_4AlC_3	HF	RT		O, F			91
	$Ti_3C_2T_x$	Ti_3AlC_2	HF 48 wt %	60	48	F			92
	V_2C	V_2AlC	HF	90	72	V, C, F, O		Li-ion battery	93
	Nb_2CT_x	Nb_2AlC	40 mL of HF	50	72−96	F, O, OH		dye adsorption	94
	$Ti_3C_2T_x$	Ti_3AlC_2	5−30 wt % HF	~850		O, OH			95
	$Ti_3C_2T_x$	Ti_3AlC_2	40% HF	RT	~408	OH, O, F			96
	$Ti_3C_2T_x$	Ti_3AlC_2	48% HF, DMSO	RT	30	O		pollutant remover	97
	$Ti_3C_2T_x$	Ti_3AlC_2	1 g of LiF, 20 mL of 9 M HCl	35	36	O		methanol oxidation	98
	$Ti_3C_2T_x$	Ti_3AlC_2	500 mg of LiF, 10 mL of HCl	40	36	O		methanol oxidation	99
	$Ti_3C_2T_x$	Ti_3AlC_2	1.98 g of LiF, 40 mL of HCl	40	24	O		Li-ion hybrid capacitor	100
	$Ti_3C_2T_x$	Ti_3AlC_2	2 g of LiF, 6 M HCl	RT	24	F, Cl, O		supercapacitor	101
	$Ti_3C_2T_x$	Ti_3AlC_2	1 g of LiF, 20 mL of 6 M HCl	35	24	O		humidity sensor	102
	$Ti_3C_2T_x$	Ti_3AlC_2	20 mL of 12 M HCl, 0.5 g of NaF powder	50	48	O, OH		Na/K-ion batteries	103

https://doi.org/10.1021/acsomega.4c04849
ACS Omega 2024, 9, 32350−32393

Table 1. continued

etching technique	MXene	precursor	etching conditions: etchants	etching conditions: temperature (°C)	etching conditions: time (h)	surface group	pros and cons	application	ref
	Ti_3C_2	Ti_3AlC_2	2 g of LiF, 40 mL of 9 M HCl	35	24	O		K-ion batteries	104
	$Ti_3C_2T_x$	Ti_3AlC_2	80 mL of 9 M HCl, 4 g of LiF	40	48	O		electromagnetic wave absorption	105
	Ti_3CNT_x	Ti_3AlCN	0.5 g of LiF in 10 mL of HCl solution (12 M)	50	24	Ti, Ni, Co, S, C, N, O		microwave absorption	106
	$Ti_3C_2T_x$	Ti_3AlC_2	HCl, LiF			O		micro-supercapacitors	107
	$Ti_3C_2T_x$	Ti_3AlC_2	2 g of LiF, 20 mL of 9 mol HCl	40	48	O		supercapacitor	108
	$Ti_3C_2T_x$	Ti_3AlC_2	0.8 g of LiF, 10 mL of 6 M HCl	35	36	O		visible light photodetector	109
	Ti_3CNT_x	Ti_3AlCN	300 mg of solid LiF, 15 mL of HCl (6 M)	150	4	O		multifunctional coating	110
	Ti_3C_2	Ti_3AlC_2	HF (48%), HCl (37%), LiF, NaF, NH_4F, and DMSO	RT	36	Br, I		NO_2 sensing	111
	$Ti_3C_2T_x$	Ti_3AlC_2	HF			O, OH, F			112
	Mo_2CT_x	Mo_2Ga_2C	3 M LiF, 12 M HCl	35		O, F			113
	Ti_2N	Ti_2AlN	HF, HCl, KF	40	3	O, F, OH			114
	Ti_3C_2	Ti_3SiC_2	HF, H_2O_2	40	45	O, F			115
	Nb_2C	Nb_2AlC	50 mL of HF (40 wt %)	60	72				116
	Ti_3C_2	Ti_3AlC_2	50 mL of HF (49 wt %)	60	36	O			116
	Ti_2CT_x	Ti_2AlC	10 wt % aqueous HF	RT	10	O		supercapacitor	117
	Ti_3C_2	$Ti_{n+1}AlC_n$	HF	RT				sensor, energy storage	118
alkaline solution chemical etching	$Ti_3C_2T_x$	Ti_3AlC_2	NaOH	270		OH	**pros:**		49
	$Ti_3C_2T_x$	Ti_3AlC_2	NaOH			O, OH, F	•due to having strong binding with A-group materials of the MAX phase, alkaline etchants are effective	wearable electromagnetic wave shielding	119
	$Ti_3C_2T_x$	Ti_3AlC_2				O, OH, F	•it requires a low concentration of alkali as an etchant	hydrogen production	120
	Mo_2C	Mo_2Ga_2C	NaOH	180	24	F, Cl	•this method exhibits highly hydrophilic products with F-free terminations	electrochemical	121
	$Ti_3C_2(OH)_2$	Ti_3AlC_2	KOH	160	24	O	**cons:**	photocatalyst	122
	Ti_3C_2	Ti_3SiC_2	HF/H_2O_2	40	45	O, F	•in some cases, in alkaline environments this method requires high pressure and temperature to remove the A-group elements from the MAX phase		115
	$Mo_2TiC_2T_x$	$Mo_2TiAlC_2T_x$	HF	250	72	O	•this method results in incomplete etching which further needs more steps to process	energy storage	123
	$Ti_3C_2T_x$	Ti_3AlC_2	NaOH		1	O	•adopting this method requires an additional step to clean the surface compared to other conventional methods, as incorporation of alkaline treatment results in the formation of other layers on the surface (like aluminum oxide/hydroxide) instead of producing MXene directly	supercapacitor	124
	Mo_4VC_4	Mo_4VAlC_4	HF			O, OH			125

https://doi.org/10.1021/acsomega.4c04849
ACS Omega 2024, 9, 32350−32393

Table 1. continued

etching technique	MXene	precursor	etching conditions: etchants	etching conditions: temperature (°C)	etching conditions: time (h)	surface group	pros and cons	application	ref
	$Ti_3C_2F_x$	Ti_3AlC_2	40% HF	RT	10			lithium storage	126
	$Ti_3C_2T_x$	Ti_3AlC_2	40% HF	40	10	OH		electrocatalyst	127
	Ti_3C_2	Ti_3AlC_2	$NaHF_2$, KHF_2, NH_4HF_2	60		O			128
	$Ti_3C_2T_x$	Ti_3AlC_2	CoF_x/HCl	~60					129
electrochemical etching	Ti_2CT_x	Ti_2AlC		500		Cl	**pros:**		58
	Mo_2CT_x	Mo_3AlC_2	Al	60	2	O, OH	•electrochemical etching method exhibits fast synthesis of MXene at room temperature	battery electrolyte	130
	V_2CT_X	V_2AlC	21 M LiTFSI + 1 M $Zn(OTf)_2$			O, F	•this etching method results in superior capacitance of all-solid-state supercapacitors based on MXene compared with other etching methods	Zn-ion battery	131
	Ti_3C_2	Ti_3AlC_2			5	O	•it has the capability to reduce the undesirable effects from the etchant	supercapacitor	132
	$Ti_3C_2F_x$	Ti_3AlC_2	[BMIM][PF_6]	60	12	OH, O, F	**cons:**	Li-ion batteries	133
	Ti_2CT_x	Ti_2AlC	HCl			O, OH	•in the electrochemical etching process, it increases the voltage and as a result the resistance is also increased, which may cause the overetching of transition metals		52
	CDC	Ti_3AlC_2	NaCl	RT			•this etching method also faces the challenge of overetching if the etching operation takes long period time		134
	CDC	Ti_2AlC	HCl	RT					134
	CDC	Ti_3SiC_2	HF	RT					134
	Ti_2CT_x	Ti_2AlC	Cl−	50	9	O		multifunctional energy materials	135
	V_2CT_x	V_2AlC		50	9	O, OH		multifunctional energy materials	135
	Cr_2CT_x	Cr_2AlC		50	9	O, OH		multifunctional energy materials	135
	Ti_3C_2	Ti_3AlC_2	NH_4HF_2	RT	1.5	F, O, OH			136
	$Ti_3C_2T_x$ MQDs	Ti_3AlC_2	TMAOH, NH_4Cl		1	OH			137
	Ti_3C_2	Ti_3AlC_2	copper(II) disodiumethylenediamine-tetraacetate tetrahydrate	1400	2	O, OH		tribology	138
	$Ti_3C_2T_x$	Ti_3AlC_2	9 M HCl, 4 M NaOH		0.5	O		electrodes	139
	$Ti_3C_2T_x$	Ti_3AlC_2	HCl 36−38 wt %	RT	12	O, C			140
	Ti_3C_2	Ti_3AlC_2	ammonium hydroxide			O, OH			132
molten salt etching	$Ti_3C_2Cl_2$	Ti_3AlC_2	$FeCl_2$ (1.14 g), NaCl (0.351 g), KCl (0.447 g)	700	7	Cl	**pros:**	microwave absorption	141
	$Ti_3C_2Cl_2$	Ti_3AlC_2	$ZnCl_2$	550	5	Cl	•Lewis acid in a molten salt exhibits a strong acidic environment the helps to displace metals from the MAX phase	photocatalytic H_2 evolution	142
	$Ti_4N_3T_x$	Ti_4AlN_3	$CuCl_2$, LiCl, KCl	600		Cl	•execution of the molten salt etching method opens a way to harness the MAX phases that are not stable thermodynamically at high temperatures		143
	$Ti_3C_2T_x$	Ti_3AlC_2	NaCl (8 g), KCl (8 g)	700	0.7	Cl	•Lewis acid in molten salt etching provides a green and viable route to formulate MXene without approaching through HF	Na-ion batteries	69
	$Ti_3C_2T_x$	Ti_3AlC_2	$CuCl_2$, NaCl, KCl	680	24	Cl, O	**cons:**		144

https://doi.org/10.1021/acsomega.4c04849
ACS Omega 2024, 9, 32350−32393

Table 1. continued

etching technique	MXene	precursor	etching conditions: etchants	etching conditions: temperature (°C)	etching conditions: time (h)	surface group	pros and cons	application	ref
	Ti_3C_2	Ti_3AlC_2	$CuCl_2$, NaCl, KCl	750	20	Cl	•the molten salt etching method requires high temperature and the presence of an argon (Ar) atmosphere for etching, which is not economically viable		145
	V_4C_3	V_4AlC_3	$CuCl_2$, $CoCl_2$	350	2	O, Cl	•the MXene produced through this etching method has lower crystallinity, excessive defects, and vacancies	aluminum batteries	146
	$Ti_3C_2T_x$	Ti_3AlC_2	$CuCl_2$	700	9	Cl	•due to having a higher energy of formation, preparation through conventional methods becomes difficult to approach	capacitive deionization	147
	$Ti_3C_2T_x$	Ti_3AlC_2	$FeCl_2$	700		Cl		energy storage	148
	$Ti_3C_2Cl_2$	Ti_3AlC_2	$CuCl_2$	700	10	O, Cl		proton supercapacitors	75
	$Ti_3C_2Br_2$	Ti_3AlC_2	$CuBr_2$	700	10	O		proton supercapacitors	75
	$Ti_3C_2I_2$	Ti_3AlC_2	CuI_2	700	10	O		proton supercapacitors	75
	Ti_3C_2	Ti_3AlC_2	$CuCl_2$	680		Cl			63
	$Ti_3C_2Cl_2$	Ti_3ZnC_2	$ZnCl_2$	1100	3	Cl			66
	Ti_2CCl_2	Ti_2ZnC	$ZnCl_2$	1100	3	Cl			66
	Nb_2CT_x	Nb_2AlC	$CuCl_2$	600−800		Cl		Li-ion Batteries	68
	$Ti_3C_2T_x$	Ti_3AlC_2	$CuCl_2$	700	0.7	Cl			149
	Ti_3CN	Ti_3AlCN	$CuCl_2$	700	24	Cl		photocatalysis	150
	$Ti_3C_2T_x$	Ti_3AlC_2	$SnCl_2$	600	24	Cl		Li-ion battery anode	151
	V_2C	V_2AlC	$NiCl_2$	750	24	Cl		secondary aluminum batteries	152
	Ti_3C_2	Ti_3AlC_2	1.0 g of $C_2H_4N_4$, 1.2 g of $Fe_2(SO_4)_3 \cdot 6H_2O$, 1 g of LiF, 10 mL of 9 M HCl		24	O		supercapacitor	153
	Ti_3C_2	Ti_3AlC_2	0.78 g of $CuCI_2$, 0.46 g of $NiCl_2 \cdot 6H_2O$	750	24	O		catalyst	154
	Ti_3C_2	Ti_3AlC_2	$CuCl_2 \cdot 2H_2O$, NaCl, KCl	750	20	O		removal of gaseous elemental mercury	145
	$Ti_3C_2T_z$	Ti_3AlC_2	SnF_2	550	6	O		water-dispersible MXene production	155
	V_2C	V_2AlC	NaCl	1400	2			vanadium pentoxide formation	156

https://doi.org/10.1021/acsomega.4c04849
ACS Omega 2024, 9, 32350−32393

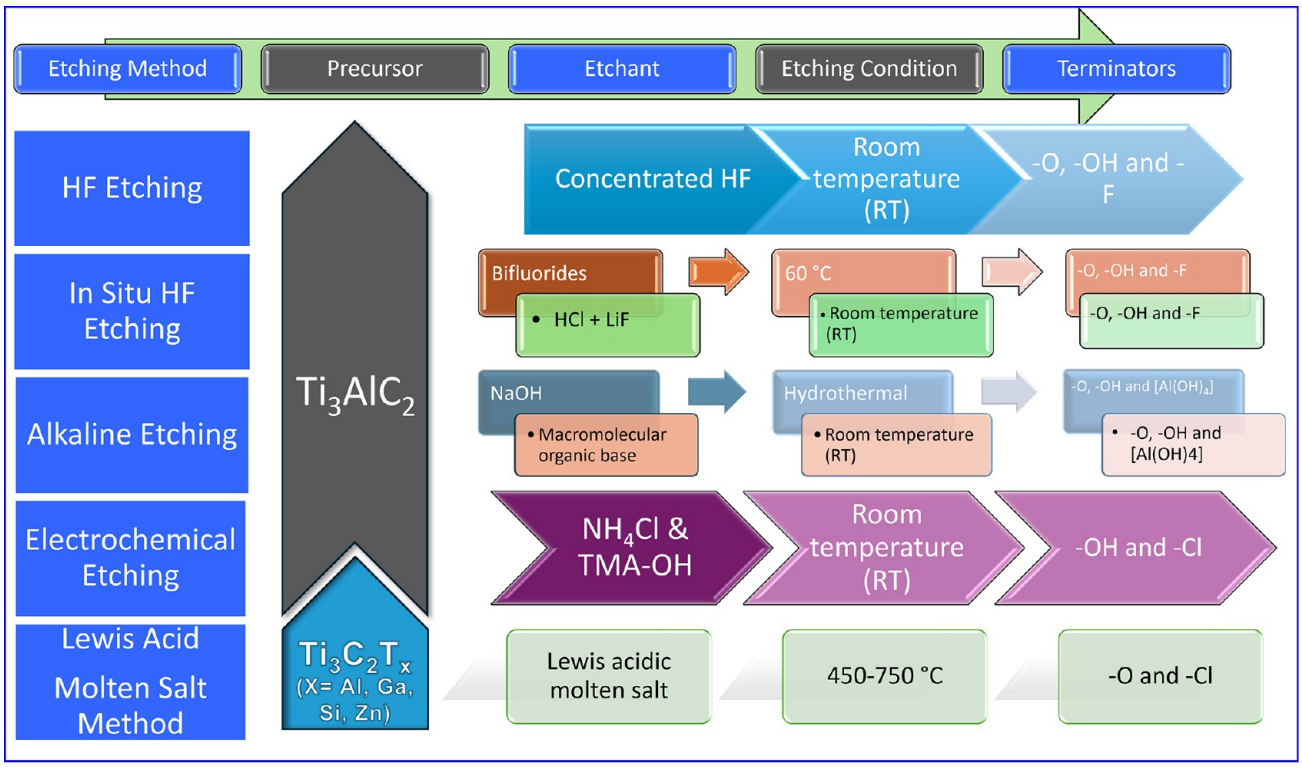

Figure 2. Different approaches for the synthesis of a titanium carbide MXene ($Ti_3C_2T_x$).

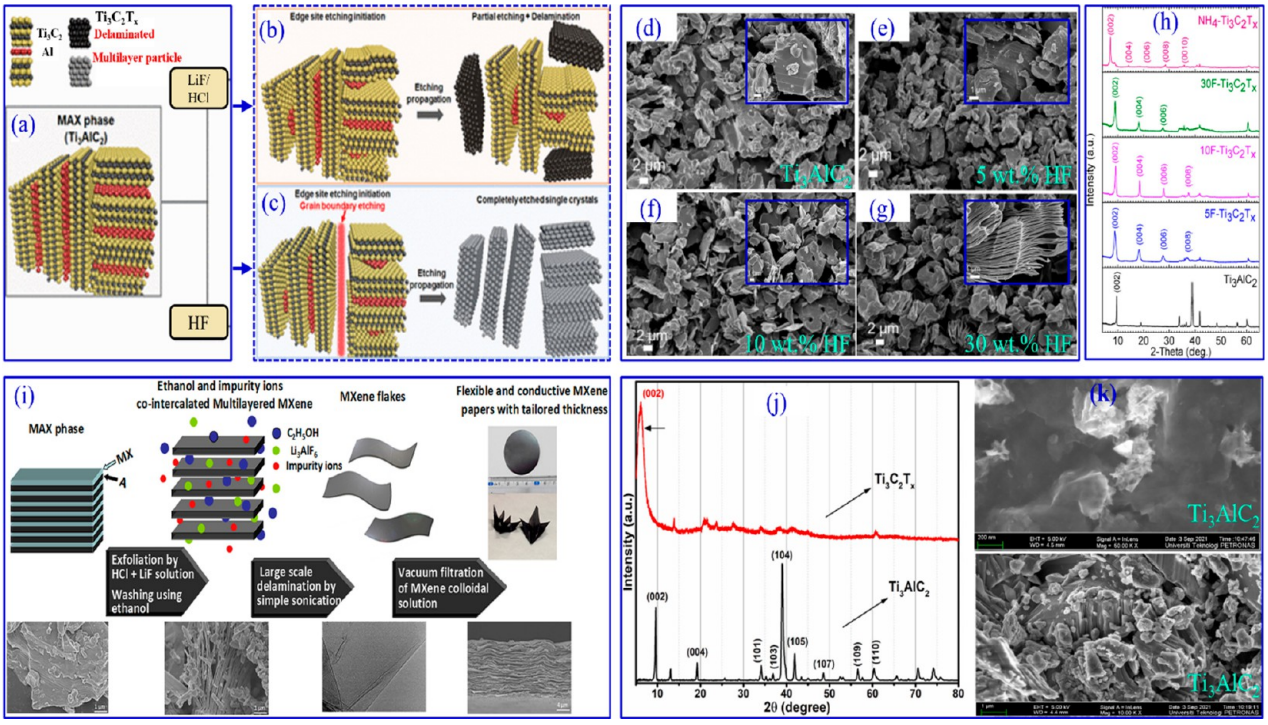

Figure 3. Comparison of schematics representing Al etching through HF and LiF solutions. (a) Ti_3C_2Al MAX phase before etching. The etching mechanisms for the MAX particle after etching with (b) LiF/HCl solution and (c) HF solution. Reproduced from ref 24. Copyright 2021 American Chemical Society. Compact layer surface morphology of Ti_3AlC_2 structures (a) before HF etching and (e−g) after etching with 5, 10, and 30 wt % HF, respectively. (h) XRD crystallinity of unetched Ti_3AlC_2 and etched $Ti_3C_2T_x$ structures with different loadings of HF. Reproduced from ref 27. Copyright 2017 American Chemical Society. (i) Schematic for the extraction of $Ti_3C_2T_x$ from Ti_3AlC_2 through LiF/HCl etching. Adapted from ref 34. Copyright 2017 Elsevier. (j) XRD spectra and (k) SEM morphology depicting the transformation of the Ti_3AlC_2 MAX phase into $Ti_3C_2T_x$ (MXene). Adapted from ref 35. Copyright 2022 Elsevier.

https://doi.org/10.1021/acsomega.4c04849
ACS Omega 2024, 9, 32350−32393

technical feasibility, commercial risk assessment, and life cycle analysis, is not provided in a single review.

This Review provides a comprehensive discussion on the synthesis of MXenes through different routes following their synthesis protocols using acid-based etchants such as HF, LiF, and HCl and non-acid-based methods such as chemical etching using alkaline solutions, electrochemical reactions, and molten salt. After that, the different properties of MXenes were overviewed, followed by structural, physical, optical, electrochemical, and magnetic characteristics that can lead to synergistic effects, enhancing the performance of MXenes in multifunctional applications. The discussion on different stability behaviors of MXenes such as thermal, mechanical, chemical, electrochemical, mechanical, and environmental stability is also provided in detail to ensure their effectiveness, reliability, and safety and enable the development of their robust employment under diverse and challenging conditions, thus maximizing their potential in advanced technologies. Also, a brief discussion on the techno-economic analysis of MXenes, including their production techniques, market demand, and commercialization with cost analysis, is provided. Lastly, the technology readiness level of MXene-based research and a description of possible challenges, outlook, and prospects for future research in the growth of MXenes are provided to explain the financial, market, and strategic factors that influence the successful development and adoption of MXene technologies, ultimately driving innovation and growth in different energy management applications.

2. SYNTHESIS AND CHARACTERIZATION OF MXENE

The synthesis and characterization of MXenes are pivotal in harnessing their unique properties. Synthesis typically involves selective etching of A-group elements from MAX phases using acid agents such as HF, LiF, and HCl and nonacidic methods through alkaline solution, electrochemical reaction, and molten salts. Characterization techniques, including X-ray diffraction (XRD), scanning electron microscopy (SEM), transmission electron microscopy (TEM), and spectroscopic methods, play crucial roles in confirming MXene's structure, morphology, and properties. This section highlights the significance of synthesis and characterization in advancing the research and development of MXenes, aiming to unlock their full potential for next-generation applications. A schematic of different routes for MXene synthesis is illustrated in Figure 2.

2.1. Etching and Delamination. *2.1.1. Hydrofluoric (HF) Acid Etching Method.* The fabrication of MXenes via HF etching encompasses the removal of the Al atomic layer from Ti_3AlC_2 utilizing a 50% HF solution. The high reactivity between the F ions and Al-supported MAX phase forms an accordion-like $Ti_3C_2T_x$ powder with strong hydrogen bonding and van der Waals forces developed by the surface group between each layer.[23] Figure 3a shows the polycrystal particle of the Ti_3AlC_2 MAX phase before its etching in both HF and LiF/HCl. In the case of LiF/HCl etching, initially, only the A layer was etched, whereas the central portions remained unetched due to poor reaction conditions and insufficient space, as shown in Figure 3b. However, in the case of HF etching (Figure 3c), a fully etched multilayer structure was attained due to the excellent ability of HF to attack the grain boundaries of MAX phase particles to initiate and propagate the exfoliation of the A layer faster than LiF/HCl etching.[24] The crystal structure and stoichiometry of the $Ti_3C_2T_x$ powder show the same consistency, following the Ti_3AlC_2 MAX phase rather than involving the Al atomic layer.[25] MAX phases were decomposed through HF etching as per the reactions given in eqs 1−4.[7]

$$TiAlC_2 + 3HF = AlF_3 = \frac{3}{2}H_2 + Ti_3C_2 \quad (1)$$

$$TiAlC_2 + 2HF = Ti_3C_2F_2 + H_2 \quad (2)$$

$$Ti_3C_2 + 2H_2O = Ti_3C_2(OH)_2 + H_2 \quad (3)$$

$$Ti_3C_2 + 2H_2O = Ti_3C_2 + 2H_2O \quad (4)$$

Specifically, the two layers of exposed Ti atoms in the unit cell require dangling bond passivation. Therefore, upon the successful removal of the A elemental layer, the surface of the Ti_3C_2 MXene nanosheet becomes rich in surface terminators like −F, −OH, and −O.[26] The scanning electron microscope (SEM) images of the morphology of MAX powders before and after the etching treatment with 5, 10, and 30 wt % HF are shown in Figure 3d−g, respectively.[27] The accordion-like morphology was not observed with 5 and 10 wt % HF-treated MXene. However, the accordion-like morphology was observed only with the MXene etched with 30 wt % HF. From the SEM analysis, it can also be observed that after the HF treatment, the morphology is different from the original MAX phase, and layers become separated from each other. However, the shifting of the X-ray diffraction (XRD) peak (002) at Ti_3AlC_2 from 9.5° to 9° for $Ti_3C_2T_x$ shows the removal of Al from Ti_3AlC_2 along with the introduction of surface terminations like −F, OH, and O at $Ti_3C_2T_x$ for all the powders with 5, 10, and 30 wt % of HF etching, as shown in Figure 3h.[27] HF etching for MXene synthesis can be scaled up from laboratory-scale batch processes to continuous production methods. Batch processes involve the sequential treatment of MAX phase precursors with HF in discrete steps, whereas continuous methods allow for a more streamlined, continuous flow of reactants, enhancing scalability. Scaling up HF etching requires careful consideration of reaction kinetics, mass transfer limitations, and heat transfer dynamics.[28] Engineering principles such as reactor design, agitation methods, and temperature control are crucial for achieving uniform etching and maximizing production rates while minimizing processing times. Scalable MXene synthesis necessitates the design and optimization of equipment such as reactors, pumps, and separation units to handle larger volumes of reactants and products efficiently. Robust equipment design ensures reproducibility, reliability, and safety in large-scale operations.[29] HF etching is a relatively cost-effective method for MXene synthesis due to the low cost and availability of raw materials (MAX phase) and HF etchant, which are commercially available at reasonable prices, contributing to cost-effectiveness.[30] The key advantages of HF etching are its convenient operation and low reaction temperature to maintain a substantial space as a substrate in the lamellar structure for a well-designed morphology.[7] Since the process was carried out in a HF-based etching system, the HF selectivity matters a lot in replacing the Al with F, which makes the Ti_3C_2 exfoliation intrinsically complex and difficult. Furthermore, the higher etching time and concentration could have a negative effect in terms of reducing the lateral size of the synthesized MXene.[31] The other drawback associated with the discussed method is that the corrosive nature of HF, which corrode and degrade the surface of the MXene under uncontrolled etching conditions. Proper safety measures and waste management protocols can minimize the risks associated with HF handling. The harmful

https://doi.org/10.1021/acsomega.4c04849
ACS Omega 2024, 9, 32350−32393

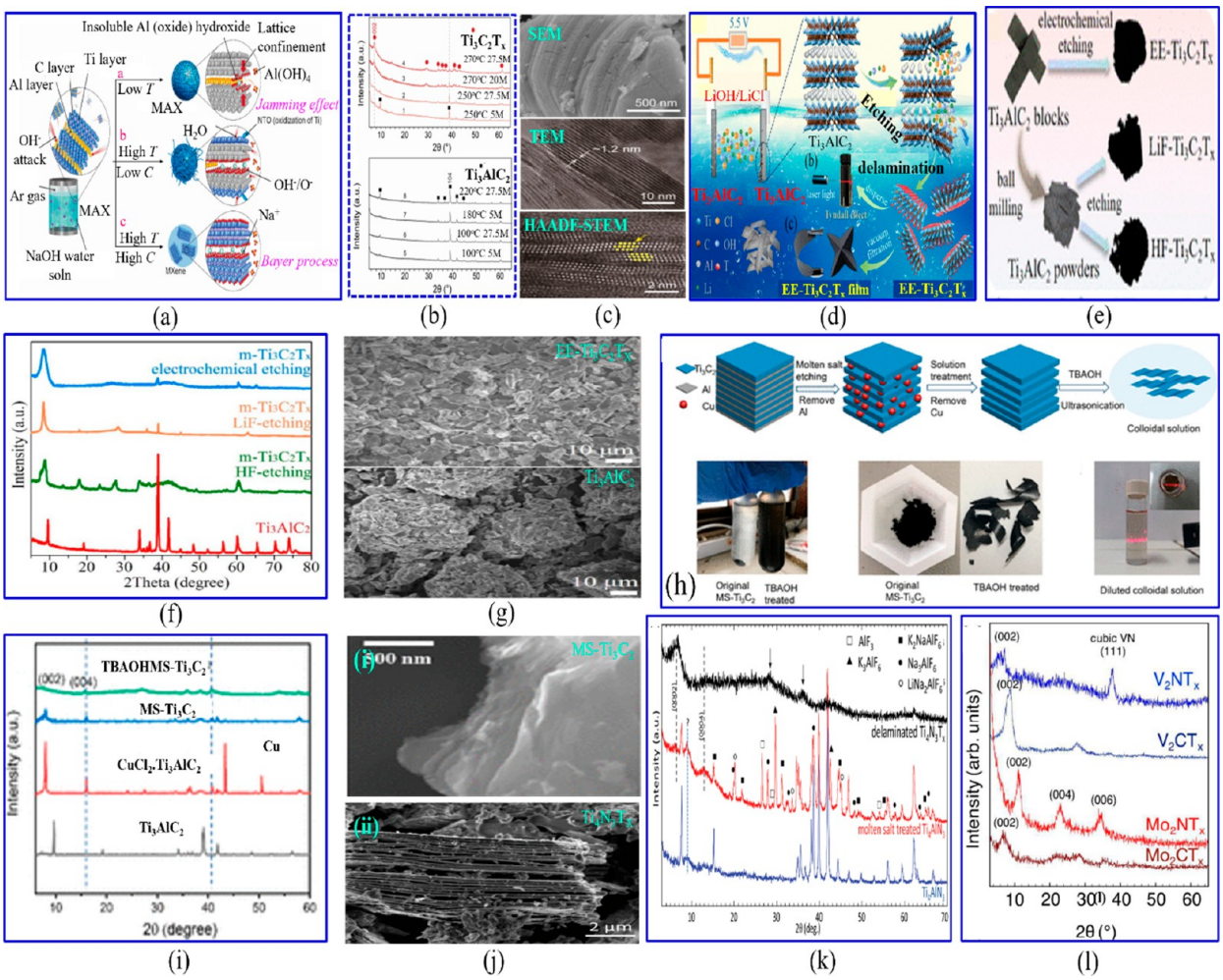

Figure 4. (a) Schematic of the reaction between Ti_3AlC_2 and NaOH water solution. (b) XRD spectra of the Ti_2AlC_2 layer and MXene etched through the alkaline treatment method. (c) Microstructure characterizations of the synthesized $Ti_3C_2T_x$ flakes. Adapted from ref 49. Copyright 2021 John Wiley & Sons, Inc. (d) Schematic of the synthesis method for EE-$Ti_3C_2T_x$. (e) Comparison of Ti_3AlC_2 raw materials and the d-$Ti_3C_2T_x$ powder product. (f) XRD spectra obtained by etching through the electrochemical method in comparison with LiF and HF acid-based etchants. (g) SEM morphology of EE-$Ti_3C_2T_x$ MXene in comparison with unetched Ti_3AlC_2. Reproduced from ref 55. Copyright 2022 American Chemical Society. (h) Synthesis schematic of a MXene etched through molten salt method inving the exfoliation of Ti_3AlC_2 in reaction with $CuCl_2$ to get multilayered MS-$Ti_3C_2T_x$ and e-MS-$Ti_3C_2T_x$ after TBAOH treatment. (i) XRD spectra and surface morphology of a MS-etched MXene. (j) SEM morphology of MS-etched Ti_3C_2 and $Ti_4N_3T_x$. Reproduced from ref 63. Copyright 2022 American Chemical Society. Adapted from ref. Copyright 2016 John Wiley & Sons, Inc. (k) Comparison of the XRD spectra of $Ti_4N_3T_x$ MXene obtained through etching of Ti_4AlN_3 with LiF, NaF, and KF. (l) XRD patterns of Mo_2CT_x and V_2CT_x before and after (Mo_2NT_x and V_2NT_x) ammonization at 600 °C for 1 h. Adapted from ref 64. Copyright 2016 Royal Society of Chemistry.

and corrosive nature of HF also limits the further usage of the HF etching method for numerous applications.[32,33]

2.1.2. LiF and HCl Etching Method. The synthesis of MXene through LiF/HCl etching is the most prominent fluorine-based etching route to avoid the highly acidic and harmful experimental conditions in HF etching.[36] This involves the right selection of the LiF/MAX phase molar ratio (7.5:1) at varying the HCl concentration (6−12 M) under stirring at room temperature to get a clear solution that yields HF with a low concentration (3−5%) following eq 5.[10,37]

$$LiF_{aq} + HCl_{aq} = HF_{aq} + LiCl_{aq} \quad (5)$$

Figure 3i shows the synthesis process of a 2D MXene through the LiF/HCl etching route.[34] A comparison of the crystalline structure (XRD) and surface morphology (SEM) after etching and delamination is shown in Figure 3j and k.[35] The successful etching of the Ti_3AlC_2 atomic layer via the HCl/LiF solution was first reported by Ghidiu et al.[38] to synthesize $Ti_3C_2T_x$ conductive clay with strong plasticity, which could be altered into film through roller pressing. The unrolled MXene clay, standing freely, exhibits favorable hydrophilic properties, notable toughness, and exceptional flexibility. Additionally, it maintains high thermal conductivity, reaching up to 1500 S cm^{-1}, even when bent into an "M" shape.[38] Similarly, Sang et al.[39] also reported the synthesis of high-quality MXene using a mild concentration of LiF/HCl instead of using a high concentration of HF (50 wt %). Similar to HF etching, the LIF/HCl etching forms a multilayer accordion-like MXene that can be directly utilized in numerous applications such as electrodes for supercapacitors, desalination, and battery management systems.[27] The LiF/HCl etching method can also be scaled up efficiently due to its relatively simple reaction setup and straightforward process. Achieving scalability may require the optimization of reaction parameters and equipment

https://doi.org/10.1021/acsomega.4c04849
ACS Omega 2024, 9, 32350−32393

design to ensure uniform etching across larger volumes.[40] Additionally, maintaining control over reaction kinetics and product quality becomes increasingly important as production scales up. Despite the relatively low cost of reagents, upfront investment in equipment and infrastructure for large-scale production can be significant. Additionally, waste management and disposal costs may need to be considered to ensure overall cost-effectiveness. LiF/HCl etching offers the potential for reduced environmental impact compared to some alternative methods. The relatively simple chemistry and fewer steps involved in this process can lead to lower energy consumption and waste generation.[41,42] One of the significant advantages of the LiF/HCl etching route is the in situ intercalation of Li ions in the resultant MXene. That is why the interlayer spacing of the m-MXene becomes larger than that of the HF-etched MXene, which permits faster ion intercalation and provides more kinetic pseudo-capacitive redox sites.[38,43] Moreover, the other advantage of this mild etching through the LiF/HCl route is that it lessens the damage of the MXene in comparison compared to the aggressive HF etching method to give a multilayer MXene of good quality.[44,45]

2.1.3. Alkaline Solution Chemical Etching. Apart from the effectiveness of using acid to etch the "A" atomic layer from MXene, it involves some environmental and health issues of being toxic and non-ecofriendly. Moreover, adding the HF solution will not only corrode the Al layer and damage the surface of the MXene but also cause the corrosion of transition metal elements in the MXene structure.[46] Therefore, a new fluorine-free strategy for removing "An atomic layer" is required. Alkalis have attracted great attention for the selective etching of the MAX phase. This process is termed the Bayer process in which a concentrated NaOH solution is used under elevated temperature and pressure to attack the Al layer in Ti_3AlC_2 to give a fluorine-free MXene.[47] In one of the studies by Li et al.,[48] 0.1 g of Ti_3AlC_2 was etched using 0.35g/0.05 mL of KOH/H_2O solution under a hydrothermal reaction with constant heating at 180 °C for 24 h in a reactor. Then, the substitution of the Al atom by the −OH group takes place to give a successful synthesis of $Ti_3C_2(OH)_2$ nanosheets.[48] Li et al.[49] in another study reported the synthesis of $Ti_3C_2T_x$ through NaOH-assisted hydrothermal etching of Ti_3AlC_2. They found that Al can be selectively etched from Ti_3AlC_2 via the NaOH solution (27.5 M) and heated at 270 °C to develop −O- and −OH-terminated multilayer $Ti_3C_2T_x$. The reaction between the $NaOH/H_2O$ solution and Ti_3AlC_2 is shown in Figure 4a. The high temperature is advantageous for the successful conversion of aluminum hydroxide $Al(OH)_3$ and aluminum oxyhydroxide AlO(OH) into soluble tetrahydroxo-aluminate ion $Al(OH)_4$. Moreover, the high concentration of the alkaline solution and low water content prevents the oxidation of the MXene surface. This was the first time the alkaline solution technique was utilized for the synthesis of a high-purity MXene, which illuminates new possibilities for the successful synthesis of fluorine-free MXene by this method. However, the operating conditions for alkali-based etching such as (27.5 M NaOH and 270 °C) make this synthesis difficult on a large scale. The structural and morphological characterization of MXene synthesized through alkali and chemical etching routes is shown in Figure 4b and c.[49] Alkaline solution etching can be conducive to scalability due to its relatively straightforward process and the availability of alkaline reagents such as sodium hydroxide (NaOH) or potassium hydroxide (KOH). These solutions can be easily prepared in large quantities, facilitating continuous production processes. Alkaline solutions are generally less expensive than some other etchants, such as HF, contributing to the cost-effectiveness of MXene synthesis. Additionally, alkaline solution etching may require less stringent safety measures and equipment compared to more hazardous etching methods.[50] Despite the lower cost of reagents, achieving cost-effectiveness may still require optimization of process parameters and energy-efficient design. Alkaline solution etching may offer a relatively reduced environmental impact compared to more hazardous etchants like HF. The chemistry involved in alkaline solution etching is generally less hazardous, and the byproducts may be less toxic if properly managed. Proper waste management practices, including neutralizing and treating alkaline byproducts, are essential to minimize environmental impact.[51] The alkali solution method for MAX phase etching is an effective method to achieve good quality, highly hydrophilic MXenes with fluorine-free termination. However, the danger in dealing with high-temperature conditions and concentrated alkalis limited their large-scale synthesis. Additionally, the acquired products are multilamellar with the accordion morphology, which needs further intercalation and delamination to give a single-layer MXene nanosheet.

2.1.4. Electrochemical Etching. Electrochemical etching for MXene synthesis involves the preferential elimination of the aluminum atomic layer facilitated by supplying a specific voltage, employing the MAX phase as an electrode. The electrochemically etched MXene ensures the fluoride ions do not appear during the etching process as compared with involving fluorine during chemically treated HF and LIF/HCl techniques. Therefore, only hydroxyl (−OH) and chlorine (−Cl) group components appear on the surface of the as-synthesized MXene.[52,53] Further studies reveal that the electrochemical etching of $Ti_3C_2T_x$ would take place in three layers. From the outside to the inside, the structure comprises carbide-derived carbon, MXene, and end-etched MAX. However, further separation of the MXene from all three layers of structures is done through ultrasonication to achieve a high-purity MXene. Based on the findings, It can be concluded that electrochemical etching can selectively eliminate the A layer from the MAX phase without involving the −F group to synthesize MXene.[54]

The etching of $Ti_3C_2T_x$ through the electrochemical route is illustrated in Figure 4d and e. Two blocks of Ti_3AlC_2 are employed as an electrode. During the etching process, the cathode part of Ti_3AlC_2 remains intact whereas the anode part remains partially intact. Then, Al becomes corroded by the Cl ion-containing electrolytes due to the vigorous reaction between Cl and Al ions. The XRD spectra of EE-$Ti_3C_2T_x$ show it possesses very good film-forming ability, as shown in Figure 4f. It can be seen that the EE-$Ti_3C_2T_x$ film synthesized by a vacuum filtration technique is highly flexible with a better surface morphology than HF/LIF-etched MXene and could be folded into a special shape without fracture, as shown in Figure 4g.[55] In one of the studies by Yang et al.,[56] the fluorine-free etching strategy based on Ti_3AlC_2 in an aqueous electrolyte was adopted through anodic etching. The electrochemical technique was used to prepare $Ti_3C_2T_x$ (T_x = OH, O) using an alkaline solution of ammonium chloride (NH_4Cl) and tetramethylammonium hydroxide (TMA−OH). The Ti_3AlC_2 acts as an anode, whereas Cl^- in the electrolyte causes the rapid corrosion of Al in the anode to break the Ti−Al bond. Furthermore, the addition of ammonium hydroxide (NH_4OH) into the nanosheets facilitates further etching under the surface, and the anode Ti_3AlC_2 was

https://doi.org/10.1021/acsomega.4c04849
ACS Omega 2024, 9, 32350−32393

fully etched during a short period of time. The reaction proposed for the successful etching is given in eqs 6−8.

$$Ti_3AlC_2 - 3e + 3Cl = Ti_3C_2 + AlCl_3 \quad (6)$$

$$Ti_3C_2 + 2OH - 2e = Ti_3C_2(OH)_2 \quad (7)$$

$$Ti_3C_2 + 2H_2O = Ti_3C_2(OH)_2 + H_2 \quad (8)$$

The electrochemical etching led to the rapid and successful synthesis of MXene at room temperature. The experimental results also revealed that the capacitance of all the solid-state MXene-based supercapacitors after electrochemical etching was higher as compared with that of the MXene etched through LIF/HCl.[56] Electrochemical etching is the safest and greenest synthetic technique with low consumption of energy. However, the inclusion of the carbide-derived carbon (CDC) layer is still a large point of criticism. Furthermore, the MAX phases as an electrode could be recycled many times through regular retching technique, which could result in a lower yield of MXene, making their utilization difficult for large-scale preparation.[57] Electrochemical etching generally utilizes inexpensive starting materials, such as bulk metallic precursors (e.g., titanium foils). These precursors are readily available and cost-effective compared to other methods of MXene synthesis.[52] Electrochemical etching often employs aqueous electrolytes and mild reaction conditions, reducing the need for harsh chemicals and minimizing environmental impact. The process can potentially be carried out at room temperature, further reducing energy consumption compared to high-temperature methods. By avoiding the use of strong acids and toxic reagents, electrochemical etching reduces chemical waste and the generation of hazardous byproducts, making it more environmentally friendly.[58,59]

2.1.5. Molten Salt Etching Method. MXene is conventionally synthesized via etching the atomically thin A layer elements from MAX phases using F-containing electrolytes such as HF, LiF, and $(NH_4)HF_2$, which results in attaching, −OH, −F, and −O surface-terminated groups to the MXene. The introduction of surface functional groups to MXenes influences not just the thermodynamic stability and optical characteristics but also the electronic properties, including the band structure and work function, as well as the electrochemical performance. Additionally, one of the major disadvantages of using the aforementioned acid-based etchants is their hazardous and toxic nature.[60,61] The successful etching of MXene through an aqueous solution is one of the most advantageous approaches to get the hydrophilic MXene phases under low operating temperatures.[62] Figure 4h shows the synthesis schematic of the exfoliation of an MXene prepared via the molten salt method with XRD. The MXene shows good crystallinity and surface morphology, as shown in Figure 4I and j(i). However, the aqueous systems may fail during the etching of non-Al or nitride MAX phases. The theoretical estimation also discovered that the transformation of $Ti_{n+1}AlN_n$ to $Ti_{n+1}N_n$ showed a high energy barrier as compared with etching $Ti_{n+1}AlC_n$ to $Ti_{n+1}C_n$, which is referred to as a thermodynamic limitation in etching $Ti_{n+1}AlN_n$ due to strong bonding between Al and Ti. Furthermore, the lower cohesive energy of $Ti_{n+1}N_n$ compared to its corresponding carbides is related to its poor structural stability, which allows its successful and easy dissolution in fluorine-containing aqueous solutions.[63] For the first time, Urbankowski et al.[64] used molten salts of lithium fluoride (LiF), sodium fluoride (NaF), and potassium fluoride (KF) for the successful etching of Ti_4AlN_3 to get nitrides of MXene (at 550 °C for 0.5 h), and the comparison of the XRD crystallinity I s shown in Figure 4k. The $Ti_4N_3T_x$ MXene formed in an accordian-like morphology and the high capacity of molten salts to produce MXene with a high formation energy and good SEM morphology of synthesized MS-etched $Ti_4N_3T_x$ MXene are shown in Figure 4j(ii).[63] One of the other advantages of molten salt etching is that HF-etched carbide MXene (Mo_2C) could be easily converted into nitride MXene (Mo_2N) via thermal treatment under ammonia (NH_3) (at 600 °C). However, this process could not be completely applied to V_2CT_x MXene. The XRD patterns of both carbide and nitride-based MXene are presented before and after treatment under NH_3 as shown in Figure 4l.[64] The material derived from V_2CT_x exhibits peaks corresponding to both V_2N and cubic VN due to structural and compositional degradation during the thermal transformation. In contrast, annealing Mo_2CT_x at 600 °C results in the formation of Mo_2NT_x, maintaining its 2D MXene structure, as indicated by the presence of the (002) peak at $2\theta = 11°$. In the case of V_2NT_x (top blue curve), a broad peak emerges at $2\theta = 7.0°$, and the presence of a non-MXene nitride is confirmed by the peak at 37°.[65]

In the molten salt etching process without fluoride, transition metal halides react with the A layer of the MAX phase, acting as an electron acceptor. One of the studies by Li et al.[66] implies the successful etching of Ti_3AlC_2, Ti_2AlC, Ti_2AlN, and V_2AlC MAX phases in a molten salt mixture of $ZnCl_2$/NaCl/KCl under a nitrogen-protected environment. $ZnCl_2$ serves as an etchant for etching the MAX phase, while NaCl/KCl is utilized to create molten salts, reducing the melting point of the eutectic system. The reaction through the molten salt HF-free etching of Ti_3AlC_2 is described in eqs 9 and 10.

$$Ti_3AlC_2 + ZnCl_2 = Ti_3ZnC_2 + Zn + AlCl_3 \quad (9)$$

$$Ti_3ZnC_2 + ZnCl_2 = Ti_3C_2Cl_2 + Zn \quad (10)$$

From the reaction, zinc chloride ($ZnCl_2$) successfully etched the Al MAX phase and Zn MAX phase to get a fluoride-free MXene. As the process is fluoride-free, the surface of the MXene gets a −Cl termination instead of attaching −F, −O, and −OH terminations to get a fluoride-free MXene. In one of the recent studies by Arole et al.,[67] the synthesis and aqueous dispersibility of Nb_2CT_Z nanosheets via molten salt etching through KOH washing showed good agreement for the successful synthesis via fluoride-free etching. Adding the KOH solution for washing adds some hydroxyl surface groups. However, the slow oxidation behavior through molten salt etching is attributed to the lesser amount of oxygen-containing terminal groups. Also, the study reported by Dong et al.[68] showed the successful employment of Nb_2CT_x MXene synthesized by molten salt Lewis acidic-based etching to achieve a high lithium storage capacity of up to 330 mAh g^{-1} at 0.05 A g^{-1}, whereas the $Ti_3C_2T_x$ MXene synthesized via molten salt etching achieved a maximum capacity of 205 mAh g^{-1}. Utilizing high-temperature molten salts such as lithium chloride (LiCl) or potassium chloride (KCl) for the targeted removal of aluminum layers, molten salt etching in MXene synthesis presents advantages such as enhanced safety and reduced environmental impact compared to traditional acid-based methods. However, challenges lie in optimizing temperature conditions and ensuring scalability for large-scale production.[69] The elevated temperature requirements may affect energy consumption, and potential alterations to MXene characteristics must be carefully evaluated. While the environ-

https://doi.org/10.1021/acsomega.4c04849
ACS Omega 2024, 9, 32350−32393

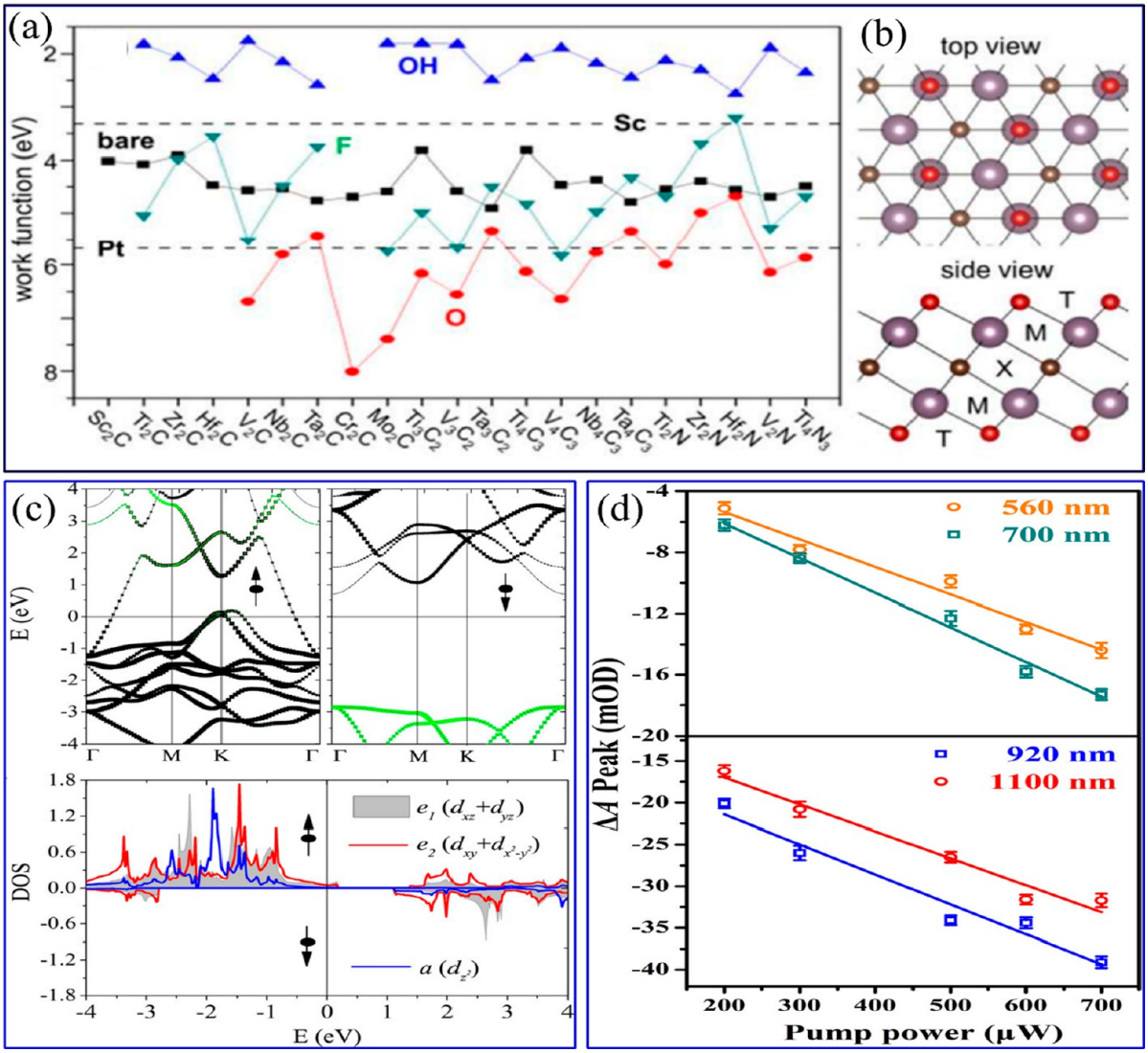

Figure 5. (a) Work functions of MXenes with different terminations. Bare surface, black square; O termination, red circle; OH, blue up-triangle; F, cyan down-triangle. (b) Atomic structure of a representative M_2XT_2. M, purple; X, gray; T, red. Reproduced from ref 162. Copyright 2016 American Chemical Society. (c) Band structure for Cr2C MXene (the black and green squares represent the weights of the Cr d and C p orbitals, respectively) and partial density of states of Cr d orbitals. The Fermi level is set to zero. Reproduced from ref 183. Copyright 2015 American Chemical Society. (d) Peak absorption versus the power intensity of the pump laser under various wavelengths. Reproduced from ref 175. Copyright 2022 American Chemical Society.

mentally friendly nature of molten salt etching shows promise, further refinement is necessary before it can be deemed suitable for industrial-scale production. Addressing these challenges and fine-tuning conditions are essential steps toward enabling its viability for large-scale synthesis.[70]

2.2. Perspective on Different Methods for MXene Synthesis. HF acid is the primary etchant used in the well-established process of synthesizing MXenes by breaking the metallic bond between titanium and aluminum, leading to the removal of aluminum layers. Despite its efficiency, HF's high toxicity raises significant safety and environmental concerns, necessitating strict precautions and disposal measures.[71] These issues make HF-based bulk production impractical, highlighting the need for new methods to reduce HF use and enable scalable, sustainable, and cost-effective industrial MXene synthesis. Mixed acid etching has become popular nowadays due to the removal of etching byproducts. However, instead of using a high concentration of HF (∼50 wt %), low concentrations of HF (<10 wt %) could be used to give high-quality MXenes.[27] For instance, Kurra et al.[72] reported the successful etching of the Ti_3AlC_2 MAX phase using a 5 wt %/25 wt % aqueous solution of HF/H_2SO_4. They achieved a high-quality MXene that showed high electrochemical energy storage for Na-ion capacitors instead of using MXene synthesized using only HF and a HF/HCl solution. Similarly, Anayee et al.[39] reported the synthesis of high-quality Ti_3C_2 MXene using low concentrations of HF acid (5 wt %) with the mixture of etchants HF/HCl and HF/H_2SO_4. They reported that HF/HCl etching resulted in −Cl terminations, contributing to larger interlayer spacing and a higher structural water content compared to the other etching methods. Etching with HF/H_2SO_4 yielded only a trace of sulfur and resulted in the highest electrical conductivity and thermal stability among the samples. The electrochemical sodium ion intercalation study indicated that the $Ti_3C_2T_x$ sample etched with HF/H_2SO_4 demonstrated lower first-cycle irreversibility and superior overall electrochemical performance. This

https://doi.org/10.1021/acsomega.4c04849
ACS Omega 2024, 9, 32350−32393

enhancement is attributed to a cleaner surface achieved through more effective removal of etching byproducts and structural water, which can limit HF-based etching.[39] The modified acid etching method, which uses LiF and HCl, offers a more controlled and customizable approach compared to HF etching. It ensures accurate removal of aluminum layers and offers benefits such as reduced toxicity and safer handling and disposal, making it suitable for large-scale manufacturing. However, challenges remain in optimizing efficiency, standardizing processes, and achieving scalability for large-scale MXene synthesis with this method.[73] Kashiwaya et al.[74] reported a method for exfoliating gold (Au) from Ti_3AuC_2 by wet-chemically etching away the carbide layers using Murakami's reagent. This reagent, consisting of low concentrations of KOH and $K_3[Fe(CN)_6]$ along with surfactants like CTAB and cysteine, provides a straightforward, scalable, and HF-free approach to obtaining high-quality Ti_3C_2 MXene.[74] Fluoride-free etching in MXene production, using concentrated HCl or nitric acid (HNO_3), offers a safer alternative by avoiding potentially harmful fluoride chemicals. This method addresses safety and environmental concerns but may result in less controlled etching, affecting selectivity and repeatability.[75] For consistent, scalable, and cost-effective large-scale MXene production, further refinement of fluoride-free etching is needed to maintain its safety benefits.[76] Molten salt etching could be effective for producing MXene by selectively removing aluminum layers from MAX-phase precursors using high-temperature molten salts like lithium chloride (LiCl) or potassium chloride (KCl).[63] This technique offers benefits such as improved safety and reduced environmental impact compared to conventional acid-based methods. However, challenges include optimizing temperature conditions, ensuring scalability for large-scale production, and managing energy consumption. While promising for its environmentally benign profile, further refinement and optimization are needed for molten salt etching to be viable for industrial-scale MXene synthesis.[67,77] Chemical vapor deposition (CVD) is employed in MXene synthesis to create films by precisely depositing precursor gases, such as organic ligands and metal chlorides, onto a substrate. This method allows for meticulous control over the film's thickness, composition, and structure, enabling the customization of MXene properties for specific applications.[78] The advantages of CVD include the ability to tune material characteristics to meet precise requirements finely. However, challenges remain, such as the need for controlled gas conditions and high temperatures, which can hinder scalability and impact MXene properties. Additionally, substrate dependency may limit application flexibility. Addressing these challenges and optimizing large-scale deposition techniques are critical for making CVD a viable method for practical and scalable MXene production.[79,80]

3. PROPERTIES OF MXENES

3.1. Structural Properties. The MXene ($M_{n+1}X_n$) structure is the output of "A" layer removal from MAX ($M_{n+1}AX_n$) and the addition of functional groups such as −O, −OH, −F, etc.[157,158] The presence of an X atom can be seen either in the TM layer or in the lower panel, resulting in two variations of hollow sites.[159] Six different structures of MXenes have been reported in various applications, although $Ti_3C_2T_x$ is used most extensively to date.[160,161] Figure 5b presents the structure of MXene, where T is seen on the FCC side of the surface and X and M layers follow ABC close packing. Non-Ti-based MXene application has led to the discovery of varied properties; for instance, some Sc-based MXenes demonstrated a rhombic structure with trigonal and oblique symmetry ,while some Cr-based MXenes promoted good HER activity and some Y-MXene configurations had two different kinds of intergrowth structures like NaCl and Al_4C_3.[162] The synthesis technique and application determine the design and reformation of the structure of MXene.[163] In the mono-M-structured MXenes like Ti_2C, the metal sites are occupied by one transition metal, whereas for solid solutions e.g., $(Cr, V)_3C_2$, randomly two metal atoms are distributed in the M site. The external layers of ordered out-of-plane double M elements like $Mo_2Ti_2C_3$ are occupied by one transition metal, and the central layer is filled by another. On the other hand, M elements are ordered in the basal plane of ordered in-plane double M elements such as $TiCrCF_2$. The "A" layer is removed and combined with an alloying M element in the vacancy ordered structure, e.g., $W_{1.33}CT_x$. A structure with randomly distributed vacancies can be seen in $Nb_{1.33}CT_x$ with two different M elements ordered in a 2:1 ratio.[161,164] The advancement of MXenes largely relies on the research conducted on MAX phases, as the structure and composition of MXenes are directly derived from their parent MAX phase. Recent focus in MAX phase studies has been directed toward ordered arrangements of alloying elements on the M site alongside random solid solutions.[89] In 2014, the discovery of the first chemically ordered MAX phase alloy, $(Cr_{2/3}Ti_1/_3)_3AlC_2$, by Liu et al.[165] marked a significant milestone. This structure, essentially reduced to M_3AX_2, exhibits out-of-plane chemical ordering, wherein alternating layers consist of one type of M element exclusively. Subsequently, similar out-of-plane ordering was achieved in an M_4AX_3 structure with the M elements in a 2:2 ratio, exemplified by $Mo_2Ti_2AlC_2$. The synthesis of the corresponding out-of-plane MXenes commonly known as o-MAX is shown in Figure S1, thus underscoring the interconnectedness of MAX phase research and MXene progress. MXene exhibits a hexagonal lattice formation, and an increase in the c-lattice parameter can occur with doping and molecular and elemental intercalation.[157,158] Active site distribution is dependent on the composition and morphology but is generally concentrated at the monolayer flake boundary.[166] MXene flakes are encircled by water molecules when dispersed due to the unrestricted movement in liquid media.[160] It was revealed via atomic force microscopy that at high temperatures Ti_3C_2 MXenes exhibit lower adhesion and friction, whereas with elevated pressure these forces increase proportionally.[167]

3.2. Optical Properties. In recent times, many interesting features have been shown regarding the optical properties of MXenes. Among these features, we have the ease of photo-thermal conversion, optical clarity, and finally favorable plasmonic behavior. The amazing ability that MXenes have to react with optics in several ways has had a significant effect on the research community.[168] In 2016, Berdiyorov et al.[169] studied the importance of external terminations for the optical characteristics of $Ti_3C_2T_2$-(MXenes) and matched the results to basic MXene. On the other hand, Halim et al.[170] focus on Nb_2CT_X and Ti_3CT_x with variations in the nature of the transition metal, which controls the optical characteristics of MXenes. The results of the above analysis showed that Nb films exhibited an enhancement in absorption rate due to the electronic configuration of M elements when moving toward the range of infrared waves. Additionally, the high absorption rate of MXene is attributed to its good surface chemistry owing

https://doi.org/10.1021/acsomega.4c04849
ACS Omega 2024, 9, 32350−32393

Table 2. Optical Characteristic Dependency on Surface Termination of MXene Flakes[a]

MXene Flakes	Surface Terminator	Highest Peak Photo Absorption Spectra Occurrence	Peak energy (eV)	μ (Debye)	PDOS Attributes
Ti_2C 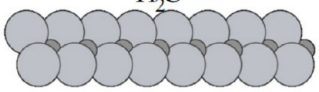	T_x	≈ 300	0.22, 1.94, 3.17	-0.6	C(p), Ti(s), Ti(p), Ti(d)
Ti_2CF_2 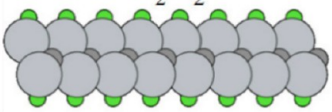	F	≈ 210	0.21, 0.90, 1.33	6.6	C(p), F(p), Ti(d)
Ti_2CFO 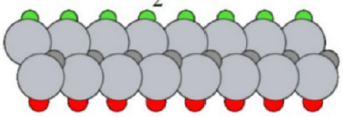	O, F	≈ 580	0.20, 0.85, 1.41	39	C(p), O(p), F(p), Ti(d)
Ti_2CO_2 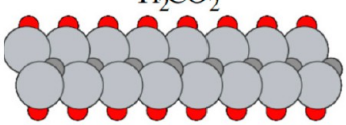	O	≈ 160	0.19, 1.15, 2.12	5.15	C(p), O(p), Ti(d)
V_2C 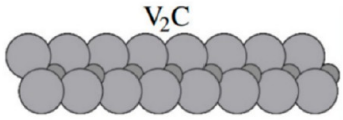	T_x	≈ 80	0.21, 0.87, 2.17	-1.77	C(p), V(s), V(p), V(d)
V_2CF_2 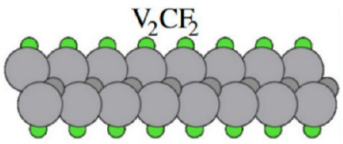	F	≈ 350	0.23, 0.96, 1.60	4.3	C(p), F(p), V(d)
V_2CFO 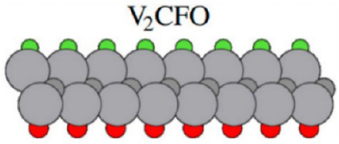	O, F	≈ 560	0.20, 0.85, 2.15	28	C(p), O(p), F(p), V(d)
V_2CO_2 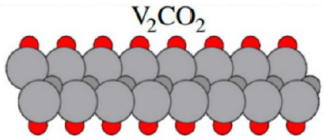	O	≈ 50	0.22, 1.26, 2.33	4.3	C(p), O(p), V(d)

[a]Adapted from ref 176. Copyright 2023 Elsevier.

to the functional groups (−F, −OH, and −O) that interact strongly with IR radiation and enhance the absorption. For example, −OH creates dipole moments that interact with IR radiation to increase the absorption. MXenes typically consist of atomically thin layers stacked on top of each other. The thickness and layering of MXene films can influence their IR absorption properties. In 2017, Li et al.[171] proved that MXenes have a greater capacity to be exposed to light when compared with carbon nanotubes (CNTs) due to the electromagnetic wave absorption property of MXene, resulting in a blockbuster electromagnetic interference shielding effect. The strong metallic conductivity of MXenes due to their unique electronic structure increases the plasmonic resonance in the IR range to increase the absorption compared to CNTs. Additionally, Jiang et al.[172] studied the optical nonlinear behavior of $Ti_3C_2T_x$ by having sources of multiple wavelengths. The results show that the rate of absorption was almost twice as large when compared with other processes. Likewise, stable MXenes have attracted a large amount of interest for plasmonic applications, as they have tunable optical properties.[173] Generally, it has been hypothesized that for both cases the linear and nonlinear optical characteristics of MXenes depend on the energy structures. For

https://doi.org/10.1021/acsomega.4c04849
ACS Omega 2024, 9, 32350−32393

use in photonics, nonlinear response is the ideal candidate. The main use of optical properties involves but is not limited to biosensing, emission/detection of light, solar technology, photocatalysis, and photoelectronic imaging.[174] Despite highlighting many applications of MXenes in the optical field, numerous changes are still required to improve their structural properties if MXenes are to be applied in wide-spread optical applications. In an experimental observation of optical properties by Gao et al.,[175] the ΔA peak is observed to increase with the pump power as shown in Figure 5d, where the transmittance is enhanced for the Pauli exclusion principle. Muhammed et al.[176] studied the dependency of surface termination in the optical properties of 6 MXene flakes, where the Janus MXene produced the narrowest and strongest infrared LSPR. While examining the projected density of states, they reported that nonterminated pristine MXene with M metal d electrons showcased a high density of states. They also investigated the photoabsorption spectra and out-of-plane time-dependent dipole moment (μ), which are briefly described in Table 2.

3.4. Electronic Eroperties. The electronic properties of MXene have different sorts of applications like the MAX phases, whereas all the pure MXenes are metallic in nature. Among all the discovered MXenes, the first MXene is $Ti_3C_2T_x$ which is still broadly utilized and exhibits the highest conductivity. To increase the electronic conductivity, different steps like incorporating hydrogen bonds, varying layer thickness, etc. were taken; depending on the functionalization of the surface, the condition turned from metallic to semiconducting in nature.[177,178] In accordance with the spin−orbital coupling (SOC), MXenes are divided into two parts that are topologically trivial and nontrivial based on the theoretical studies, whereas depending on the strength of relativistic SOC they can be outlined into metal, semimetal, and semiconductor. The main portion of MXenes follow metallic characteristics, but Sc_2CT_2 (T = F, OH, and O), Ti_2CO_2, Zr_2CO_2, and Hf_2CO_2 behave like semiconductors after the functionalization of the surface and have energy gaps based on general gradient approximation of 0.24 eV for Ti_2CO_2, 0.88 eV for Zr_2CO_2, and 1.0 eV for Hf_2CO_2. However, in the case of Sc_2CT_2 (T = F, OH, and O) with calculated energy gaps of 1.03, 0.45, and 1.8 eV, respectively, the band gap is direct. As Ti, Zr, and Hf are the members of the same group in the periodic table, they also have similar electron distributions in their last orbital, which is partially filled, and their band gaps are indirect; this family of MXenes demonstrates similar metallic to semiconductive characteristics.[157,159] Figure 5a demonstrates the work function of MXene where the −OH-terminated MXenes have ultralow (<2.8 eV) work functions. When a surface dipole moment is induced by functionalization, the workforce changes. Among Ti_2CO_2, Zr_2CO_2, and Hf_2CO_2 MXenes, their good electronic properties and quantum capacitance were recently analyzed by comparing pristine Hf_2CO_2(PH) and N-doped Hf_2CO_2 through density functional theory (DFT). By enhancing the N-doping concentration, the red shift of the valence bands of C p, Hf d, O p, and Hf p states progressively increased.[162] In an aqueous system, for specific electrode materials, 100% of the n-doped concentration and 89% of PH systems are suitable.[179] Topologically nontrivial semimetal and semiconductor MXenes consist of 4d and 5d heavy metals, and these types of MXenes can be symbolized as M_2CO_2 (M = Mo, W) and $M'_2M''C_2O_2$ (M'=Mo, W; M''=Ti, Zr, W). Without accounting for SOC, these semiconductors exhibit zero energy gap for the peak valence band and their conduction band is the lowest, which makes both conduction and valence band parabolic.[159] In spintronic applications, topological materials are utilized as potential candidates, and topological insulators can be called quantum spin hall (QSH) insulators, which enable the uniform spread of energy with no scattered spin and gapless states.[180]

3.5. Magnetic Properties. Spin-polarized DFT demonstrated that the MXenes are the nonmagnetic majority at the ground state because of the strong covalent interaction between the T_x, transition metals M, and C/N.[159] The band gap could be manipulated by applying strain, which was shown to release d electrons while providing magnetism.[159,181] Additionally, certain pure MXenes show intrinsic magnetism like Ti_2N and Ti_2C, which are almost half-metallic ferromagnetic and have magnetic moments of 1.0 and 1.91 μB per unit formula, respectively.[182] On account of the existence of d electrons, chromium (Cr), chromium nitride (Cr_2N), and chromium carbide (Cr_2C) are magnetic in the case of Cr-MXene. Cr_2C is a semimetallic ferromagnetic that changes into an antiferromagnetic semiconductor due to functionalization. V_2N and V_2C are nonmagnetic and antiferromagnetic metals in a monolayer, respectively, yet compressive and biaxial strain can create a significant magnetic moment. Additionally, a functionalized V_2C containing OH or F can become a semiconductor with a narrow antiferromagnetic gap. The semimetallic characteristic is demonstrated via a half-metallic gap in Figure 5c. On the other hand, the projected density of states shows the appearance of metallicity. The surface of Cr_2N was functionalized with O, F, or OH to give semimetallic behavior.[183] Nonmagnetic MXenes could be made magnetic, for instance, by doping Sc_2CT_2 with Mn, V, Cr, or Ti.[184] Lei et al.[185] found the effect of element vacancy on the magnetic properties of a monolayer SC_2CF_2 MXene. The vacancy of Sc induces magnetism that is delicate against tensile strains but stable under compressive strains. Table 3 shows the magnetic and electronic properties of various MXenes. In one of the studies by Yue et al.,[186] the authors projected that the 2D Fe_2C MXene will be intrinsically ferromagnetic and metallic, with a total magnetic moment of 3.95 μB per unit cell. The strong negative magnetic anisotropy energy surrounding the borders of the hexagonal Brillouin zone is the cause of Fe_2C's in-plane magnetism. Bandyopadhyay et al.[187] found that, due to the existence of unpaired electrons in the spin, point defects like Frenkel and Schottky vacancies created during the synthesis of the materials may drastically change the MXenes' electromagnetic properties divided by d orbitals.

3.3. Electrochemical Properties. The next generation of electrochemical energy storage devices require outstanding electrochemical performance coupled with high power and energy density, both of which are directly dependent on the properties of the electrode materials. That is why it is crucial to develop good contact between the electrolyte and electrode to maintain their long-term cyclic stability with a controlled morphology, which could be developed through adopting an effective synthesis synthesis technique, precursor selection, and reaction conditions.[219,220] The importance of different materials like activated carbon, graphene, and carbon nanotubes (CNTs) has been highlighted in the electrochemical energy storage application of supercapacitors. However, low energy density (<20 mWhcm^{-3}), low volumetric capacitance (200F/cm^3), and low operating voltage (<2.7 V) are the major challenges.[221,222] Recently, MXene has garnered significant attention from researchers as a unique electrode material due to its rapid ion diffusion, large surface area, high thermal and electrical

https://doi.org/10.1021/acsomega.4c04849
ACS Omega 2024, 9, 32350−32393

Table 3. Magnetic and Electronic Properties of Different MXenes

MXene	magnetic moment (μ_B)	band gap (eV)	ref
Ti_2C	1.92	~0.2	188, 189
Ti_3C_2	1.87	0.3−2.1	190
Zr_2C	1.25		188
Cr_3C_2	3.9	1.2	191
Co_2C	2−5	1−3	192, 193
Fe_2C	3.9196		194
Fe_2CF_2	2−5	1.58	192, 195
$Fe_2C(OH)_2$	2−5		192
Mn_2C	~6		196
Mn_2CO_2	3	1.9−2.3	193, 197
Mn_2NF_2	~9		197
$Mn_2N(OH)_2$	8.8		197
Cr_2NO_2	~5		197
Fe_2C	3.95		186
Sc_2Na_2CNC	3	1.18	198
Sc_2K_2CNC	3	1.31	198
$Sc_2Na_2CNCF_2$	5	2.87	198
$Sc_2Na_2CNCCl_2$	5	3.25	198
Ti_2N	1.09		199
V_2N	0		200
$ScCr_2C_2F_2$	~5		201
Sc_2COHC	3.98		202
Cr_2COOH	5		203
Cr_2CuC_2	5	0.569	204
$Sc_2Li_2N_3$	3		205
bMn_2ZnN_2	6−9		206
Ti_2ZnC_2	4		207
Sc_2CF_2	1	0.55−0.24	208, 209
Hf_2CO_2		1.657	210
Sc_2CO_2		1.84	211
$ScNbCO_2$		~1.40	211
Fe_2CCl_2		1.28	195
Ti_2NO_2	0.27	2.28	212
Fe_2CO_2	2−5	0.66	192
Co_2CF_2	2−5	1.53	192
$Co_2C(OH)_2$	2−5	1.12	192
Ni_2CF_2	2−5	0.51	192
Hf_2C	1.5	1.0058	188, 213
Mn_2N	~4		214
$Hf_2MnC_2O_2$	3	0.282	215
$Mo_3N_2F_2$		0.47	216
$Cr_2Ti_2C_3O_2$		1.75−2.18	217
$Cr_2Ti_2C_3T_2$	1.983		217
$Cr_2V_2C_3T_2$	2.015		217
Sc_2CO_2	1.28	0.565	218
$Sc_2C(OH)_2$	1	0.532	218

conductivity, and controllable thickness and composition to boost the electrochemical performance of energy storage devices. The exceptional characteristics of MXene, including fast electron transfer, hydrophilicity, fast ion diffusion capability, and high electronic conductivity (~24 000 S cm^{-1}) and pseudocapacitive performance, along with a multilayer morphology and surface functionalities, play a vital role in making it a superior candidate for electrochemical energy storage compared to other 2D materials.[223,224] While pure MXene demonstrates superior electrochemical properties, its practical application in dense structures for commercial purposes is impeded by inherent layer restacking driven by van der Waals interactions. This phenomenon results in compromised capacitance retention, reduced stability, and hindered electrolyte ion diffusion over extended cyclic usage.[225,226] Fine-tuning the interlayer distance, surface terminations, and chemical composition of MXene-based materials offers avenues for optimizing their electrochemical performance. The strategic integration of MXenes with other materials to form composites has emerged as a highly promising approach in energy storage applications.[227] Among the diverse range of MXenes synthesized, $Ti_3C_2T_x$ has garnered significant attention due to its redox-active Ti atom and consequent high volumetric capacitance, aided by the conductive carbide layer facilitating ion transport and electron mobility. Thus, the controlled synthesis of MXene-based materials, focusing on composition, metal/carbon ratio, and surface characteristics, holds immense potential for enhancing their utility in lithium-ion batteries and supercapacitors.[228] Furthermore, the creation of MXene-based hybrid materials presents an opportunity for synergistically improving MXene's electrochemical characteristics. Additionally, MXenes possess a unique combination of metallic conductivity, hydrophilicity, and high surface area, rendering them particularly promising for a variety of niche applications. MXenes demonstrate high capacitance, rapid charge−discharge rates, and excellent cycling stability, which are critical for supercapacitor applications. Their performance in electrochemical capacitors is further enhanced by their surface chemistry and tunable interlayer spacing.[229,230] In lithium-ion and sodium-ion batteries, MXenes can serve as anodes due to their high conductivity and ability to accommodate large ionic species, facilitating rapid charge and discharge processes.[231] Their conductive and catalytic properties also make MXenes suitable for the oxygen reduction reaction (ORR), which is essential for fuel cells and metal−air batteries.[232] The high surface area and conductive nature of MXenes enable the development of highly sensitive electrochemical sensors for the detection of various biomolecules and environmental pollutants.[233] Moreover, MXenes can be utilized in membranes for water desalination and filtration, effectively leveraging their surface charge and hydrophilicity to remove salts and contaminants.[234]

4. STABILITY OF MXENE

4.1. Thermal Stability. MXenes have exhibited good thermal properties that make them fitting candidates for energy management systems, especially for thermal energy storage units. However, understanding the thermal stability of MXenes is crucial to determining their practical performance values.[235] Aslfattahi et al.[236] conducted thermogravimetric analysis (TGA) on MXene-based nanocomposites and observed that when the MXene concentration is increased in the nanocomposites they become more thermally stable. The focal degradation temperature for the nanocomposites of PW70 (362.5 °C) with different MXene loadings (0.1, 0.2, and 0.3 wt %) is achieved at 363.9, 380.9, and 384.0 °C. This can be seen in Figure 6a, with the increased concentration of Ti_3C_2 increasing the thermal stability of the nanocomposites. The enthalpy curve for MXene/PW-70 also showed good agreement in the melting enthalpy of 69.8 °C with the highest weight loading of 0.3 wt %, as shown in Figure 6b, which suggests the high durability of MXene-based composites for thermal storage applications. Lu et al.[237] employed vacuum impregnation by using MXene as a framework along with polyethylene glycol (PEG). The resulting MXene/PEG composite exhibited favorable freezing and

https://doi.org/10.1021/acsomega.4c04849
ACS Omega 2024, 9, 32350−32393

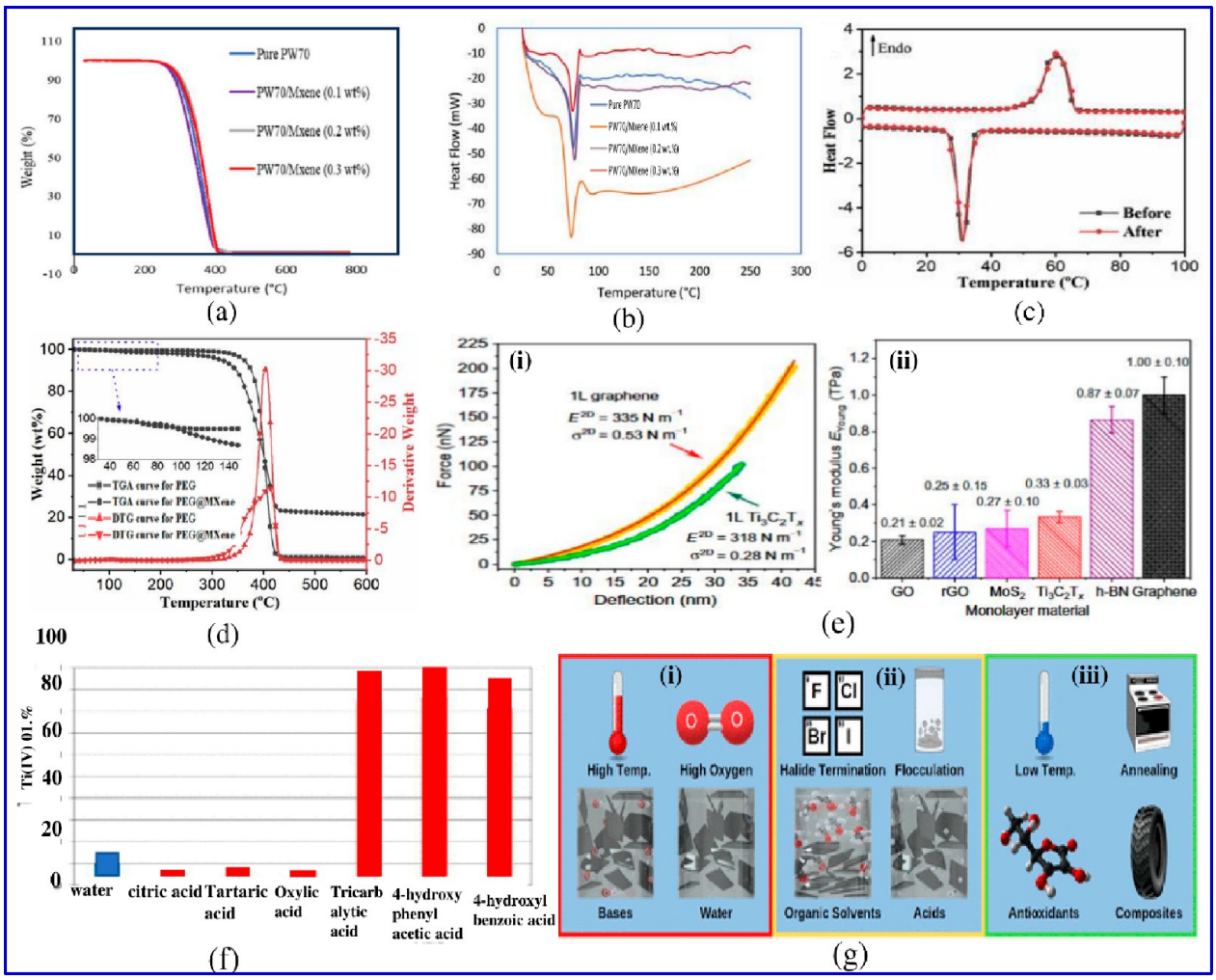

Figure 6. (a) TGA curves and (b) melting heat enthalpies of pure PW-70 and a MXene-loaded PW-70 composite. Adapted from ref 236. Copyright 2020 Elsevier. (c) Freezing and melting enthalpy. (d) TGA and DTG curves of pure PEG and MXene-loaded PEG composites. Adapted from ref 237. Copyright 2020 Elsevier. (e) *F*−*d* curve and Young's modulus of MXene in comparison with other nanomaterials. Adapted from ref 244. Copyright 2018 American Association for the Advancement of Science. (f) Degradation percentage of $Ti_3C_2T_z$ in different aqueous acidic solutions. Adapted from ref 253. Copyright 2022 John Wiley & Sons, Inc. (g) Degradation of MXene under environmental conditions: (i) oxidization environment, (ii) reduced rate environment, and (iii) methods to provide degradation resistance. Reproduced from ref 264. Copyright 2023 American Chemical Society.

melting enthalpy values of 131.2 and 129.5 J/g, respectively, after undergoing 100 thermal cycles, as illustrated in Figure 6c. Figure 6d compares TGA and DTG curves of pure MXene and a prepared form-stable phase change material. The weight loss of PEG@MXene at the temperature range of 30−100 °C is lower than 1 wt %, which is similar to pure PEG. This suggests that the acquired PEG@MXene demonstrates reliable thermal stability below 100 °C, making it crucial for practical applications in thermal storage. The obtained PCM indicated a stable thermal performance below 100 °C and 76.6 wt % weight loss, confirming the homogeneous dispersion of PEG in the MXene. The T_5 value was observed to be lower, for which the low thermal stability of MXene was suspected. Shape-stable biomass-based MXene phase change composites were prepared by Cao et al,.[238] and the composite went through two steps of thermal deterioration, where the first stage occurred within the temperature range of 85−220 °C and the range for the second stage was 215−300 °C. No weight loss was seen below 85 °C, indicating the ability to withstand a higher operative temperature. An MXene-doped microcapsule was designed by Mo et al.,[239] which was run through 50 melting and solidifying cycles. The microcapsules appeared to have 49.6% degradation in supercooling temperature. This beneficial characteristic was a result of the reduction of the free energy of nucleation during solidification. Huang et al.[240] designed a biobased hybrid composite of MXene that could function above the temperature point of phase transition, as no weight loss was recorded below 100 °C. A drastic decline was monitored between 220 and 310 °C, which is the result of the volatilization and disintegration of alkane molecules. The experimental and theoretical values of residual carbon content were almost similar. A composite was designed along with cellulose nanofibers and MXene by Quan et al.,[241] and they used a heated stage to observe more than 1000 thermal cycles. The melting and freezing enthalpies were similar in both the first and 1000th cycles. The highest decomposition temperature was higher in the prepared composite, which indicates a wide temperature range during operation. Gao et al.[242] observed no mass loss in MXene-incorporated Fe_3O_4 for the temperature range of 40−800 °C. The composite was thermally stable within 200 °C, which made it suitable for medium to low temperature applications. The composite showed a 30% mass fraction after reaching 800 °C.

https://doi.org/10.1021/acsomega.4c04849
ACS Omega 2024, 9, 32350−32393

4.2. Mechanical Stability. Nanosheets made up of the delaminated MXene nanomaterial are extremely flexible, especially the monolayer of MXene.[243] Even though vacuum-filtering a delaminated MXene solution to measure the Young's modulus is a relatively easy method, it cannot be used with monolayers and bilayer nanosheets. Lipatov et al.[244] used nanoindentation combined with some atomic force microscope tips to measure the elastic properties of monolayer and bilayer $Ti_3C_2T_x$. The force−displacement curves collected during the experiments were used to calculate the effective Young's modulus of the $Ti_3C_2T_x$ single layer, which was found to be 0.33 TPa. $F-d$ curves for monolayer graphene and $Ti_3C_2T_x$ with a comparison of the effective Young's moduli for several 2D materials are shown in Figure 6e(i and ii).[244] The measured value of the Young's modulus is close to the predicted value for monolayer $Ti_3C_2T_x$.[245] However, by adding polymers like polyethylene and chitosan, the mechanical properties of $Ti_3C_2T_x$ films could be enhanced.[246] For example, Ling et al.[247] combined $Ti_3C_2T_x$ MXene with polydiallyldimethylammonium (PDDA) chloride and poly(vinyl alcohol) (PVA) to fabricate an MXene/polymer composite, which successfully improved the flexibility, tensile strength, and intercalation. The volumetric capacitance improved to ∼530 Fcm^{-3} at 2 mVs^{-1}, and the composite could withstand 15000× its weight. Similarly, Wan et al.[248] incorporated 30 wt % poly(3,4-ethylenedioxythiophene)/poly(styrenesulfonate) (PEDOT/PSS) on a $Ti_3C_2T_x$ MXene film with a thickness of 6 μm, which gave a 150% improvement in tensile strength to 38.5 ± 2.9 MPa in comparison with pure MXene. Kilikevičius et al.[249] investigated the elastic properties of a novel hybrid composite made of MXene with graphene nanosheets and found that the novel nanoengineered high-strength multifunctional composite materials exhibited improved mechanical properties with improved tensile/shear stress and Young's moduli, providing future directions to develop hybridized composites with improved mechanical properties. The model properties of M_2X_1 MXene are illustrated by Yorulmaz et al.[250] The mechanical strength could be greatly affected by the functionalized MXene.[250] The mechanical properties of MXene were determined by Guo et al.[251] The results reveal that 2D Ti_2C can endure substantial strains of 18% and 9.5% under uniaxial and biaxial tension, respectively. The stretchable capacity of Ti_2CO_2 increases to 28% from 20% when incorporating −O terminations, showcasing the inhibitory impact of surface terminations on Ti_2C collapse.[251] The properties related to how nanosheets behave in directions other than their length, along with the force holding them together, are called tribological properties.[252] The tribological properties of MXenes are comparable with those of graphene just because of the weak contact and easy shareability between the nanosheets.[252]

4.3. Chemical Stability. MXenes are typically composed of transition metal carbides or nitrides, which can be susceptible to oxidation in aqueous environments. Exposure to oxygen and water can lead to the formation of metal oxides or hydroxides on the surfaces of MXenes, altering their properties and potentially degrading their performance.[177] There are several strategies to achieve chemical stability discussed by different researchers. For example, Zhao et al.[253] studied the chemical stability of $Ti_3C_2T_z$ and Ti_2CT_z nanosheet dispersions in aqueous solutions containing α-hydroxy acids, poly(carboxylic acid), and phenolic acids. They measured the degradation through XPS and the zeta potential. Figure 6f shows the degradation percentage of $Ti_3C_2T_z$ in different aqueous acidic solutions. They proposed that the interaction between the antioxidant molecule and $Ti_3C_2T_z$ nanosheet leads to the creation of a stable chelation complex. This complex prevents the $Ti_3C_2T_z$ structure from reacting with water. Wang et al.[177] studied hydrogen bonds with the coordination bond established through occupying and attacking the water and oxygen molecules of reaction sites of $Ti_3C_2T_x$ to achieve chemical and colloidal stability of the MXene at 0.1 mg mL^{-1}. Due to the chemical instability, MXenes are affected by the severe oxidation degradation in aqueous media. Fan et al.[254] introduced sodium dodecyl sulfate (SDS) to establish efficient long-term storage of a $Ti_3C_2T_x$-MXene aqueous dispersion protectant, whereas the experimental data support the ability to protect $Ti_3C_2T_x$ nanosheets from site oxidation up to 213 days of colloidal stability. Among all discovered MXenes, the titanium carbide ($Ti_3C_2T_x$) MXene exhibits the best utilization for energy storage, high conductivity, and catalysis. In addition, its lamellar structures work very well as an efficient barrier that protects against corrosion. However, in harsh surroundings, MXenes are receptive to oxidation degradation, which hinders their anticorrosive capability.[254] To mitigate this issue, Ning et al.[255] demonstrated the modification of imidazolium salt (I-$Ti_3C_2T_x$) to protect against the oxidization of $Ti_3C_2T_x$ MXene, which increased the stability of antioxidants. In an aqueous solution, the crystalline structure of the imidazolium salt (I-$Ti_3C_2T_x$) remained unchanged for 30 days and the lamellar structure remained stable for an extended duration. Because of the formation of metal oxide, the oxidation of MXene becomes a very critical challenge in its application and oxidation resistance. Nam et al.[256] introduced a novel bimetallic cobalt−manganese organic framework (CMT) on an MXene sheet. In addition, to increase the electrocatalytic properties for the evaluation of oxidation and reduction reactions, a solvothermal treatment was achieved to establish a strong resistance to oxidation. The CMT@MXene exhibits high stability as an electrocatalyst at a specific capacity of 1000 mAh g^{-1}.[256] The oxidation of MXene in the presence of aqueous media leads to the degradation of its structure and properties. This oxidation of MXene could occur in the presence of oxygen-containing functional groups such as −O and −OH and other reactive species in water. However, storing MXenes in inert atmospheres, functionalization, or the use of protective coatings can effectively work to prevent oxidation.[257]

4.4. Environmental Stability. MXenes are very reactive to environmental conditions and highly sensitive to oxygen and water. When exposed to water and air, an impulsive phase transition will occur with visible changes in the microstructure. Additionally, illumination and temperature will assist the degradation activity. However, under hydrothermal activities, MXene exhibited structural evolution and a better phase transition. Nowadays, MXene solutions are stored in the dark at reduced temperature to keep them apart from oxygen and moisture contents.[258] Lipatov et al.[45] investigated the environmental stability of single-layer MXene flakes and found that exposing delaminated MXene to air resulted in complete oxidation within a short period. They also observed degrading environmental effects first occur rapidly at the exposed edges of the MXene flakes rather than in the basal plane. Wei et al.[259] worked with MXene-based organic hydrogels that can withstand rapid temperature changes in lengthy operations. Although at tensile testing the sample's stretchability decreased at −24 °C, it still reached almost 1380% stretched strain. There was no crystallization peak in the DSC curve for temperature from −80 to 50 °C, which indicates high resistivity toward freezing. Also,

https://doi.org/10.1021/acsomega.4c04849
ACS Omega 2024, 9, 32350−32393

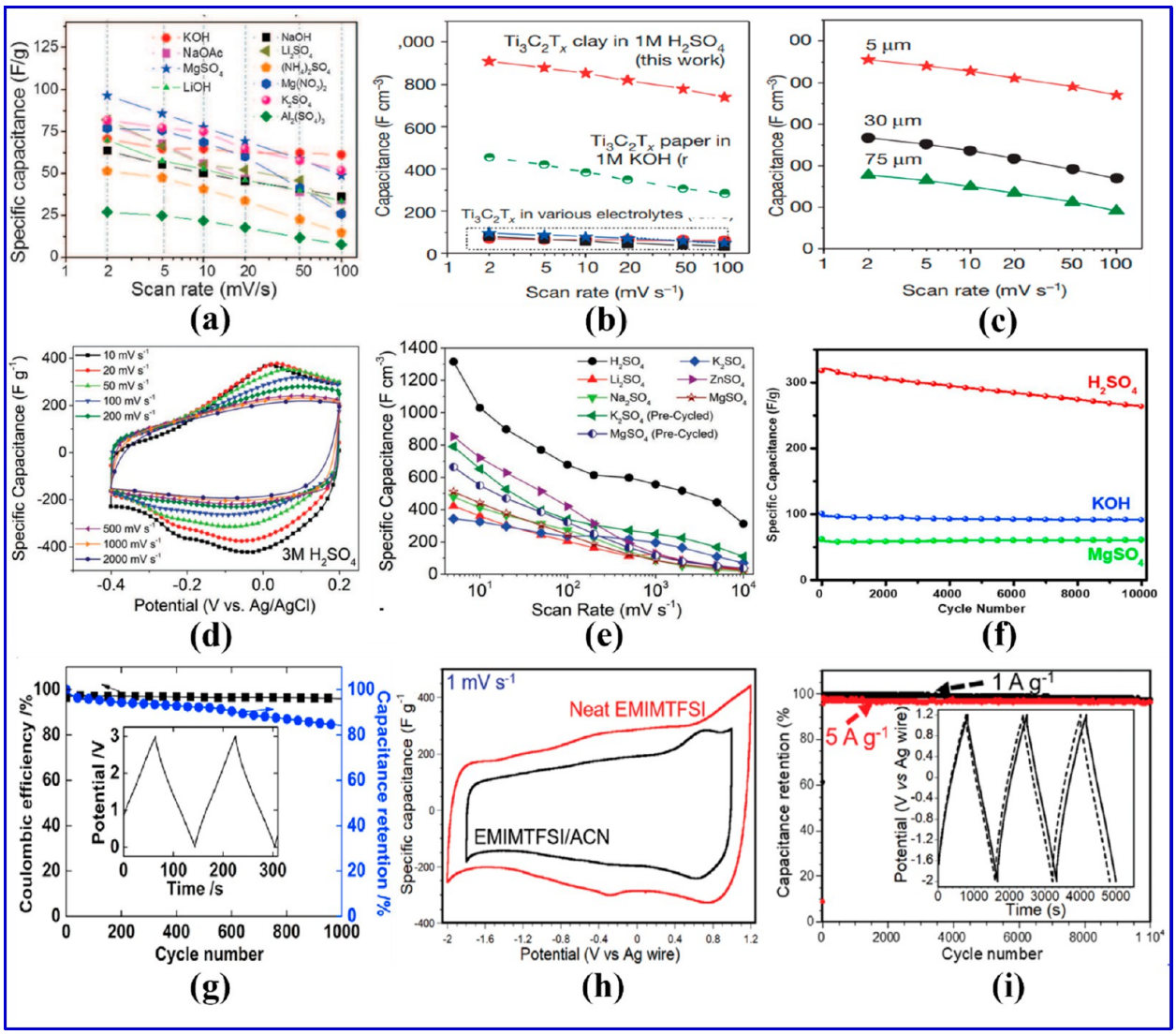

Figure 7. (a) Performance of multilayer $Ti_3C_2T_x$ electrodes in different aqueous electrolyte solutions. Adapted from ref 267. Copyright 2013 American Association for the Advancement of Science. (b) Comparison of volumetric capacitances. (c) Degrading trend in volumetric capacitances. Adapted from ref 269. Copyright 2014 Nature. (d and e) CV profiles of a MXene electrode under different solutions at different voltage and scan rates. Adapted from ref 271. Copyright 2018 John Wiley & Sons, Inc. (f) Capacitance retention after 10 000 cycles. Adapted from ref 272. Copyright 2018 Elsevier. (g−i) Specific capacitance and cyclic stability of a $Ti_3C_2T_x$ electrode in a neat (EMIMTFSI) electrolyte along with sterile $Ti_3C_2T_x$ in an EMIMTFSI/ACN electrolyte. Adapted from ref 226. Copyright 2016 Elsevier.

the sample maintained 80% weight after 7 days of exposure to open air. Wang et al.[260] also designed an MXene-incorporated organo-hydrogel that could tolerate high stretching even at −20 °C along with great resistance toward frosting and moisture. The protective shell from gelatin chains and MXene hindered the oxidation process and at the same time stabilized the aqueous dispersion of nanosheets.[260] Ternary titanium carbides, a new family of 2D MXenes, were produced by Chen et al.[261] that showed sustained resistance in various humidity ranges. The authors recommended using polyanionic salts to prevent oxidation in the MXene nanosheets, and their sample exhibited outstanding hydration stability in the recorded XRD pattern. Shekhirev et al.[262] delaminated MXene nanosheets with salts and performed an 85/85 aging test, after which they concluded that increasing the HCl concentration during the etching process will increase the intermolecular spacing and aid delamination. Minor changes during synthesis can result in behavioral differences in the MXene. Liu et al.[263] decorated MXene with a core−shell fiber that was stable not only in humid and extreme temperature environments but also in alkali and acidic media. The sample showed stability even after aging for 8 months and did not burn after being torched by an alcohol lamp. The sample showed resistance to degradation after being subjected to cryogenic cooling. Athavale et al.[264] reported the degradation of MXene under oxidation and reduced rate environments and discussed the methods to avoid the degradation in the environment, as illustrated in Figure 6g, which gives suitable pathways to maintaining the environment stability.

4.5. Electrochemical Stability. The electrochemical stability of electrodes in both aqueous and nonaqueous electrolytes is essential for ensuring the longevity, safety, efficiency, and overall performance of supercapacitors and batteries. Stable electrodes prevent material degradation, maintain capacity, and ensure safe operation, whether in the high ionic conductivity environment of aqueous electrolytes or

https://doi.org/10.1021/acsomega.4c04849
ACS Omega 2024, 9, 32350−32393

the wide voltage range provided by nonaqueous electrolytes. The electrochemical stability of MXens electrodes in aqueous and nonaqueous electrolytes was also investigated by researchers compared to its effect on the capacitance performance of supercapacitors and batteries.[265,266] Lukatskaya et al.[267] reported the high affinity of the $Ti_3C_2T_x$ MXene electrode to gather a number of cations such as NH^{4+}, Li^+, K^+, Na^+, Mg^{2+}, and Al^{3+} from different aqueous and natural electrolytes. They achieved a high volumetric capacitance of 300 F cm^{-3}, which is three times higher than that of porous carbon. The performance of multilayer $Ti_3C_2T_x$ electrodes in different aqueous electrolyte solutions is shown in Figure 7a. Yaqoob et al.[268] found that the MXene/Ag_2CrO_4 nanocomposite electrode exhibits a capacitance of 525 F g^{-1} in a 0.1 M H_2SO_4 electrolyte at a scan rate of 10 mV s^{-1}, compared to a lower capacitance of 75 F g^{-1} at 20 mV s^{-1} in a 1 M KOH electrolyte. This indicates that the pseudocapacitive behavior in acidic media maximizes charge storage for the $Ti_3C_2T_x$/Ag_2CrO_4 electrode in contrast to its performance in basic media. Ghidiu et al.[269] reported the high volumetric capacitances of $Ti_3C_2T_x$ MXene electrodeS up to 900 F cm^{-3} using acidic aqueous electrolyte H_2SO_4, which is higher as compared with the carbon-based electrolytes with A volumetric capacitance of 300F cm^{-3} illustrated in Figure 7b. From Figure 7c it can be seen that a decreasing trend in THE volumetric capacitance of electrodes was observed with an increase in electrode thickness, but overall $Ti_3C_2T_x$ MXene electrodes showed good cyclability without significant degradation over 10 000 cycles. Yang et al.[270] reported that the nitrogen doping of Ti_3C_2 to form urea-assisted and monoethanolamine-assisted N-Ti_3C_2 electrodes gives high CV performance of (2836 and 2643 Fcm^{-3}) in a 3 M H_2SO_4 electrolyte solution along with excellent stability (good capacitance retention time and Coulombic efficiency). Mohammadi et al.[271] reported that V_2CT_x MXene electrodes in H_2SO_4 electrolyte showed a high volumetric capacitance of 1300 F cm^{-3} (~420 F g^{1-}). However, specific capacitances of ≈180 and ≈100 F g^{-1} were achieved, which are higher than volumetric capacitance of $Ti_3C_2T_x$ MXene electrodes achieved at the scan rates of 1 and 10 V s^{-1} respectively. Figure 7d and e shows the CV profile, capacitance, and rate performance of various electrodes in different sulfide-based solutions. The fabricated electrodes exhibited no capacitance decay after 10 000 cycles at 10 A g^{-1} and maintained approximately 77% of their capacitance after one million cycles at 100 A g^{-1}. This performance sets a new benchmark for pseudocapacitive materials, demonstrating an exceptionally long cycle life. Shan et al.[272] compared the performance of V_2C MXene electrode in three different electrolytes, H_2SO_4, $MgSO_4$, and KOH. They achieved capacitances of 487 F g^{1-} in 1 M H_2SO_4, 225 F g^{-1} in 1 M $MgSO_4$, and 184 F g^{1-} in 1 M KOH. After 1000 live cycles, the capacitance exhibited a slight decline with increasing cycle numbers in H_2SO_4, whereas it remained stable in KOH and $MgSO_4$, as shown in Figure 7f. After 10 000 cycles, the capacitance retention was 83% in 1 M H_2SO_4, 94% in 1 M KOH, and 99% in 1 M $MgSO_4$, respectively. Wustoni et al.[273] reported the aqueous dispersion of EDOT and NaPSS with MXene to fabricate a EDOT:PSS:MXene monomer solution film and achieved a high volumetric capacitance of 607.0 ± 85.3 F cm^{-3} along with a capacitance retention of ~78% after 500 CV cycles in comparison with the PEDOT:PSS film, which loses half of its charging ability and exhibits a capacitance retention of ~37% after 500 CV cycles.

MXenes display fabulous capacitance at peak scan rates in corrosive watery electrolytes, i.e., sulfuric acid, but the energy density is restricted by the contract potential window of fluid electrolytes. Natural electrolytes and room-temperature ionic fluids (RTILs) can give higher potential windows, leading to improved energy density. The conventionally used electrolytes for ECs are nonaqueous electrolytes based on propylene carbonate (PC) or acetonitrile (ACN), which could be used as solvents with conducting salts of Et_4N-BF_4, Pyr-FSI, EMI-TFSI, EMI-BF_4, and Li-TFSI. Using nonaqueous electrolytes such as organic and IL electrolytes the high stability and potential for batteries could achieve capacitance up to 3 V. Adding MXene nonaqueous electrolytes produced a significant potential window for battery capacitance. Lin et al.[274] reviewed the behavior of $Ti_3C_2T_x$ MXene in ionic fluid 1-ethyl-3-methylimidazolium bis(trifluoromethyl sulfonyl)imide (EMIMTFSI), a well-formed ionic fluid electrolyte, and accomplished a capacitance of 70 F g^{-1} alongside an astonishing voltage window of 3 V at a filter rate of 20 mV s^{-1}. After 1000 cycles, the capacitance retention exceeds 80% of the initial value, with the Coulombic efficiency remaining above 95% as shown in Figure 7g. Liang et al.[226] observed that the $Ti_3C_2T_x$ electrode in neat 1-ethly-3-methylimidazolium bis(trifluoromethylsulfonyl)-imide (EMIMTFSI) electrolyte showed higher specific capacitances and cycling stabilities than sterile $Ti_3C_2T_x$ in 1-ethly-3-methylimidazolium bis(trifluoromethylsulfonyl)-imide EMIM-TFSI/ACN electrolyte, as shown in Figure 7h and i, respectively. Preintercalated MXene with an interlayer divide of ≈2.2 nm can provide a huge particular capacitance of 257 F g^{-1} (492 F cm^{-3}) in neat EMIMTFSI electrolyte driving to unmatched energy density. Zheng et al.[275] developed a high-voltage and high-energy adaptable ionogel-based MXene-based miniaturized scale supercapacitor with interdigital micro-electrodes of ionic fluid preintercalated MXene films. Benefiting from the preintercalation of the ionic liquid, the as-fabricated M-MSCs, working at 3 V in 1-ethyl-3-methylimidazolium tetrafluoroborate ($EMIMBF_4$), displayed noteworthy areal and volumetric energy densities of 13.9 μWh cm^{-2} and 43.7 mWh cm^{-3}, respectively. Dall'Agnese et al.[276] employed $Ti_3C_2T_x$MXene anodes in 1 M EMI-TFSI in acetonitrile and achieved a capacitance value of 245 F cm^{-3} at 2 mV s^{-1} with great cyclability and humongous rate capability.

MXenes, two-dimensional materials noted for their metallic conductivity and large surface area, show great potential for high-rate energy storage applications. However, their practical implementation is hindered by poor ionic conductivity.[277] This limitation arises from restricted interlayer spacing, restacking of layers, and hydrophilic surface functional groups that impede ion transport. Structural defects and variations in composition also trap ions, while significant volume changes during ion intercalation can create mechanical stress and disrupt pathways. Furthermore, the compatibility between MXenes and electrolytes can affect ionic mobility.[278,279] Improving the ionic conduction pathways of MXenes, which are promising for high-rate energy storage, involves several cost-effective strategies. Interlayer engineering, such as ion intercalation with larger ions or molecules and mechanical exfoliation, can increase the spacing between MXene layers, enhancing ion transport. Surface functionalization through chemical treatments and surface charge modifications optimizes the electrostatic environment, facilitating better ionic mobility. Forming composites with conductive polymers or inorganic nanomaterials, like polyaniline or metal oxides, can create synergistic effects that improve conductivity.[280,281] Optimizing electrolyte compatibility by using low-cost aqueous or gel electrolytes can also enhance

https://doi.org/10.1021/acsomega.4c04849
ACS Omega 2024, 9, 32350−32393

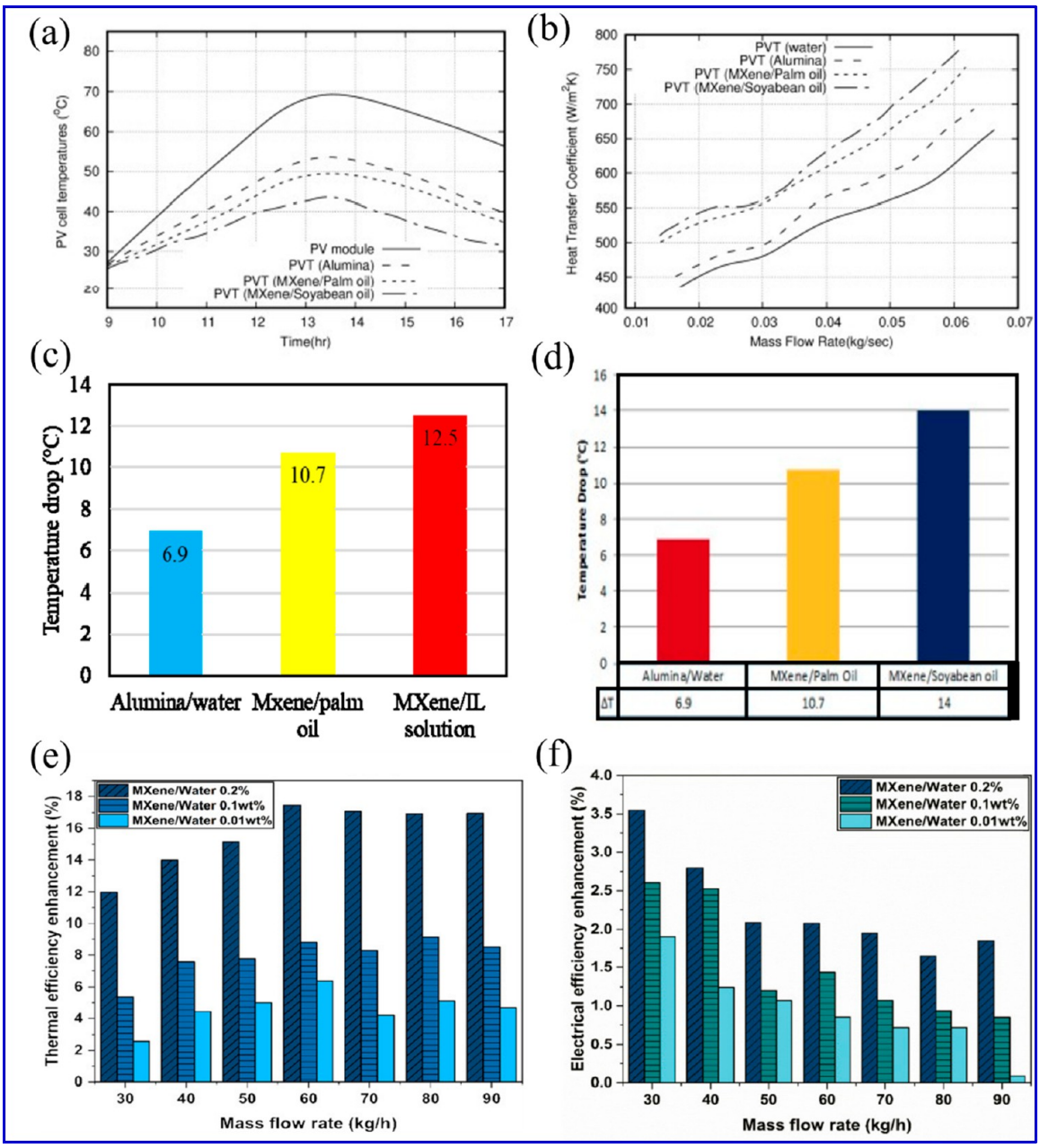

Figure 8. Performance evaluation of a hybrid PV/T collector with different coolant types. (a) PV cell temperature variation with respect to time during the day period at a flow rate of 0.07 kgs^{-1}. (b) Variation in the heat transfer coefficient against varying flow rates at 1000 W/m^2. Temperature drop of the PV panel with different cooling fluids: (c) MXene/IL solution and (d) MXene/soybean oil. (a, b, d) Adapted from ref 286. Copyright 2020 Elsevier. (c) Adapted from ref 289. Copyright 2020 MDPI. (e) Percentage enhancement in the thermal efficiency of a NF-based system over water. (f) Percentage enhancement of the electrical efficiency of a nanofluid-based system over water. Adapted from ref 291. Copyright 2022 Elsevier.

ionic pathways.[282] Additionally, reducing structural defects through controlled synthesis and postsynthesis treatments, such as thermal annealing, can improve ion transport. Techniques like electrophoretic deposition and spray coating enable the creation of well-ordered and minimally restacked MXene films, further enhancing ionic conductivity.[283−285] These strategies collectively offer a cost-effective approach to overcoming the ionic conductivity bottleneck in MXenes, advancing their potential in energy storage applications.

5. MXENE-BASED ENERGY MANAGEMENT SYSTEMS

Energy management systems (EMSs) encompass a broad range of technologies and strategies aimed at optimizing the generation, storage, distribution, and consumption of energy. These systems are characterized by their ability to enhance energy efficiency, reduce operational costs, and integrate renewable energy sources. The significance of EMSs lies in their potential to contribute to sustainable energy practices, mitigate environmental impacts, and improve grid stability and reliability. Incorporating MXenes into EMSs can lead to advancements in energy storage efficiency, enhanced energy conversion processes, and effective thermal management. This integration not only improves the overall performance and reliability of EMSs but also supports the development of more sustainable and resilient energy systems, addressing both present and future energy challenges. The boundary-breaking employ-

https://doi.org/10.1021/acsomega.4c04849
ACS Omega 2024, 9, 32350−32393

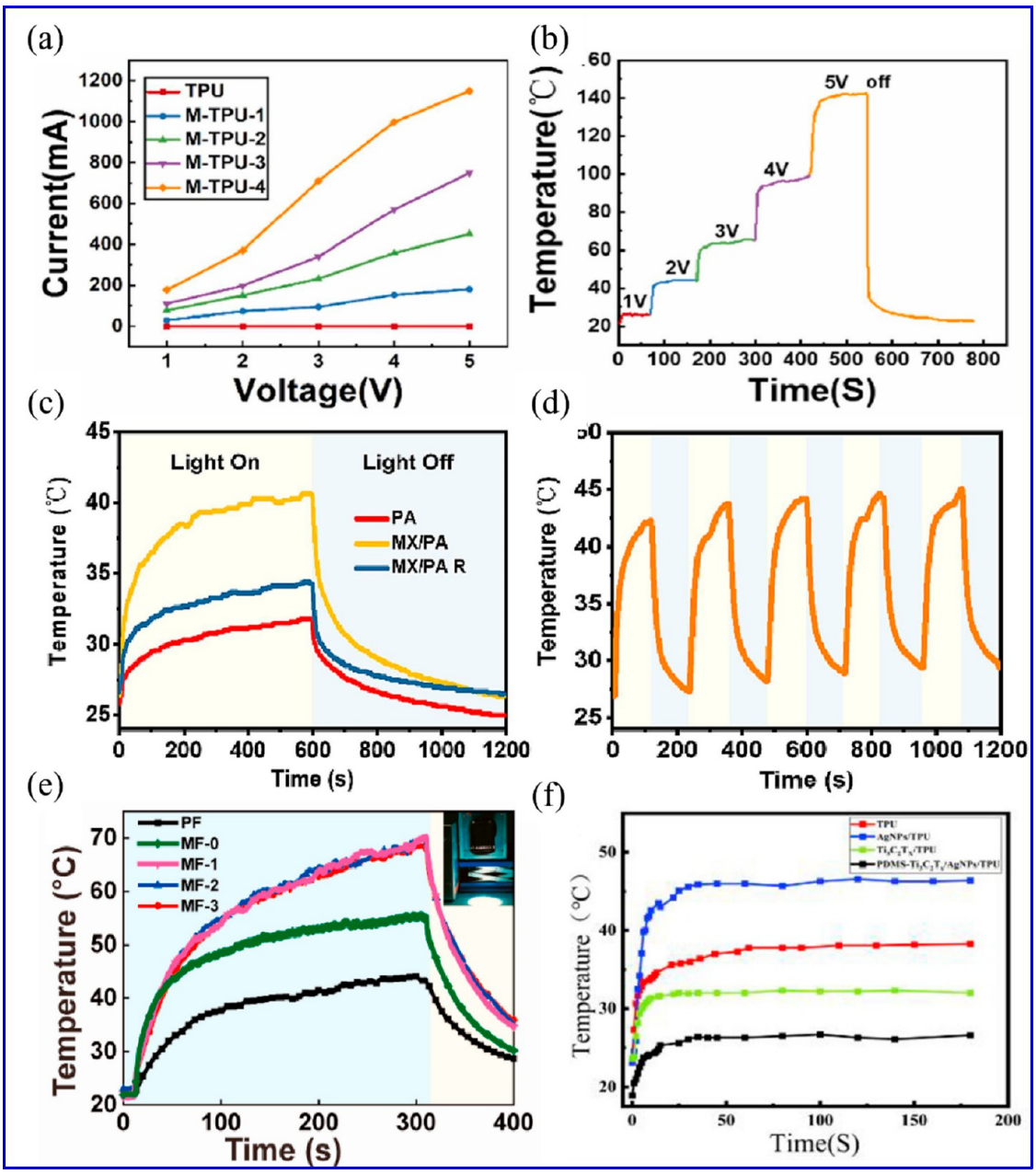

Figure 9. Electrothermal performance of M-TPU. (a) *I*−*V* curves of TPU and M-TPUs. (b) Temperature evolution of M-TPU-4 under gradually increasing voltage input (photothermal heating performances). Adapted from ref 294. Copyright 2023 Elsevier. (c) Cyclic stability of MX/PA photothermal performance. (d) Curves of irradiation time and fabric temperature under different light intensities. Adapted from ref 295. Copyright 2023 Elsevier. (e) Temperature distribution of different fabrics under a xenon lamp with an optical density of 1000 W m^{-2}. Adapted from ref 298. Copyright 2022 Elsevier. (f) Photothermal conversions of TPU, $Ti_3C_2T_x$/TPU, AgNPs/TPU, and PDMS-$Ti_3C_2T_x$/AgNPs/TPUnano fiber membranes. Reproduced from ref 300. Copyright 2022 American Chemical Society.

ment of MXene in numerous energy management applications is discussed in the following section.

5.1. Photovoltaic/Thermal (PV/T) System. A photovoltaic/thermal (PV/T) system is a hybrid system consisting of thermal along with photovoltaic components to ensure maximum use of the heat lost from radiation. In photovoltaic designs, a large amount of heat is wasted in the environment that can be utilized by integrating a thermal management system. Rubbi et al.[286] improved the performance of a hybrid PV/T system after composing a pristine thermally stable nanofluid from MXene (Ti_3C_2) and soybean oil. After using water/alumina as the cooling fluid, they observed increases in both electrical and thermal effectiveness and electrical output by 84.25% and 15.44%, respectively. Their system also boosted the thermal conductivity up to 60.82%, with the improved thermal storage capacity increased to 24.49%. Figure 8a, b, and d shows the performance evaluation of MXene/soybean oil against reducing the cell temperature and improving the heat transfer coefficient. MXene/soybean oil performed well as compared to the alumina-based nanofluid. Similarly, Sreekumar et al.[287] reported the performance of MXene/C.dot to enhance the thermohydraulic performance of a PV/T system, with an enhancement in thermal efficiency to 57.45%, which is 9.45% improved over DI-water. Awis et al.[288] reported the sky-high

https://doi.org/10.1021/acsomega.4c04849
ACS Omega 2024, 9, 32350−32393

thermohydraulic performance of MXene/SO in achieving a thermal efficiency of 31% with a low entropy generation rate when compared to water. Another hybrid PV/T module was designed by Das et al.[289] with a binary solution of MXene dispersed in an ionic liquid. Their experiment consisted of 1,3-dimethyl imidazolium dimethyl phosphate [MMIM][DMP]/MXene as the ionic fluid, which showed excellent electrical and thermal properties with increases 13.95% and 81.15% in the consecutive efficiencies for 0.2 wt %. They also simulated palm oil with MXene and water with alumina nanofluids to compare the performance, but IL with water and MXene exhibited the best results in reducing the PV/T cell temperature, as shown in Figure 8c. Samylingam et al.[290] suspended a chemical formula of Ti_3C_2 in the pure form of olein palm oil via the wet chemistry method and then compared it with an Al_2O_3/water-based nanofluid for PV/T solar thermal storage. In their experiment, the viscosity did not change with the increment in the concentration of nanoparticles; on the other hand, it decreased with a 40% elevation in temperature. In the case of removing heat from the PV/T thermal system, they achieved an 8.5% increase when compared to the alumina nanofluid. A 3D numerical simulation was conducted by Sreekumar et al.[291] where they included a feasibility study with emission cost analysis along with energy−exergy analysis. The results favored a nanofluid-assisted system at a concentration of 0.2 wt %, with 17% thermal and 3.5% electrical efficiency enhancements with a maximum heat transfer coefficient of 261.95 W m^{2-} K^{-1} and a mass flow rate of 90 kg h^{-1}, as illustrated in Figure 8e and f. They proved the possibility of a 4.5−14.5% reduction in size via an optimization study. However, a secondary heat exchanger is required during practical use which affects the cost of the system, and this numerical model was unable to characterize the nanofluid stability. Abdelrazik et al.[292] studied optical performance and stability incorporated with varying concentrations of MXene and surfactants, namely, CTAB and SDBS. Transmittance was conducted with the Rayleigh method, and effects were prominent between the wavelengths of 300−1350 nm. The optical filtration facility concluded that the hybrid system becomes inefficient in terms of electricity above the MXene concentration of 0.05 wt %. Visual observation indicated high concentration degradation after 5 days; for highly concentrated nanoflakes, the CTAB surfactant showed more stability, whereas SDBS was stable for lower concentrations. Silicon oil nanofluid was integrated with Ti_3C_2 by Aslfattahi et al.,[293] and for a 0.1 wt % concentration of silicon oil mixed with MXene they measured the highest thermal conductivity, which was 64%. The viscosity is independent of nanoparticle concentration but affected by temperature, and the mixture showed thermal stability until ∼380 °C due to greater cooling of the system.[293]

5.2. Wearable Light Heaters. Shi et al.[294] contrived a multifunctional heater by depositing MXene on a thermoplastic polyurethane (TPU) fiber membrane. The M-TPU-modified fiber membrane showed good electrical conductivity (IV-curve) and gained more surface temperature than the TPU membrane, as illustrated in Figure 9a and b. The fiber pattern not only stabilizes the conductive pathways through MXene but also ensures good air permeability. Their designed electronics reached 150 °C at a voltage of 5 V and could also observe the movement of humans with a promising joule heating effect, which increases the expectations toward wearable product performance. Lan et al.[295] utilized MXene's dual high photothermal conversion ability and mid-infrared exhalation to radiate heating with Janu fabric. After being coated with MXene, the fabric exhibited a 3.4 °C increment in temperature via the suppression of body radiation loss and 13% photothermal conversion efficiency, which means that the MXene coating on PA enables the system to efficiently convert light to thermal energy, as shown in Figure 9c. During cycle tests under a light intensity of 125 mW cm^{-2}, the temperature distribution remained consistently uniform without degradation. This observation underscores the excellent reproducibility and stability of MX/PA, as depicted in Figure 9d. Due to its one-of-a-kind asymmetric structure, Janus fabric can be used in both the energy and healthcare industries. A heterostructured multifunctional fabric with MoSe2 and MXene was designed by Xie et al.[296] by growing $MoSe_2$ nanoflakes on MXene sheets. Their design was stable even after 1000 cycles and also showed a 230 °C heating response against the supplied 4 V voltage. With 37 dB electromagnetic interference shielding effectiveness, >90% antibacterial performance, and 400 mW cm^{-2} light intensity rate, their MXene-decorated cellulose fabric ensured effective heating therapy. Ye et al.[297] used a coaxial wet-spinning assembly strategy to fabricate the hollow core of a 6 μm thick MXene layer with polyvinylidene fluoride with enhanced interaction due to ammonium hydroxide during coagulation. Electromagnetic wave scattering and lightweight fiber of a hollow structure enhanced the absorption of electromagnetic waves. Great chemical resistance, improved ductility, around 3.08 × 105 S m^{-1} electrical conductivity, 16% elongation at break, and hydrophobicity make these core−shell fibers effectively applicable. Considering fire protection, He et al.[298] mixed viscose fibers that are flame retardant with alginate fibers and coalesced them with MXene. This study introduces successful fabric integration with a spray drying technique, reduced heat release, 55 dB EMI shielding performance, and a novel electro/photoprompted heater. With 2Ω sq^{-1} electrical performance and 123 °C Joule heating performance at 3.5 V, this multifunctional fire-resistant fabric showed superiority regarding safety. The temperature on the surface of the base fabric increased from 20 to 44 °C, while the MXene-modified fabric (MF-0), incorporating just 0.3 wt % MXene, demonstrated a heightened temperature of 55 °C. This suggests that even a minimal addition of MXene can substantially enhance the photothermal performance of the modified fabric, as illustrated in Figure 9e. To address the overheating issue, Wang et al.[299] introduced an MXene-containing nonwoven fabric with the assistance of plasma treatment. An electromagnetic efficiency of 35.7 dB was seen just in one layer of the fire-retardant fabric along with some integrated electrothermal and photothermal properties. With an 18.87 wt % MXene concentration, a TiO_2 flame-barring layer is formed on the surface, and the flexibility and permeability of this modified fabric are enhanced. Li et al.[300] prepared a self-heating device by integrating MXene, Ag nanoparticles, and thermoplastic polyurethane. The photothermal conversion performances of TPU, $Ti_3C_2T_x$/TPU, AgNPs/TPU, and PDMS-$Ti_3C_2T_x$/AgNPs/TPU nanofiber membranes are illustrated in Figure 9f. The PDMS-$Ti_3C_2T_x$/AgNPs/TPU membrane showed great stability and great electromagnetic properties with a 72.7 dB shielding effectiveness and 400−5000 Pa sensing range. With great hydrophobicity and photothermal properties make this membrane suitable for cold and damp environments.

5.3. Solar Water Desalination. The use of MXene for solar desalination technology renders a commendable approach to mitigate the problem of pure drinking water because it has outstanding physicochemical characteristics with higher surface

https://doi.org/10.1021/acsomega.4c04849
ACS Omega 2024, 9, 32350−32393

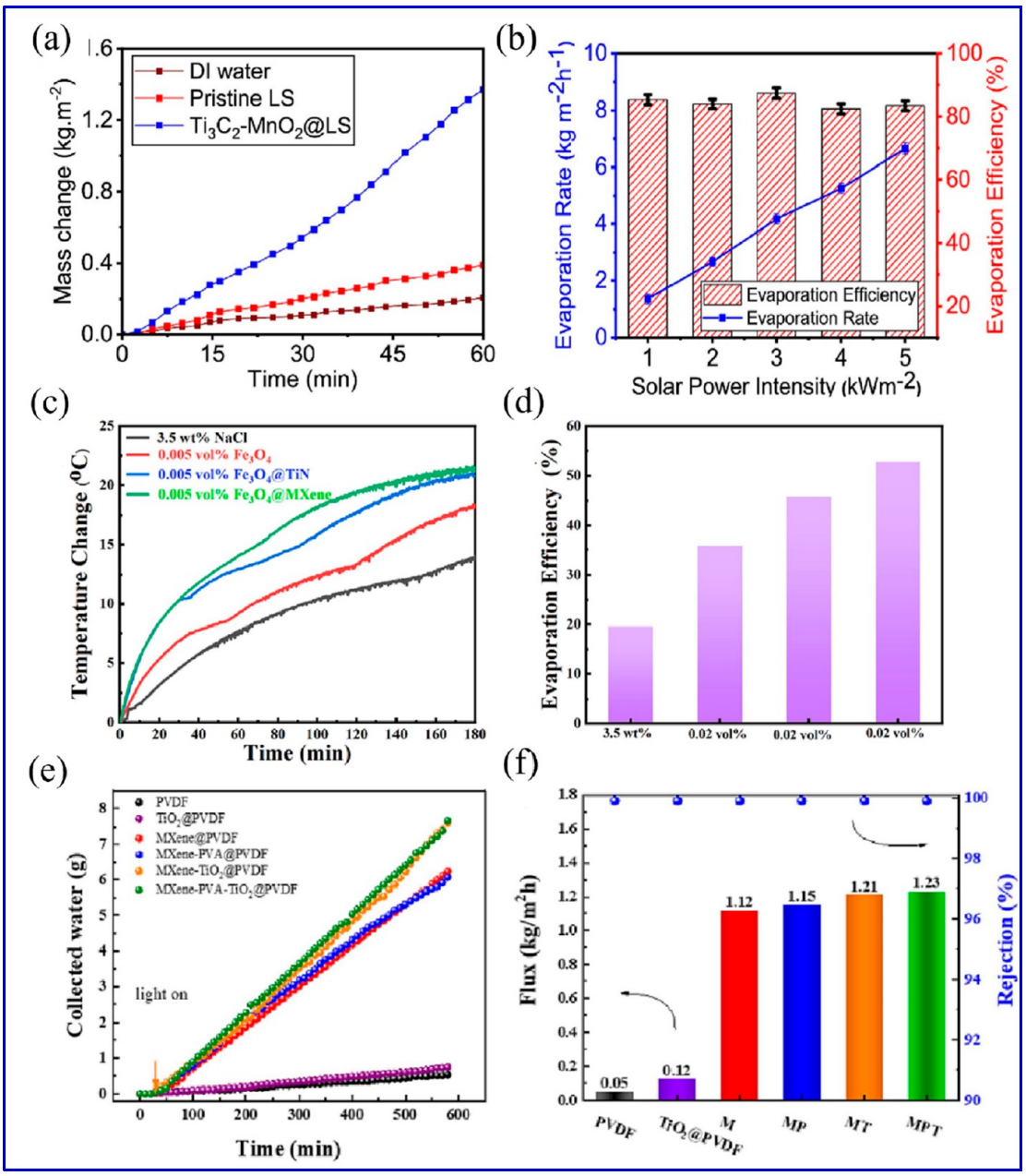

Figure 10. (a) The solar water evaporation mass change over time of the systems with water only, pristine LS, and Ti_3C_2-MnO_2@LS under one sun irradiation. (b) Corresponding evaporation rate (line) and evaporation efficiency (bars) with error bars under varying solar irradiance. Adapted from ref 303. Copyright 2023 Elsevier. (c and d) Temperature increase comparison picture and Evaporation efficiency of Fe_3O_4, Fe_3O_4@TiN solutions, and Fe_3O_4@ MXene. Adapted from ref 304. Copyright 2023 Elsevier. Photothermal properties of the prepared membranes: (e) the surface temperature as a function of time under 1 sun irradiation in air and (f) the surface temperature increase rates. Adapted from ref 305. Copyright 2023 Elsevier.

area and high conductivity. Earlier applications for producing freshwater by utilizing solar energy were conducted through the interfacial solar steam generation system, where different photothermal materials were used at the interface of air or water to absorb the solar energy and afterward transform it into thermal energy. To enhance the evaporation rate and performance for producing an efficient amount of pristine water, the use of MXene with different nanomaterial technologies represents a promising approach toward the solar desalination process.[301,302] Saleque et al.[303] explored the application of a biodegradable solar evaporator, the MXene/MnO_2 luffa sponge (Ti_3C_2-MnO_2@LS), for efficient solar steam generation. They found that Ti_3C_2-MnO_2@LS enhanced the stability and surface area with a significant mass change, exhibiting a high solar evaporation rate and solar steam conversion efficiency of 1.36 kg m^{-2} h^{-1} and 85.28%, respectively, under 1 sun illumination, as shown in Figure 10a and b. Moreover, Ti_3C_2-MnO_2@LS gives excellent water purification performance and superior salt rejection properties under highly concentrated saltwater desalination. Jiang et al.[304] worked on solar direct contact membrane-based distillation using Fe_3O_4@MXene light-absorbing particles to heat the feedwater for membrane desalination by absorbing the sunlight without involving the additional heat. They found that the addition of MXene to Fe_3O_4 increased the rate of water production of direct contact membrane distillation. They found that the temperature of Fe_3O_4@MXene nanofluids

https://doi.org/10.1021/acsomega.4c04849
ACS Omega 2024, 9, 32350−32393

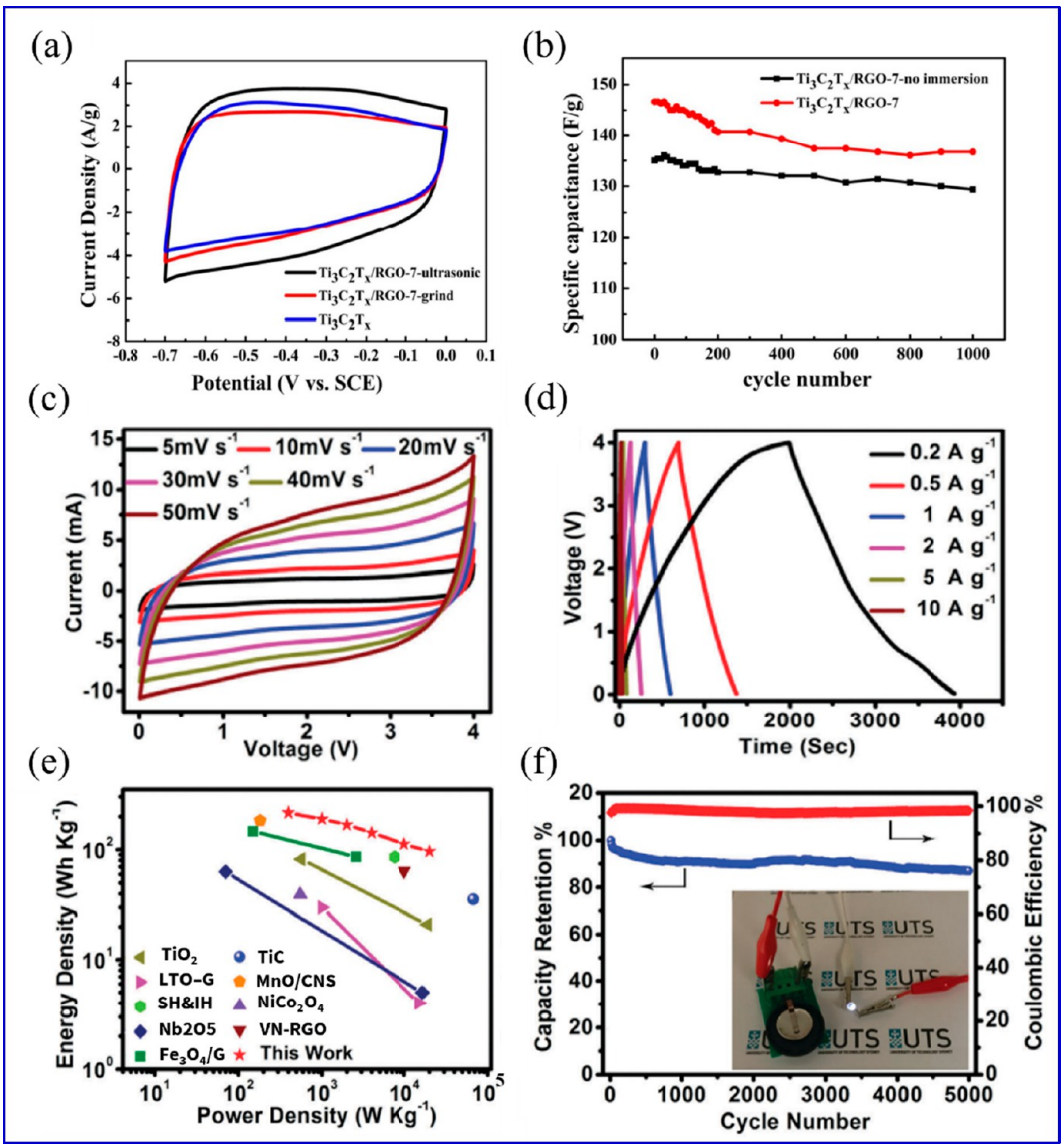

Figure 11. (a) CV curves were obtained for three different electrodes: $Ti_3C_2T_x$/RGO-7, $Ti_3C_2T_x$/RGO-7-grind, and $Ti_3C_2T_x$. (b) Cycling performance of $Ti_3C_2T_x$/RGO-7 and $Ti_3C_2T_x$/RGO-7. Reproduced from ref 312. Copyright 2016 American Chemical Society. (c) CV curves and (d) charge−discharge curves of the $Ti_3C_2T_x$@Fe_2O_3//NS-DPC LIC device. (e) Ragone plots of the $Ti_3C_2T_x$@Fe_2O_3//NS-DPC LIC device and other previously reported devices modified with TiO_2,[315] LTO-G,[316] SH&IH,[317] Nb_2O_5,[318] Fe_3O_4/G,[319] TiC,[320] MnO/CNS,[321] $NiCo_2O_4$,[322] and VN−RGO.[323] (f) Cycling stability of the $Ti_3C_2T_x$@Fe_2O_3//NS-DPC device. Reproduced from ref 313. Copyright 2018 Royal Society of Chemistry.

increased more rapidly than those of the Fe_3O_4@TiN and Fe_3O_4 nanofluids, and Fe_3O_4@MXene NPs used in the direct contact membrane distillation method exhibited a higher water production rate with a flux of 2.26 kg h^{-1} m^{-2} and could be recycled to decrease the material consumption and overall operating cost, as illustrated in Figure 10c and d. Sun et al.[305] used a photothermal catalytic membrane distillation process to desalinate the water by integrating MXene with a PVA-TiO_2@PVDF membrane. They observed that the improved MXene-PVA-TiO_2@PVDF membrane displayed a higher photothermal degradation flux (1.23 kg/m^2h) while maintaining a 99.9% salt rejection rate. Additionally, it exhibited effective photodegradation capabilities, achieving a methylene blue removal rate of over 95% under 1 sun irradiation. Based on the data illustrated in Figure 10e, it is evident that the MXene-PVA-TiO_2@PVDF membrane displays a notably higher solar-to-heat conversion efficiency compared to PVDF and TiO_2@PVDF. When exposed to solar irradiation, the MXene-PVA-TiO_2@PVDF membrane's surface temperature rapidly increased from 27.9 to 74.1 °C within just 300 s. In contrast, PVDF and TiO_2@PVDF membranes showed comparatively moderate temperature increases of 38.1 and 36.2 °C, respectively, attributed to their lower solar-to-heat conversion efficiency. Given the rapid and significant temperature surge observed within the initial 30 s of light exposure, the authors assessed the temperature increase rate, as illustrated in Figure 10f. The MXene-PVA-TiO_2@PVDF membrane displayed the most favorable photothermal properties among the tested membranes, with a temperature increase rate of 1.27 °C s^{-1}. Mu et al.[306] investigated solar-driven evaporation-based desalination by combining MXene polypyrrole with melamine foam (MF-MXene/PPy) through in situ polymerization. They found that MF-MXene/PPy showed high porosity (89.13%) and excellent light absorption capacity (94%) and exhibited excellent performance in solar desalination, water

https://doi.org/10.1021/acsomega.4c04849
ACS Omega 2024, 9, 32350−32393

purification, and photodegradation of dyes. Hao et al.[6] analyzed MXene with Ag incorporation by using a 3D chitosan hydrogel for solar desalination, which exhibited a higher solar energy utilization of almost 94.9% with an efficient evaporation rate of 3.22 kg m^{-2} h^{-1}. The 3D Ag/MXene@chitosan hydrogel nanocomposites work by following the synergistic system where chitosan with Ag/MXene as 3D Ag/MXene@chitosan hydrogel has the ability to eliminate the microbe and ensure the production of fresh drinkable water. The combination of Ag Mxene with a chitosan hydrogel exhibited a high capacity to absorb dye molecules from water in addition to enriched flexibility and chemical stability, which makes this analysis far more promising.

5.4. Supercapacitors. Supercapacitors are popular energy storage devices for their swift discharging−charging, long life cycle, and high energy density. Based on their working mechanism, supercapacitors can be distinguished into two categories: pseudocapacitors (dominated by chemical effects) and electrical double-layer capacitors (dominated by physical effects).[307] The capacitance of MXene-based supercapacitors is mostly dependent on the MXene surface oxidation−reduction process. The capacitance is mostly the result of the surface chemical reaction, as in nonaqueous electrolytes the double layer structure disintegrates due to the distinct potential difference. However, to reduce the effect of the low density of MXene, composites are formed with a pseudocapacitance or electric double-layer property. For layered structures, MXene redeposits ions during cyclic discharging/charging. Pressure resistance and extraordinary tensile properties make MXene suitable for most preparation techniques. MXene is coated on a current collector in a conventional three-electrode system to detect the electrochemical performance.[308] Wen et al.[309] synthesized a novel electrode material by doping MXene with nitrogen. The doped MXene materials, under optimized conditions, showed significantly enhanced electrochemical capacitances. Specifically, they achieved capacitances of 192 F g^{-1} in a 1 M H_2SO_4 electrolyte and 82 Fg^{-1} in a 1 M $MgSO_4$ electrolyte. These values are remarkably higher than those of the undoped $Ti_3C_2T_x$ materials, which exhibited capacitances of 34 F g^{-1} in 1 M H_2SO_4 and 52 F g^{-1} in 1 M $MgSO_4$. Some researchers have introduced two electrode systems, but they obscure the physical properties of MXene-based substances. Rakhi et al.[310] formed electrodes with ε-MnO_2 whiskers on the MXene nanosheet surface for the first time, and they observed a three order magnitude enhancement of the specific capacitance. The ε-MnO_2/MXene supercapacitors, in addition to their enhanced pseudocapacitance, demonstrated outstanding cycling stability. After 10 000 cycles, approximately 88% of the initial specific capacitance was retained. This performance significantly surpasses that of pure ε-MnO_2-based supercapacitors, which retained only around 74% of their initial capacitance. Yang et al.[311] developed a wet-spinning assembly method to fabricate MXene-based fibers continuously. This approach leverages the synergistic effect between graphene oxide liquid crystals and MXene sheets. Specifically, MXene sheets are precisely aligned within graphene oxide liquid crystalline templates, resulting in hybrid fibers. These fibers achieve an impressive MXene mass ratio of 95 w/w %. Notably, the integrated supercapacitor constructed from these fibers exhibits excellent overall electrical conductivity (2.9×10^4 S m^{-1}) and superior volumetric capacitance (586.4 F cm^{-3}). These performance metrics surpass those of neat reduced graphene fibers. Zhao et al.[312] fabricated a $Ti_3C_2T_x$/RGO composite where RGO acted as a conductive bridge and increased the volume during charging and discharging. The 3D hierarchical $Ti_3C_2T_x$@$NiCo_2S_4$−reduced graphene oxide (RGO) heterostructure hydrogel achieved an ultrahigh specific capacitance of 717.1 F g^{-1} at 1 A g^{-1}, surpassing the $Ti_3C_2T_x$−RGO hydrogel (155.5 F g^{-1}) as shown in Figure 11a, and exhibited outstanding capacity retention (124.7 F/g) after 1000 cycles, as depicted in Figure 11b. Tang et al.[313] designed a hybrid capacitor with a 3D nitrogen sulfur dual-doped porous carbon cathode and MXene-wrapped Fe_2O_3 nanosphere anode. Lithium-ion capacitors (LICs) can achieve impressive energy density and power density; Figure 11c demonstrates the cyclic voltammetry curves, suggesting superior capacitive behavior, and Figure 11d reconfirms the good capacitive behavior of the device. Specifically, LICs can demonstrate a high energy density of 216 Wh kg^{-1} at a power density of 400 W kg^{-1}. Additionally, LICs can achieve a high-power density of 20 kW kg^{-1} at an energy density of 96.5 Wh kg^{-1}. This research highlights the feasibility of achieving both high energy density and power density in hybrid lithium-ion capacitors, and a comparison with previous research is shown in Figure 11e. Figure 11f demonstrates the practical application, as the device can successfully power a 2.5 V LED. In some cases, MXene-based special supercapacitors have been designed via electrophoretic deposition, the electrostatic spray method, the substrate loading method, the filtration-peeling method, and the fiberization method. Laser etching, printing, and spray coating methods have been used to generate microsupercapacitors.[270] Using MXene in microsupercapacitors is possible because of the amazing adhesion property of MXene, which facilitates binderless electrode preparation. Additionally, a hybrid capacitor combining an activated carbon cathode and MXene anode has sustained up to 60% overall performance.[308,314]

5.5. Batteries. The battery manufacturing industry has grown significantly, driven by the widespread adoption of lead−acid, lithium-ion, nickel−metal hydride, and nickel−cadmium batteries in global markets. Among these, lithium-ion batteries (LIBs) have emerged as leaders due to their superior efficiency, cost-effectiveness, and continuous innovation. LIBs are expected to dominate future applications because they offer high energy density and competitive pricing. Moreover, the exploration of new battery electrode materials presents substantial opportunities for materials scientists. Recent research has focused on enhancing the performance of LIBs by improving their Coulombic efficiency and cyclic stability. This involves using MXenes to mitigate lithium dendrite growth, a critical challenge in battery technology. Concurrently, the development of MXene-based batteries like lithium−sulfur, aluminum, and zinc-ion types is progressing rapidly, demonstrating ongoing advancements in the field. Different MXene materials, including $Ti_3C_2T_x$, $Mo_2TiC_2T_x$, Nb_2CT_x, V_2CT_x, $Nb_4C_3T_x$, and Mo_2CT_x, have been reported as promising candidates for anodes in lithium-ion batteries (LIBs). When utilized as an anode material by Tang et al.[324] for lithium-ion batteries (LIBs), $Nb_4C_3T_x$ MXene exhibits an impressive reversible specific capacity of 430 mAh g^{-1} at 0.1 A g^{-1}. Notably, this capacity ranks among the highest values achieved for pure-MXene-based anodes. The superior lithium storage performance of $Nb_4C_3T_x$ MXene can be attributed to its high conductivity, rapid Li^+ diffusion kinetics, and robust structural stability. The composite of potassium iron hexacyanoferrate (KFF) and MXene prepared by Jiang et al.[325] demonstrates improved electrochemical reaction kinetics and lithium storage capabilities. The excellent electronic conductivity and layered structure of MXene contribute to these

https://doi.org/10.1021/acsomega.4c04849
ACS Omega 2024, 9, 32350−32393

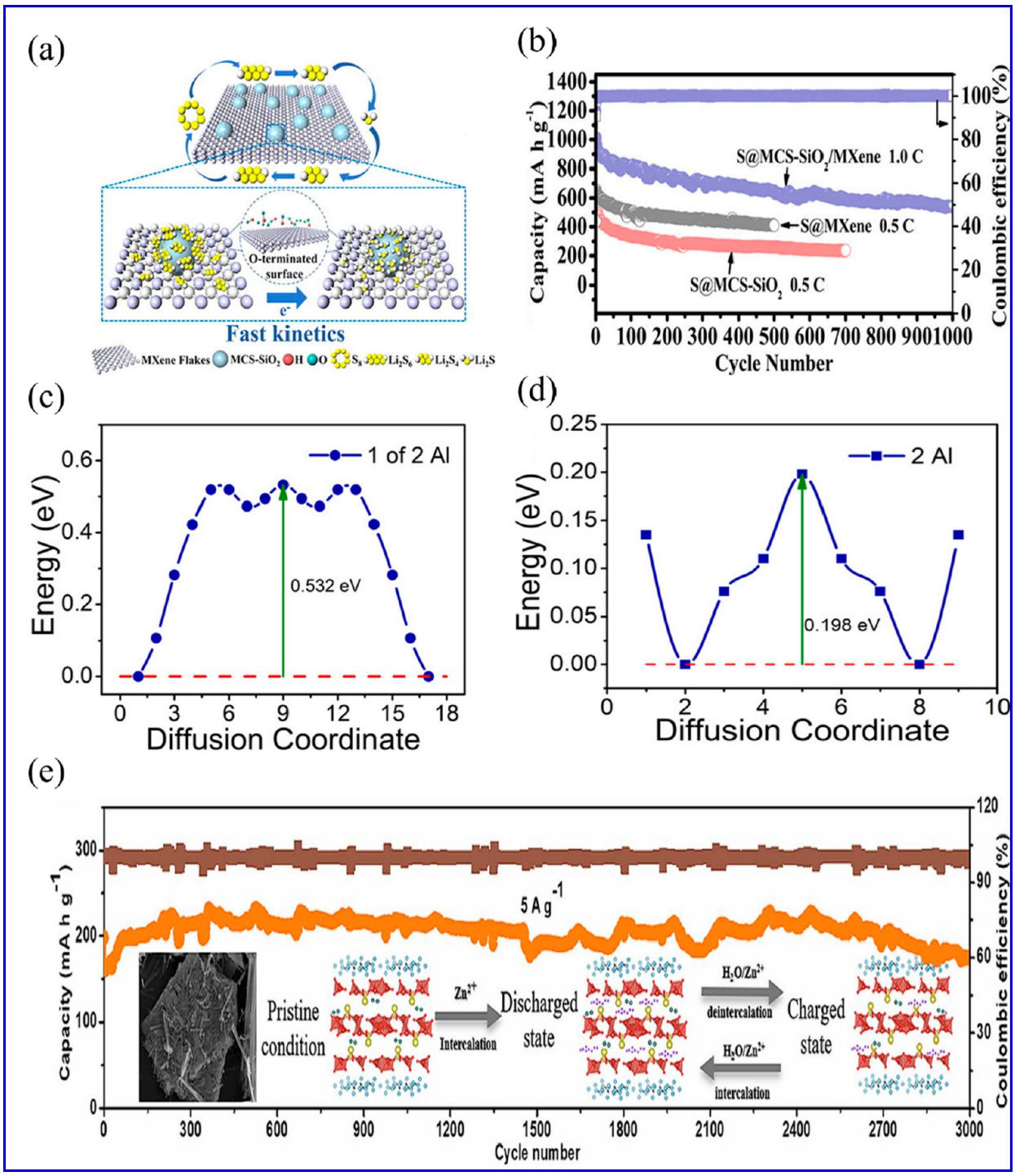

Figure 12. (a) Electrode structure resembling a chessboard. (b) Discharge capacity with 1000 cycles. Reproduced from ref 327. Copyright 2022 American Chemical Society. (c) Diffusion energy profile for A−B−B−A. (d) Diffusion energy profile. Reproduced from 330. Copyright 2020 American Chemical Society. (e) Discharge−capacity with 3000 cycles. Adapted from ref 331. Copyright 2024 Elsevier.

enhancements. Additionally, the stable structure of KFF effectively prevents agglomeration and stacking of the MXene host. As anticipated, the optimized KFF-MXene composite anode achieves a high reversible capacity (approximately 405 mAh g^{-1}), superior rate capacity (133 mAh g^{-1} at 3.2 A g^{-1}), and stable cycling performance over 1000 cycles. Furthermore, researchers have investigated the lithium storage behavior and mechanism of KFF, and Li-ion full batteries (KFF-MXene//$LiFePO_4$) have been assembled to explore practical applications.

Gong et al.[326] considered an alternative sea-urchin-like anode material. The CoP@Ti_3C_2 electrode, benefiting from the excellent electronic conductivity and layered structure of MXene, demonstrated satisfactory cycling and rate performance. Specifically, it exhibited a specific capacity of 420 mAh g^{-1} after 1000 cycles at 1 A g^{-1}. The pore structure formed by MXene reduced accumulation during material preparation, improved conductivity, and allowed adaptation to volume expansion during lithiation/delithiation processes

https://doi.org/10.1021/acsomega.4c04849
ACS Omega 2024, 9, 32350−32393

In the realm of current lithium-ion battery (LIB) technology, lithium−sulfur batteries (LSBs) are emerging as strong contenders for broader commercial adoption due to their exceptionally high specific energy. According to literature sources, LSBs boast a theoretical capacity of 1675 mAh g^{-1} and a specific energy density of 2600 Wh/kg, marking a significant 4-fold increase compared to LIBs. However, their widespread deployment faces notable challenges, including sulfur's low electrical conductivity and the migration of soluble polysulfides ($Li_2S_4^{-8}$) across the separator during charge and discharge cycles, known as the "shuttle effect". Zhao et al.[327] proposed a novel electrode structure resembling a chessboard (Figure 12a) to address lithium−sulfur (Li−S) battery challenges. In this design, MXene nanosheets act as "chessboards", providing a conducive framework for rapid conversion of polysulfides to Li_2S. Meanwhile, sulfur-loaded mesoporous carbon nanospheres (S@MCS-SiO_2) serve as "chesspieces", confining and adsorbing polysulfides. Experimental results demonstrate uniform Li_2S precipitation with high capacity and highly reversible solid−liquid/liquid−solid phase reactions. The S@MCS-SiO_2/MXene electrode exhibits excellent electrochemical performance, including an initial discharge specific capacity of 1303.6 mA h g^{-1} at 0.1 C and minimal capacity attenuation (0.046%) over 1000 cycles at 1 C (Figure 12b).

Aluminum batteries (ALBs) are a promising option for energy storage due to aluminum's superior safety and cost-effectiveness compared to lithium. However, they encounter challenges related to the high charge density of Al^{3+} cations and their strong interactions with the host lattice, which impact cyclic stability. Additionally, the narrow potential window restricts the achievable energy density in ALBs. Aluminum-based batteries have garnered significant interest due to their compelling advantages, including cost-effectiveness, high energy density, and safety performance compared to other metal-based batteries. Specifically, the Ti_3C_2@CTAB-Se electrode, prepared by Li et al.,[328] demonstrates a reversible discharge specific capacity of 583.7 mAh g^{-1} at 100 mA g^{-1}, and even after 400 cycles its capacity remains at 132.6 mAh g^{-1}. Furthermore, Ti_3C_2@CTAB-Se exhibits superior voltage and capacity characteristics when compared to graphite-based, oxide, and sulfide electrode materials in both aluminum-based and other battery cathodes. Du et al.[329] designed a heterostructured g-C_3N_4/$Ti_3C_2T_x$ hybrid to address the long-standing challenges of aluminum's storage capacity and rate. This hybrid structure provides a conductive framework that maintains structural integrity and accelerates electron transport. During cycling, the energy storage mechanism involves reversible intercalation. DFT calculations confirm that the heterostructured g-C_3N_4/$Ti_3C_2T_x$ possesses enhanced electrical conductivity and an aluminum trapping capability. Consequently, the heterostructured g-C_3N_4/$Ti_3C_2T_x$ cathode exhibits excellent aluminum-storage properties, reaching 237 mAh g^{-1} at 0.5 A g^{-1}, and considerable rate capability (174 mAh g^{-1} at 4 A g^{-1}). These results position it among state-of-the-art cathode materials for aluminum batteries. Liu et al.[330] designed a heterostructured g-C_3N_4/$Ti_3C_2T_x$ hybrid to address the long-standing challenge of aluminum storage capacity and rate. This hybrid structure provides a conductive framework that maintains structural integrity and accelerates electron transport. Figure 12c shows the calculated diffusion energy profile, where the obtained migration energy barrier is about 0.532 eV, and Figure 12d demonstrates the predicted the migration energy profile. Additionally, the battery capacitance model mechanism in these hybrids may enhance the kinetics of electrode reactions.

In addition to the conventional battery types noted earlier, rechargeable zinc-ion batteries (ZIBs) are also a battery technology that has garnered significant attention. When used by Sun et al.[331] as the cathode material for aqueous zinc-ion batteries (AZIBs), NVO@MXene exhibits a remarkable rate capability and excellent reversible capacity. After 3000 cycles (Figure 12e) at 5 A g^{-1}, it retains 88.9% of its initial discharge capacity (175 mAh g^{-1}). The outstanding performance is attributed to MXene layers with high conductivity, which accelerate ion diffusion and reduce the agglomeration of $Na_2V_6O_{16}\cdot 3H_2O$ nanowires during charge and discharge. Additionally, the stable layered structure of $Na_{16}V_6O_6\cdot 3H_2O$, with wide interlamellar spacing (d = 7.9 Å), facilitates fast Zn^{2+} intercalation/deintercalation. Mao et al.[332] developed a novel 3D interconnected heterostructure material composed of VS_2 nanosheets uniformly distributed on the surface of V_4C_3 MXene. The $VS_2\perp V_4C_3T_x$ cathode demonstrates a high specific capacity of 273.9 mAh g^{-1} at 1 A g^{-1}. It also exhibits an excellent rate capability, reaching 143.2 mAh g^{-1} at 20 A g^{-1}. V_4C_3 MXene, when used as a protective layer for the Zn anode, effectively suppresses zinc dendrite growth. The resulting $V_4C_3T_x$@Zn symmetric cell maintains a stable voltage profile for approximately 1700 h.

To summarize, MXenes have been reported as superior candidates for utilization in battery application systems, but the low specific gravimetric capacity, heterostructure blending, and interlayer spacing enlargement have been explored to improve the electrochemical properties of MXene. When pure MXene is used in Li-ion batteries, it is necessary to create an active electrode composite-based material due to easy oxidation, insufficient performance of electrochemical properties, and restack tendency.[333] Composites created with CNTs, MOFs, graphene, and Ag can improve ion and electric conductivity.[209,334] Doping MXene with nonmetallic elements can also increase conductivity. In the context of Li−S batteries, addressing issues related to the dissolution of lithium polysulfides (LiPSs) and the shuttle effect is crucial. MXene-based composite cathode materials with hydrophilic surfaces effectively restrict LiPSs and result in impressive cycling performance. In the case of MXene-based sodium-ion batteries, the reaction between Ti_3C_2 and sodium ions results in the formation of Ti_3C_2NaX, demonstrating a notable reversible capacity. To prevent MXene restacking during cycling, interlayers like CNTs can be employed. Besides lithium and sodium ions, MXene layers can accommodate potassium, magnesium, and aluminum ions. Consequently, MXene-based materials have potential applications in hybrid batteries such as potassium (K^+), magnesium (Mg^{2+}), aluminum (Al^{3+}), and zinc (Zn^+) cells. MXene composites have shown outstanding electrocatalytic activity when applied in metal−air batteries. The performance is stronger when a transition metal is used in the MXene-based composite.

6. ECONOMIC ASSESSMENT OF MXENE FOR ENERGY MANAGEMENT SYSTEMS

The first step involves selecting MXene preparation method, which could be HF etching, fluoride-free etching, or any other variation of this process. The company is noticing specific indicators, for example, expenses on raw materials, personnel, and the cost of cutting. The adequacy of raw materials is evaluated via their prices in the market, reviewing if supply can

https://doi.org/10.1021/acsomega.4c04849
ACS Omega 2024, 9, 32350−32393

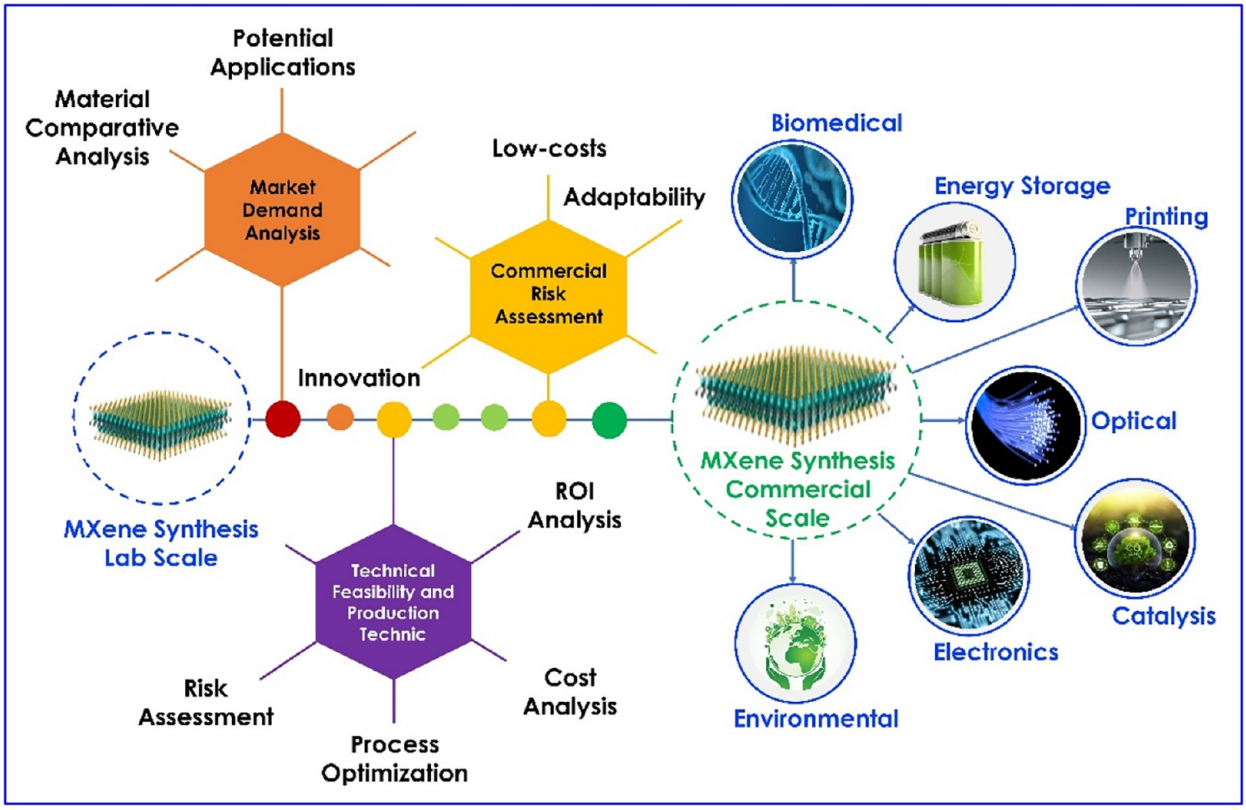

Figure 13. Economic assessment of MXene from synthesis to commercialization.

be stable with reasonable fluctuations in prices and considering the energy consumption patterns during synthesis. Scalability is also an important factor in ensuring the process is an endless source of high-quality products.[335] Monitoring the ecological footprint of MXene manufacturing processes through emissions assessments, waste generation assessments, and adherence to standards is the key activity of environmental impact assessments.[336] Market analysis includes an analysis of the demand for MXenes in various applications, seeking to comprehend and project their present demand as well as future demand. Market power, or attaining advantages in comparison with rivals, is treated as an image that boosts competitiveness. Figure 13 shows the competitive market analysis for the synthesis of MXenes on lab scale, along with the feasibility of each production method as per market demand. Through sensitivity analysis, relationships between the model and the parameters are examined. This allows us to know what the reaction might be in an event where an external change occurs due to key factors. Risk assessments discover prospective problems in regulations, market conditions, and doubtful technologies.[337] The financial modeling process is always the most crucial part of the business plan through conducting cash flow projections and ROI management and estimate the repayment period. In the comparison of studies conducted on materials and production processes, the only reason for these studies is either validity or further advancement. Transparent communication of economic viability as well as hardships that are specific to mass-scale MXene manufacture is fundamentally being discussed by people interested in MXenes: stakeholders, investors, and researchers. The bullet point of a detailed TEA methodology for commercial-sized MXene manufacturing is aimed at enhancing the decision-making, strategic planning, and sustainability of a plant.[338]

6.1. Market Demand Analysis. The huge appetite for MXene materials for the market is supported by their prized combination of properties, which adapt themselves to meet the highly demanding industrial needs. MXene takes the lead with excellent electrical conductivity, meaning that MXene is the prime material for energy management as it boosts the performance of batteries and supercapacitors.[339] A wide range of applications, including catalysis and energy conversion, gain more power from fuel cells and electrolyzers.[340] The MXene surface demonstrates these advantages that raise efficiency. It is unique because its chemical surface can be changed to suit specialized needs for biomedical, electronic, and other applications.[341] Beyond being an exceptional material in terms of mechanical, electrical, and thermal applications, MXene is also a promising candidate for use in the therapeutic and diagnostic markets. Also on the list of its features is its versatility, as seen in its use in water purification, sensors, and flexible electronics.[342]

In time, research and development processes have shown that MXene is competent for a wide range of applications. At the same time, the collaboration and industry connections speed up its entry into the market. Demand for MXene is not only dictated by its application in other technologies but also largely affected by the potential of MXene to be a significant contributor to the world's desire for sustainable technology. This makes MXene a godsend for advanced material manufacturers. It is a clear indicator of its utmost importance in the current markets. MXenes can be used successfully in many different areas, being very powerful, for example, for pressing global issues. The water purification field has benefited from the MXenes' property of excess surface area, along with their ability to tune both the surface chemistry and the proximity of contaminants like heavy metals, organic pollutants, and so on. Water filtration

https://doi.org/10.1021/acsomega.4c04849
ACS Omega 2024, 9, 32350−32393

membranes create solutions to both the problem of wastewater treatment and the issue of water safety in water-poor areas. Extensive research conducted on MXenes has put them in a position to be the key players in storing and converting energy and contributing to devices such as batteries, supercapacitors, and solar cells.[343]

The remarkable electrochemical properties of MXenes as conductors, space-expanders, and capacitors to store ions are what make them good choices for high-energy management systems. MXene technology not only contributes to energy management efficiency but also helps reduce costs.[344] Thus, technology plays a significant role in advancing an affordable clean energy solution that aligns with the global trend of sustainability. In smart cities and human settlements, MXenes show their worth in inclusive, secure, resilient, and sustainable parameters, which are the results of smart sensor and device applications. These materials play a role in building sensory mechanisms for assessing environmental pollution, constructing smart buildings, and monitoring energy consumption. As a result, they are beneficial to the development of modern smart, sustainable cities. Energy efficiency is also enhanced with MXene-based building materials for the construction industry, which leads to the adoption of sustainable practices in building designs. Specially, MXene materials pave the way to face the critical challenge of combating climate change by improving the efficiency of renewable energy systems such as fuel cells and electrolyzers with special catalysts based on MXene nanomaterials.

6.2. Technical Feasibility and Production Techniques. It should be noted that the LiF-HCl technique has developed as a highly scalable method for the synthesis of MXenes for production in milligram quantities for industrial large-scale manufacturing based on numerous factors. The main advantage is accessibility due to its popular procedure, which is straightforward and thus more acceptable than the HF method.[345]

This puts us at a vantage point to strategically deal with the cost, especially when we must generate high quantities of MXene. Nevertheless, synthesis may face the challenge of obtaining and managing huge quantities of the precursor materials, making sure that every batch is of consistent quality, and eliminating waste disposals, mainly byproducts. To guarantee the financial return and stability of MXene production on an industrial scale, the solution to process engineering and automation, and quality control is the core question,[346] with the highest possible purity and quality as stipulated by the specific industry standards. It is of paramount importance to maintain the supply of reliable suppliers for raw materials through effective waste management systems and continuous improvements in the method of synthesis to provide production with guaranteed high-quality output at a low cost. Investments in partnering with top universities for the transfer of research knowledge and training of human resources are fundamental to the commercialization of the MXene synthesis process.[347] This encompasses lean system management, automatic control technology, and environmentally friendly projects. The allocation of funds to research and development activities pursuing both process efficiency and standard observance in the constantly evolving industry can be guaranteed. Overall, the comprehensible and sustainable industrialization of MXene synthesis technology is a trend that demands integrated consideration of cooperative links, meticulous quality control, and ongoing research and development works.

6.3. Commercial Risk Assessment. Interestingly, there are some compounds that MXene comes from that also present risks, like the introduction of industry regulations and market changes that could affect the time and costs associated with production, among other things. Environmental standards, safety procedures, or precursor material regulations may be altered, and the processes shall therefore be pulled back, as it may increase costs of time and establish delays in timelines.[348] The raw material costs are counterbalanced by the price fluctuations used in MAX and MXene. This principle could directly influence the overall production costs. An appearance in the market of materials that are competitive or sophisticated technologies may become a threat to MXene demand, which will in turn put their profitability in jeopardy. The technological uncertainties, for instance, the technical limitations of carrying out new formation methods or the availability of materials for MXene in the market with comparable or better properties, can hinder its position in the market and demand. Challenges such as the sourcing of precursors, along with supply chain complications, pose potential limitations on manufacturing scale-up, whereas uncertainty regarding legal IP matters representing intellectual property rights and patents might affect the companies' competitiveness and market access.[349] To efficiently mitigate such power generation risks, vertical platforms must guarantee different sources of energy precursors, different production strategies, and scenario planning. Partnering with regulatory agencies, constantly monitoring the markets, and making sure that manufacturing technologies are primary in the research and development of MXenes are some of the essential ways that will help a business stay one step ahead and not risk producing in mass.[350] The easy adaptability of flexible synthetic procedures that can comply with regulatory changes, whether they are increasing or decreasing, gives a nice position to this regulatory framework. Process efficiency enhancement, energy-saving improvements, and new ways of getting rid of waste create operational expenditures and environmentally friendly outcomes, as they are in line with the norms in the field of environmental management.

Depicting a risk management strategy that works in varying markets requires scenario exercises and identifying support measures. A purposeful intellectual property protection system is reflective of the active maintenance of patents and licensing.[351] This multifaceted risk prevention measure shields the inventor from legal and intellectual property rights risks that can impair market access. Hence, success in risk adaptation is dependent on a holistic approach encompassing agility, supply chain resilience, incurring low costs, innovation, and being responsive to market dynamics, which should be ensured to pave the way for the successful and more enhanced production of MXene at a large scale.[352]

6.4. Cost Analysis. Cost is one of the major challenges for MXenes. To minimize the cost, there are a few ways already published in different journals. The cost of MXene depends on precursors, processes, and characterization techniques.[19] This research group shows the method of how to perform the cost analysis and where focus is required reduce the cost of the materials. One of the research groups expresses a way to reduce the cost (e.g., introducing recycled materials, extracting precursors from nature, and process optimization).[42] One of the ways to reduce cost is to introduce recycled materials for the synthesis of MXene. One of the research groups extracts carbon from tires and Ti from TiO_2 (nature-based) for the synthesis of MXene.[353] Another research group synthesizes MXene using car

https://doi.org/10.1021/acsomega.4c04849
ACS Omega 2024, 9, 32350−32393

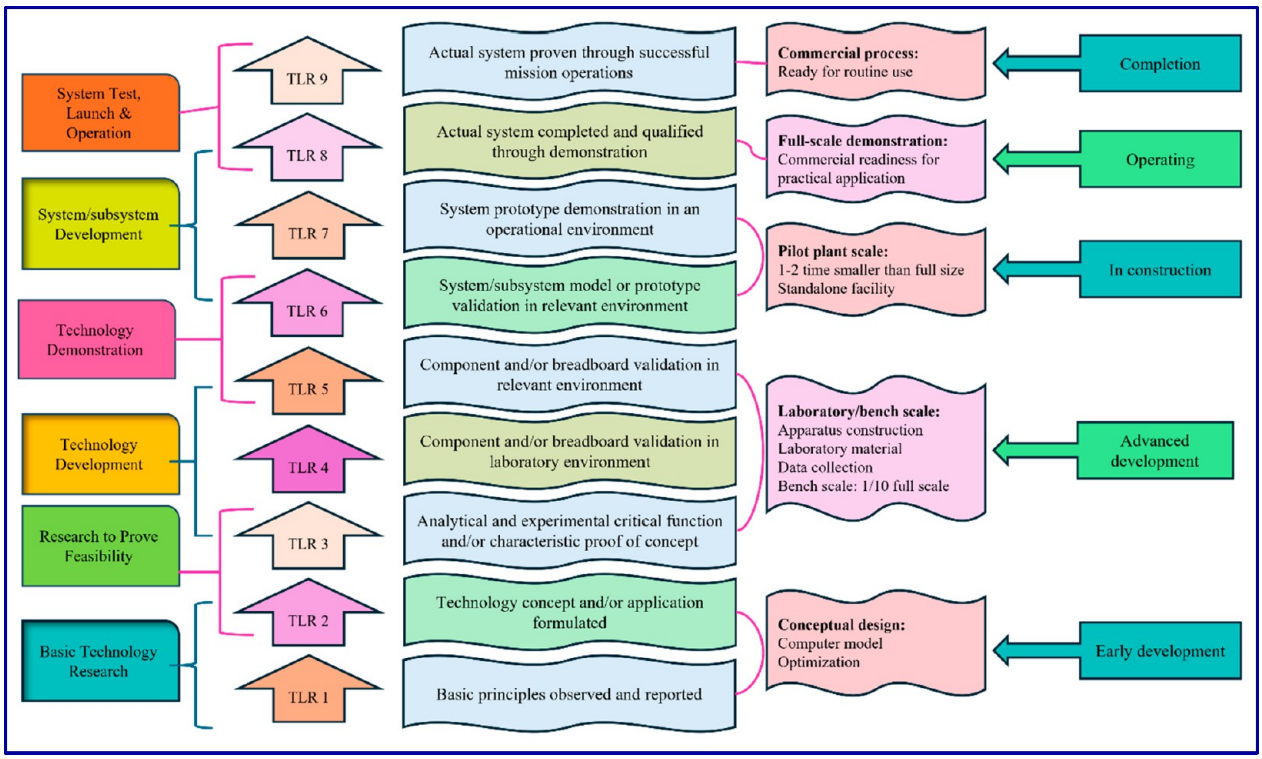

Figure 14. Description of technology readiness levels. Produced from ref 357. Copyright U.S. Department of Energy 2018.

exhaust and applies this MXene for desalination applications.[354] Another important point is to know the lifecycle analysis of the materials. Firouzjaei and colleagues are applying MXene materials for EMI shielding in communication satellites, and they also discuss the environmental impact of $Ti_3C_2T_x$ MXene production and the cumulative energy demand of $Ti_3C_2T_x$ MXene production.[81]

6.5. Technology Readiness of Level of MXene-Based Research. After the invention of MXenes at Drexel Laboratories in 2011,[25] researchers have discovered more than 50 MXene compositions. Computers have predicted thousands more, and around 70 000 researchers from over 100 countries are studying MXenes. Scientific symposia and journals with special issues have been dedicated by research organizations to explore these materials. The impressive and diverse list of potential applications identified by researchers includes long-lasting batteries, desalination, thermal energy management, wearable heaters, green hydrogen production, and kidney dialysis.[355] Nearly 15 years after their discovery, MXenes are on the brink of a commercial breakthrough. Tech giants such as Samsung and Intel have obtained MXene-related patents. The Japanese electronic component manufacturer Murata Manufacturing plans to launch an MXene-based product in the near future.[356] These pioneering commercial products will determine the future of the materials. "The only bottleneck now is to find the killer application that requires tons of the material" https://drexel.edu/engineering/research-design/centers-institutes-labs/drexel-nanomaterials-institute/research/energy-applications/.

However, it is rare for newly discovered materials to hit the market in just a few years. Global initiatives have supported early innovation, helping to advance these materials through the Technology Readiness Level (TRL) ladder. TRL is a nine-point scale defined by the U.S. Government Accountability Office (US GAO) to measure a technology's maturity, as shown in Figure 14.[357] Higher TRL levels indicate closer proximity to commercialization. Typically, new technology must reach TRL 8 or 9 to be considered mature and ready for practical implementation. Introducing unproven technologies prematurely can result in delays and budget overruns, whereas projects that incorporate mature technologies tend to stay on schedule and within budget.

The evaluation of MXene technology indicates that it is currently at MCLR-4 (laboratory validation), suggesting it is on the brink of transitioning from laboratory scale to manufacturing environments. This progression points to the near-future mainstream adoption of MXene for a wide range of applications, including energy management, desalination, separation/purification, friction stir additive manufacturing (FSAM), etc.

7. CONCLUSION AND FUTURE RECOMMENDATION

Energy management is gaining importance with the fast depletion of fossil fuels and the intermittent nature of renewable energy resources. MXene, due to its outstanding properties and stability, holds revolutionary power, especially in energy management systems. The current Review aims to provide details discussion of various strategies used for the synthesis of MXene through linking their properties, stabilization, economic assessment, and energy management applications. Although MXenes have been reported through widespread synthesis routes in recent years and have revolutionized the energy sectors, researchers still continue to explore novel methods, etchants, low-cost precursors, and surface modification strategies to enhance properties and stabilization in more sustainable ways. However, there are still unresolved issues and challenges that must be addressed by researchers in the future, which could be handled through potential pathways given below.

https://doi.org/10.1021/acsomega.4c04849
ACS Omega 2024, 9, 32350−32393

(i) The synthesis route for MXene necessitates secure synthesis aimed at achieving efficient, cost-effective, high-quality, and reproducible production of MXene. Research should focus on optimizing existing synthesis techniques and exploring new methods to produce high-quality MXenes with controlled properties. Greener chemical routes need to be explored to avoid environmental and health risks. Mixed acid etching became popular due to the removal of etching byproducts. The focus on mixed etching of MXene could lead to new gateways of research for optimizing acid-based etching to make it less toxic, prevent equipment corrosion, limit surface contamination, and reduce chemical burns and inhalation risks due to high concentrations of the acidic etchant.

(ii) To fully exploit the potential of MXenes, a deeper understanding of their surface chemistry and functionalization is essential. Investigating the interactions between MXenes and various chemical groups can facilitate the development of novel functional materials with tailored properties for specific applications. Employing MXene as a metal precursor with ligands to synthesize MXene-derived metal−organic frameworks (MX-MOFs) and MXene with ionic liquid through ionanomaterials (INMs) could be an effective integration strategy for its further utilization in a wide range of boundary-breaking applications.

(iii) The synthesis of MXenes using low-cost precursors is crucial for their bulk synthesis and commercialization. Economically viable production methods facilitate scalable manufacturing, ensuring that MXenes can meet market demands while remaining cost-effective. This approach enhances the economic feasibility of MXene-based technologies and promotes sustainability by reducing reliance on scarce and expensive raw materials. Ultimately, the ability to produce high-quality MXenes at a reduced cost will drive innovation, expand their industrial and research applications, and provide a competitive advantage, accelerating the integration of MXenes into various advanced technological sectors.

(iv) MXene has recently attracted considerable interest in the research community and is currently at the laboratory validation stage (TRL-4). Soon MXene will come under the project consortium, which includes European manufacturers and semiconductor fabrication lines and plans to establish an industrially compatible infrastructure to scale up the production of 2D devices. These devices are expected to achieve Technology Readiness Levels (TRLs) 7−8, indicating fully operational system prototypes in their intended environments. However, the boundary-breaking career of MXene could be the point of future investigations as a reinforcement to enhance the properties of alloy composites through FSAM with improved process parameters.

Based on the above recommendations, it is suggested that further investigation on MXene-based research is still required to make their commercialization straightforward for energy management applications.

■ ASSOCIATED CONTENT

Supporting Information

The Supporting Information is available free of charge at https://pubs.acs.org/doi/10.1021/acsomega.4c04849.

Reported chemically ordered MXenes with three different general formulas: M_2X, M_3X_2, and M_4X_3, where M is an early transition metal and X is carbon and/or nitrogen (PDF)

■ AUTHOR INFORMATION

Corresponding Authors

Khairul Habib − *Department of Mechanical Engineering, Universiti Teknologi PETRONAS, 32610 Bandar Seri Iskandar, Perak Darul Ridzuan, Malaysia*; Email: khairul.habib@utp.edu.my

Syed Awais Ali − *Department of Mechanical Engineering, Universiti Teknologi PETRONAS, 32610 Bandar Seri Iskandar, Perak Darul Ridzuan, Malaysia*; orcid.org/0000-0001-5284-3518; Email: awaissyed480@gmail.com, SYED_22009995@utp.edu.my

Authors

Mumtahina Mim − *Department of Mechanical Engineering, Universiti Teknologi PETRONAS, 32610 Bandar Seri Iskandar, Perak Darul Ridzuan, Malaysia*

Sazratul Nayeem Farabi − *Department of Mechanical Engineering, Universiti Teknologi PETRONAS, 32610 Bandar Seri Iskandar, Perak Darul Ridzuan, Malaysia*

Md Abu Zaed − *Research Centre for Nanomaterials and Energy Technology (RCNMET), School of Engineering and Technology, Sunway University, 47500 Petaling Jaya, Selangor, Malaysia*

Mohammad Younas − *Department of Chemical Engineering, Faculty of Mechanical, Chemical and Industrial Engineering, University of Engineering and Technology, 25120 Peshawar, Pakistan; CAS Key Laboratory of Urban Pollutant Conversion, Institute of Urban Environment, Chinese Academy of Sciences, Xiamen, Fujian 361021, China*; orcid.org/0000-0003-3234-3297

Saidur Rahman − *Research Centre for Nanomaterials and Energy Technology (RCNMET), School of Engineering and Technology, Sunway University, 47500 Petaling Jaya, Selangor, Malaysia; School of Engineering, Lancaster University, Lancaster LA1 4YW, U.K.*

Complete contact information is available at: https://pubs.acs.org/10.1021/acsomega.4c04849

Author Contributions

M.M.: writing original draft, data curation. K.H.: Formal analysis and review. S.N.F.: writing, review and editing. S.A.A.: conceptualization, writing review and editing. M.A.Z.: writing review and editing. M.Y.: writing review and editing. S.R.: Formal analysis and review

Notes

The authors declare no competing financial interest.

■ ACKNOWLEDGMENTS

This research was funded by Yayasan Universiti Teknologi Petronas (YUTP) Grants 015LC0-520 and 015LC0-532.

NOMENCLATURE

CAN	Acetonitrile
Ag	Silver
Al	Aluminum
ALB	Aluminum Battery
$AlCl_3$	Aluminum Chloride
Al_4C_3	Aluminum Carbide
AlF_3	Aluminum Fluoride
Al_2O_3	Alumina
$Al(OH)_3$	Aluminum Hydroxide
AlO(OH)	Aluminum Hydroxide Oxide
$Al(OH)_4$	Aluminate
As	Arsenic
AZIB	Aqueous Zinc Ion Battery
C	Carbon
Cd	Cadmium
CDC	Carbide Derived Carbon
CdS	Cadmium Sulfide
CH_4	Methane
CH_3OH	Methanol
Cl	Chlorine
CMT	Cobalt−Manganese Organic Framework
CO	Carbon Monoxide
CO_2	Carbon Dioxide
COE	Cost of Electricity
Cr	Chromium
Cr_2C	MXene
CNTs	Carbon Nanotubes
CTAB	Cetrimonium Bromide
CT	Computed Tomography
CDC	Carbide-Derived carbon
DFT	Density Functional Theory
F	Florine
Fe_3O_4	Iron(II) Oxide
FSAM	Friction Stir Additive Manufacturing
FSPCM	Form Stable Phase Change Materials
Ga	Gallium
GAO	Government Accountability Manufacturing
Ge	Germanium
H_2	Hydrogen
HCl	Hydrochloric Acid
HCOOH	Formic Acid
HER	Hydrogen Evolution Reaction
Hf	Hafnium
HF	Hydrofluoric Acid
Hf_2CO_2	MXene
H_2O	Water
IL	Ionic Liquid
In	Indium
KCl	Potassium Chloride
KF	Potassium Fluoride
KOH	Potassium Hydroxide
Li	Lithium
LIB	Lithium Ion Battery
LIC	Lithium Ion Capacitor
LiCl	Lithium Chloride
Lif	Lithium Fluoride
LSF	Lithium Sulfur Battery
[MMIM][DMP]	*N*-Methyl-*N*-methylimidazolium Dimethyl Phosphate
Mo	Molybdenum
MoN_2	Molybdenum Nitride
$MoTi_2C_3$	MXene
MRI	Magnetic Resonance Imaging
N	Nitrogen
NaCl	Sodium Chloride
NaOH	Sodium Hydroxide
Nb	Niobium
Nb_2CT_x	MXene
$Nb_{1.33}CT_x$	MXene
NH_3	Ammonia
NH_4Cl	Ammonium Chloride
NH_4F	Ammonium Fluoride
$(NH_4)HF_2$	Ammonium Bifluoride
O	Oxygen
OH	Hydroxide
P	Phosphorus
PA	Phytic Acid
Pb	Lead
PCM	Phase Change Materials
PDMS	Polydimethylsiloxane
PEG	Polyethylene Glycol
PPy	Polypyrrole
PVA	Poly(vinyl alcohol)
PVT	Photovoltaic Thermal
PVDF	Polyvinylidene Difluoride
QSH	Quantum Spin Hall
RR	Respiration Rate
S	Sulfur
Sc	Scandium
SC	Super Capacitor
Sc_2CF_2	MXene
SDS	Sodium Dodecyl Sulfate
SDBS	Sodium Dodecylbenzenesulfonate
SEM	Scanning Electron Microscope
SHE	Self-Healing Efficiency
Si	Silicon
SOC	Spin Orbital Coupling
Sn	Tin
Ta	Tantalum
TEG	Thermoelectric Generator
TEM	Transmission Electron Microscope
TES	Thermal Energy Storage
TGA	Thermogravimetric Analysis
Ti	Titanium
Ti_2AlC	Titanium Aluminum Carbide
Ti_3AlC_2	Titanium Aluminum Carbide
Ti_2AlN	Titanium Aluminum Nitride
Ti_4AlN_3	Titanium Aluminum Nitride
Ti_3C_2	Titanium Carbide
$Ti_3C_2F_2$	MXene
$Ti_3C_2O_2$	MXene
$Ti_3C_2(OH)_2$	MXene
$Ti_3C_2T_x$	MXene
$TiCrCF_2$	MXene
TiO_2	Titanium Oxide
TMA−OH	Tetramethylammonium Hydroxide
TMDs	Transition Metals Dichalcogenides
TPU	Thermoplastic Polyurethane
TRC	Technology Readiness Level
V	Vanadium
V_2AlC	Vanadium Aluminum Carbide
V_2N	MXene
VN	Vanadium Nitrite
V_2CT_x	MXene

https://doi.org/10.1021/acsomega.4c04849
ACS Omega 2024, 9, 32350−32393

$W_{1.33}CT_x$	MXene
XRD	X-ray Diffraction
ZIB	Zinc Ion Battery
Zn	Zinc
$ZnCl_2$	Zinc Chloride
Zr	Zirconium
Zr_2CO_2	MXene

REFERENCES

(1) Gohar, O.; Zubair Khan, M.; Bibi, I.; Bashir, N.; Tariq, U.; Bakhtiar, M.; Ramzan Abdul Karim, M.; Ali, F.; Bilal Hanif, M.; Motola, M. Nanomaterials for advanced energy applications: Recent advancements and future trends. *Materials & Design* **2024**, *241*, No. 112930.

(2) Liu, Y.; Zhou, G.; Liu, K.; Cui, Y. Design of Complex Nanomaterials for Energy Storage: Past Success and Future Opportunity. *Acc. Chem. Res.* **2017**, *50* (12), 2895−2905.

(3) Liu, C.-j.; Burghaus, U.; Besenbacher, F.; Wang, Z. L. Preparation and Characterization of Nanomaterials for Sustainable Energy Production. *ACS Nano* **2010**, *4* (10), 5517−5526.

(4) *Nanomaterials for sustainable energy*; Li, Q., Ed.; Springer, 2016.

(5) Tao, W.; Kong, N.; Ji, X.; Zhang, Y.; Sharma, A.; Ouyang, J.; Qi, B.; Wang, J.; Xie, N.; Kang, C.; et al. Emerging two-dimensional monoelemental materials (Xenes) for biomedical applications. *Chem. Soc. Rev.* **2019**, *48* (11), 2891−2912.

(6) (a) Halim, J. *Synthesis and transport properties of 2D transition metal carbides (MXenes)*. Ph.D. Thesis, Linköping University, Linköping, Sweden, 2018. (b) Rasool, K.; Pandey, R. P.; Rasheed, P. A.; Berdiyorov, G. R.; Mahmoud, K. A. MXenes for Environmental and Water Treatment Applications. In *2D Metal Carbides and Nitrides (MXenes)*; Springer, 2019; p 417.

(7) Wei, Y.; Zhang, P.; Soomro, R. A.; Zhu, Q.; Xu, B. Advances in the Synthesis of 2D MXenes. *Adv. Mater.* **2021**, *33* (39), No. 2103148.

(8) Wyatt, B. C.; Rosenkranz, A.; Anasori, B. 2D MXenes: Tunable Mechanical and Tribological Properties. *Adv. Mater.* **2021**, *33* (17), No. 2007973.

(9) An, Y.; Tian, Y.; Shen, H.; Man, Q.; Xiong, S.; Feng, J. Two-dimensional MXenes for flexible energy storage devices. *Energy Environ. Sci.* **2023**, *16* (10), 4191−4250.

(10) Shahzad, U.; Marwani, H. M.; Saeed, M.; Asiri, A. M.; Rahman, M. M. Two-dimensional MXenes as Emerging Materials: A Comprehensive Review. *ChemistrySelect* **2023**, *8* (25), No. e202300737.

(11) (a) Zhang, C.; Ma, Y.; Zhang, X.; Abdolhosseinzadeh, S.; Sheng, H.; Lan, W.; Pakdel, A.; Heier, J.; Nüesch, F. Two-Dimensional Transition Metal Carbides and Nitrides (MXenes): Synthesis, Properties, and Electrochemical Energy Storage Applications. *ENERGY & ENVIRONMENTAL MATERIALS* **2020**, *3* (1), 29−55. (b) Zhang, X.; Ren, T.; Li, Z. Recent advances of two-dimensional lubricating materials: from tunable tribological properties to applications. *Journal of Materials Chemistry A* **2023**, *11* (17), 9239−9269.

(12) Li, X.; Huang, Z.; Shuck, C. E.; Liang, G.; Gogotsi, Y.; Zhi, C. MXene chemistry, electrochemistry and energy storage applications. *Nature Reviews Chemistry* **2022**, *6* (6), 389−404.

(13) Xiong, D.; Shi, Y.; Yang, H. Y. Rational design of MXene-based films for energy storage: Progress, prospects. *Mater. Today* **2021**, *46*, 183−211.

(14) Lim, K. R. G.; Handoko, A. D.; Nemani, S. K.; Wyatt, B.; Jiang, H.-Y.; Tang, J.; Anasori, B.; Seh, Z. W. Rational Design of Two-Dimensional Transition Metal Carbide/Nitride (MXene) Hybrids and Nanocomposites for Catalytic Energy Storage and Conversion. *ACS Nano* **2020**, *14* (9), 10834−10864.

(15) Wang, J.; Shen, M.; Liu, Z.; Wang, W. MXene materials for advanced thermal management and thermal energy utilization. *Nano Energy* **2022**, *97*, No. 107177.

(16) Zhang, X.; Wang, L.; Liu, W.; Li, C.; Wang, K.; Ma, Y. Recent Advances in MXenes for Lithium-Ion Capacitors. *ACS Omega* **2020**, *5* (1), 75−82.

(17) Das, P.; Katheria, A.; Jana, A.; Das, M.; Roy, B.; Nayak, J.; Nath, K.; Ghosh, S. K.; De, A.; Das, N. C. Super-Stretchable, Self-Healing 2D MXene-Based Composites for Thermal Management and Electromagnetic Shielding Applications. *ACS Applied Engineering Materials* **2023**, *1* (4), 1186−1200.

(18) Tan, K. H.; Zaed, M. A.; Saidur, R.; Abdullah, N.; Ishak, N. A. I. M.; Cherusseri, J. Strategic Insights for Bulk Production of MXene: A Review. *E3S Web Conf.* **2024**, *488*, 01003.

(19) Zaed, M. A.; Tan, K. H.; Saidur, R.; Abdullah, N.; Pandey, A. K. Invited viewpoint: pathways to low-cost MXene synthesis. *J. Mater. Sci.* **2024**, *59* (18), 7575−7594.

(20) Saharudin, M. S.; Ayub, A.; Hasbi, S.; Muhammad-Sukki, F.; Shyha, I.; Inam, F. Recent advances in MXene composites research, applications and opportunities. *Materials Today: Proceedings* **2023**, DOI: 10.1016/j.matpr.2023.02.435.

(21) Lamiel, C.; Hussain, I.; Warner, J. H.; Zhang, K. Beyond Ti-based MXenes: A review of emerging non-Ti based metal-MXene structure, properties, and applications. *Mater. Today* **2023**, *63*, 313−338.

(22) Bibi, F.; Soomro, I. A.; Hanan, A.; Lakhan, M. N.; Khan, A.; Goraya, N. R.; Rehman, Z. U.; Hussain, I.; Zhang, K. Advances in 2D/2D MXenes-based heterostructures for energy storage/conversion applications. *Journal of Materials Science & Technology* **2024**, *202*, 82−118.

(23) (a) Naguib, M.; Mashtalir, O.; Carle, J.; Presser, V.; Lu, J.; Hultman, L.; Gogotsi, Y.; Barsoum, M. W. *ACS Nano* **2012**, *6*, 1322−1331. (b) Naguib, M.; Kurtoglu, M.; Presser, V.; Lu, J.; Niu, J.; Heon, M.; Hultman, L.; Gogotsi, Y.; Barsoum, M. W. *Adv. Mater.* **2011**, *23*, 4248−4253. (c) Mashtalir, O.; Naguib, M.; Dyatkin, B.; Gogotsi, Y.; Barsoum, M. W. Kinetics of aluminum extraction from Ti3AlC2 in hydrofluoric acid. *Mater. Chem. Phys.* **2013**, *139* (1), 147−152.

(24) Kim, Y.-J.; Kim, S. J.; Seo, D.; Chae, Y.; Anayee, M.; Lee, Y.; Gogotsi, Y.; Ahn, C. W.; Jung, H.-T. Etching Mechanism of Monoatomic Aluminum Layers during MXene Synthesis. *Chem. Mater.* **2021**, *33* (16), 6346−6355.

(25) Naguib, M.; Kurtoglu, M.; Presser, V.; Lu, J.; Niu, J.; Heon, M.; Hultman, L.; Gogotsi, Y.; Barsoum, M. W. Two-Dimensional Nanocrystals Produced by Exfoliation of Ti3AlC2. *Adv. Mater.* **2011**, *23* (37), 4248−4253.

(26) (a) Wang, L.; Tao, W.; Yuan, L.; Liu, Z.; Huang, Q.; Chai, Z.; Gibson, J. K.; Shi, W. Rational control of the interlayer space inside two-dimensional titanium carbides for highly efficient uranium removal and imprisonment. *Chem. Commun.* **2017**, *53* (89), 12084−12087. (b) Wang, H.; Wu, Y.; Yuan, X.; Zeng, G.; Zhou, J.; Wang, X.; Chew, J. W. Clay-Inspired MXene-Based Electrochemical Devices and Photo-Electrocatalyst: State-of-the-Art Progresses and Challenges. *Adv. Mater.* **2018**, *30* (12), No. 1704561.

(27) Alhabeb, M.; Maleski, K.; Anasori, B.; Lelyukh, P.; Clark, L.; Sin, S.; Gogotsi, Y. Guidelines for Synthesis and Processing of Two-Dimensional Titanium Carbide (Ti3C2Tx MXene). *Chem. Mater.* **2017**, *29* (18), 7633−7644.

(28) Murali, G.; Reddy Modigunta, J. K.; Park, Y. H.; Lee, J.-H.; Rawal, J.; Lee, S.-Y.; In, I.; Park, S.-J. A Review on MXene Synthesis, Stability, and Photocatalytic Applications. *ACS Nano* **2022**, *16* (9), 13370−13429.

(29) Hui, X.; Ge, X.; Zhao, R.; Li, Z.; Yin, L. Interface Chemistry on MXene-Based Materials for Enhanced Energy Storage and Conversion Performance. *Adv. Funct. Mater.* **2020**, *30* (50), No. 2005190.

(30) Biswas, S.; Alegaonkar, P. S. MXene: Evolutions in Chemical Synthesis and Recent Advances in Applications. *Surfaces* **2022**, *5*, 1−34.

(31) Sang, X.; Xie, Y.; Lin, M.-W.; Alhabeb, M.; Van Aken, K. L.; Gogotsi, Y.; Kent, P. R. C.; Xiao, K.; Unocic, R. R. Atomic Defects in Monolayer Titanium Carbide (Ti3C2Tx) MXene. *ACS Nano* **2016**, *10* (10), 9193−9200.

(32) Zhou, J.; Zha, X.; Zhou, X.; Chen, F.; Gao, G.; Wang, S.; Shen, C.; Chen, T.; Zhi, C.; Eklund, P.; et al. Synthesis and Electrochemical Properties of Two-Dimensional Hafnium Carbide. *ACS Nano* **2017**, *11* (4), 3841−3850.

(33) Tang, Q.; Zhou, Z.; Shen, P. Are MXenes Promising Anode Materials for Li Ion Batteries? Computational Studies on Electronic

Properties and Li Storage Capability of Ti3C2 and Ti3C2 × 2 (X = F, OH) Monolayer. *J. Am. Chem. Soc.* **2012**, *134* (40), 16909−16916.
(34) Zhang, T.; Pan, L.; Tang, H.; Du, F.; Guo, Y.; Qiu, T.; Yang, J. Synthesis of two-dimensional Ti3C2Tx MXene using HCl+LiF etchant: Enhanced exfoliation and delamination. *J. Alloys Compd.* **2017**, *695*, 818−826.
(35) Numan, A.; Rafique, S.; Khalid, M.; Zaharin, H. A.; Radwan, A.; Mokri, N. A.; Ching, O. P.; Walvekar, R. Microwave-assisted rapid MAX phase etching and delamination: A paradigm shift in MXene synthesis. *Mater. Chem. Phys.* **2022**, *288*, No. 126429.
(36) Sinha, A.; Ma, K.; Zhao, H. 2D Ti3C2Tx flakes prepared by in-situ HF etchant for simultaneous screening of carbamate pesticides. *J. Colloid Interface Sci.* **2021**, *590*, 365−374.
(37) Pang, J.; Mendes, R. G.; Bachmatiuk, A.; Zhao, L.; Ta, H. Q.; Gemming, T.; Liu, H.; Liu, Z.; Rummeli, M. H. J. C. S. R. *Applications of 2D MXenes in energy conversion and storage systems* **2019**, *48* (1), 72−133.
(38) Ghidiu, M.; Lukatskaya, M. R.; Zhao, M.-Q.; Gogotsi, Y.; Barsoum, M. W. Conductive two-dimensional titanium carbide 'clay' with high volumetric capacitance. *Nature* **2014**, *516* (7529), 78−81.
(39) Anayee, M.; Kurra, N.; Alhabeb, M.; Seredych, M.; Hedhili, M. N.; Emwas, A.-H.; Alshareef, H. N.; Anasori, B.; Gogotsi, Y. Role of acid mixtures etching on the surface chemistry and sodium ion storage in Ti3C2Tx MXene. *Chem. Commun.* **2020**, *56* (45), 6090−6093.
(40) Carey, M. S.; Barsoum, M. W. Scalable and sustainable production of Ti 3 C 2 T z MXene and fluorine recovery from wastewater through cryolite precipitation. *RSC Adv.* **2022**, *12* (47), 30846−30850.
(41) Li, C.; Kota, S.; Hu, C.; Barsoum, M. W. On the synthesis of low-cost, titanium-based MXenes. *J. Ceram. Sci. Technol.* **2016**, *7* (3), 301−306.
(42) Zaed, M. A.; Tan, K. H.; Abdullah, N.; Saidur, R.; Pandey, A. K.; Saleque, A. M. Cost analysis of MXene for low-cost production, and pinpointing of its economic footprint. *Open Ceramics* **2024**, *17*, No. 100526.
(43) Hong Ng, V. M.; Huang, H.; Zhou, K.; Lee, P. S.; Que, W.; Xu, J. Z.; Kong, L. B. Recent progress in layered transition metal carbides and/or nitrides (MXenes) and their composites: synthesis and applications. *Journal of Materials Chemistry A* **2017**, *5* (7), 3039−3068.
(44) Benchakar, M.; Loupias, L.; Garnero, C.; Bilyk, T.; Morais, C.; Canaff, C.; Guignard, N.; Morisset, S.; Pazniak, H.; Hurand, S.; et al. One MAX phase, different MXenes: A guideline to understand the crucial role of etching conditions on Ti3C2Tx surface chemistry. *Appl. Surf. Sci.* **2020**, *530*, No. 147209.
(45) Lipatov, A.; Alhabeb, M.; Lukatskaya, M. R.; Boson, A.; Gogotsi, Y.; Sinitskii, A. Effect of Synthesis on Quality, Electronic Properties and Environmental Stability of Individual Monolayer Ti3C2MXene Flakes. *Advanced Electronic Materials* **2016**, *2* (12), No. 1600255.
(46) Zhou, C.; Zhao, X.; Xiong, Y.; Tang, Y.; Ma, X.; Tao, Q.; Sun, C.; Xu, W. A review of etching methods of MXene and applications of MXene conductive hydrogels. *Eur. Polym. J.* **2022**, *167*, No. 111063.
(47) Maleski, K.; Alhabeb, M. Top-down MXene synthesis (selective etching). *2D Metal Carbides and Nitrides (MXenes) Structure, Properties and Applications* **2019**, 69−87.
(48) Li, G.; Tan, L.; zhang, Y.; Wu, B.; Li, L. Highly Efficiently Delaminated Single-Layered MXene Nanosheets with Large Lateral Size. *Langmuir* **2017**, *33* (36), 9000−9006.
(49) Li, T.; Yao, L.; Liu, Q.; Gu, J.; Luo, R.; Li, J.; Yan, X.; Wang, W.; Liu, P.; Chen, B.; et al. Fluorine-Free Synthesis of High-Purity Ti3C2Tx (T = OH, O) via Alkali Treatment. *Angew. Chem., Int. Ed.* **2018**, *57* (21), 6115−6119.
(50) Yan, Z.; Jiang, J.; Zhang, Y.; Yang, D.; Du, N. Scalable and low-cost synthesis of porous silicon nanoparticles as high-performance lithium-ion battery anode. *Materials Today Nano* **2022**, *18*, No. 100175.
(51) (a) Sohn, M.; Kim, D. S.; Park, H.-I.; Kim, J.-H.; Kim, H. Porous Silicon−Carbon Composite Materials Engineered by Simultaneous Alkaline Etching for High-Capacity Lithium Storage Anodes. *Electrochim. Acta* **2016**, *196*, 197−205. (b) Yu, M.; Zeng, X.; Song, Q.; Liu, L.; Li, J. Examining regeneration technologies for etching solutions: a critical analysis of the characteristics and potentials. *Journal of Cleaner Production* **2016**, *113*, 973−980.
(52) Sun, W.; Shah, S. A.; Chen, Y.; Tan, Z.; Gao, H.; Habib, T.; Radovic, M.; Green, M. J. Electrochemical etching of Ti2AlC to Ti2CTx (MXene) in low-concentration hydrochloric acid solution. *Journal of Materials Chemistry A* **2017**, *5* (41), 21663−21668.
(53) Lukatskaya, M. R.; Halim, J.; Dyatkin, B.; Naguib, M.; Buranova, Y. S.; Barsoum, M. W.; Gogotsi, Y. Inside Cover: Room-Temperature Carbide-Derived Carbon Synthesis by Electrochemical Etching of MAX Phases (Angew. Chem. Int. Ed. 19/2014). *Angew. Chem., Int. Ed.* **2014**, *53* (19), 4728−4728.
(54) Xu, D.; Li, Z.; Li, L.; Wang, J. Insights into the Photothermal Conversion of 2D MXene Nanomaterials: Synthesis, Mechanism, and Applications. *Adv. Funct. Mater.* **2020**, *30* (47), No. 2000712.
(55) Chen, J.; Chen, M.; Zhou, W.; Xu, X.; Liu, B.; Zhang, W.; Wong, C. Simplified Synthesis of Fluoride-Free Ti3C2Tx via Electrochemical Etching toward High-Performance Electrochemical Capacitors. *ACS Nano* **2022**, *16* (2), 2461−2470.
(56) Yang, S.; Zhang, P.; Wang, F.; Ricciardulli, A. G.; Lohe, M. R.; Blom, P. W. M.; Feng, X. Fluoride-free synthesis of two-dimensional titanium carbide (MXene) using a binary aqueous system. *Angew. Chem.* **2018**, *130* (47), 15717−15721.
(57) (a) Saxena, S.; Johnson, M.; Dixit, F.; Zimmermann, K.; Chaudhuri, S.; Kaka, F.; Kandasubramanian, B. Thinking green with 2-D and 3-D MXenes: Environment friendly synthesis and industrial scale applications and global impact. *Renewable and Sustainable Energy Reviews* **2023**, *178*, No. 113238. (b) Liu, A.; Liang, X.; Ren, X.; Guan, W.; Gao, M.; Yang, Y.; Yang, Q.; Gao, L.; Li, Y.; Ma, T. Recent Progress in MXene-Based Materials: Potential High-Performance Electrocatalysts. *Adv. Funct. Mater.* **2020**, *30* (38), No. 2003437.
(58) Liu, L.; Zschiesche, H.; Antonietti, M.; Gibilaro, M.; Chamelot, P.; Massot, L.; Rozier, P.; Taberna, P.-L.; Simon, P. In Situ Synthesis of MXene with Tunable Morphology by Electrochemical Etching of MAX Phase Prepared in Molten Salt. *Adv. Energy Mater.* **2023**, *13* (7), No. 2203805.
(59) Jiang, Q.; Lei, Y.; Liang, H.; Xi, K.; Xia, C.; Alshareef, H. N. Review of MXene electrochemical microsupercapacitors. *Energy Storage Materials* **2020**, *27*, 78−95.
(60) Yadav, M.; Kumar, M.; Sharma, A. Review of Ti3C2Tx MXene Nanosheets and their Applications. *ACS Applied Nano Materials* **2024**, *7* (9), 9847−9867.
(61) Chen, N.; Yang, W.; Zhang, C. Perspectives on preparation of two-dimensional MXenes. *Sci. Technol. Adv. Mater.* **2021**, *22* (1), 917−930.
(62) Zhang, T.; Shevchuk, K.; Wang, R. J.; Kim, H.; Hourani, J.; Gogotsi, Y. Delamination of Chlorine-Terminated MXene Produced Using Molten Salt Etching. *Chem. Mater.* **2024**, *36* (4), 1998−2006.
(63) Liu, L.; Orbay, M.; Luo, S.; Duluard, S.; Shao, H.; Harmel, J.; Rozier, P.; Taberna, P.-L.; Simon, P. Exfoliation and Delamination of Ti3C2Tx MXene Prepared via Molten Salt Etching Route. *ACS Nano* **2022**, *16* (1), 111−118.
(64) Urbankowski, P.; Anasori, B.; Makaryan, T.; Er, D.; Kota, S.; Walsh, P. L.; Zhao, M.; Shenoy, V. B.; Barsoum, M. W.; Gogotsi, Y. Synthesis of two-dimensional titanium nitride Ti4N3 (MXene). *Nanoscale* **2016**, *8* (22), 11385−11391.
(65) Urbankowski, P.; Anasori, B.; Hantanasirisakul, K.; Yang, L.; Zhang, L.; Haines, B.; May, S. J.; Billinge, S. J. L.; Gogotsi, Y. 2D molybdenum and vanadium nitrides synthesized by ammoniation of 2D transition metal carbides (MXenes). *Nanoscale* **2017**, *9* (45), 17722−17730.
(66) Li, M.; Lu, J.; Luo, K.; Li, Y.; Chang, K.; Chen, K.; Zhou, J.; Rosen, J.; Hultman, L.; Eklund, P.; et al. Element Replacement Approach by Reaction with Lewis Acidic Molten Salts to Synthesize Nanolaminated MAX Phases and MXenes. *J. Am. Chem. Soc.* **2019**, *141* (11), 4730−4737.
(67) Arole, K.; Blivin, J. W.; Bruce, A. M.; Athavale, S.; Echols, I. J.; Cao, H.; Tan, Z.; Radovic, M.; Lutkenhaus, J. L.; Green, M. J. Exfoliation, delamination, and oxidation stability of molten salt etched

Nb2CTz MXene nanosheets. *Chem. Commun.* **2022**, *58* (73), 10202−10205.
(68) Dong, H.; Xiao, P.; Jin, N.; Wang, B.; Liu, Y.; Lin, Z. Molten Salt Derived Nb2CTx MXene Anode for Li-ion Batteries. *ChemElectroChem.* **2021**, *8* (5), 957−962.
(69) Hu, W.; Yang, M.; Fan, T.; Li, Z.; Wang, Y.; Li, H.; Zhu, G.; Li, J.; Jin, H.; Yu, L. A simple, efficient, fluorine-free synthesis method of MXene/Ti3C2Tx anode through molten salt etching for sodium-ion batteries. *Battery Energy* **2023**, *2* (5), No. 20230021.
(70) Shen, M.; Jiang, W.; Liang, K.; Zhao, S.; Tang, R.; Zhang, L.; Wang, J. Q. One-pot green process to synthesize MXene with controllable surface terminations using molten salts. *Angew. Chem.* **2021**, *133* (52), 27219−27224.
(71) Ramírez, R.; Melillo, A.; Osella, S.; Asiri, A. M.; Garcia, H.; Primo, A. Green, HF-Free Synthesis of MXene Quantum Dots and their Photocatalytic Activity for Hydrogen Evolution. *Small Methods* **2023**, *7* (6), No. 2300063.
(72) Kurra, N.; Alhabeb, M.; Maleski, K.; Wang, C.-H.; Alshareef, H. N.; Gogotsi, Y. Bistacked Titanium Carbide (MXene) Anodes for Hybrid Sodium-Ion Capacitors. *ACS Energy Letters* **2018**, *3* (9), 2094−2100.
(73) Gong, S.; Zhao, F.; Zhang, Y.; Xu, H.; Li, M.; Qi, J.; Wang, H.; Wang, Z.; Hu, Y.; Fan, X.; et al. Few-layered Ti3C2Tx MXene synthesized via water-free etching toward high-performance supercapacitors. *J. Colloid Interface Sci.* **2023**, *632*, 216−222.
(74) Kashiwaya, S.; Shi, Y.; Lu, J.; Sangiovanni, D. G.; Greczynski, G.; Magnuson, M.; Andersson, M.; Rosen, J.; Hultman, L. Synthesis of goldene comprising single-atom layer gold. *Nature Synthesis* **2024**, *3*, 744.
(75) Khan, U.; Luo, Y.; Kong, L. B.; Que, W. Synthesis of fluorine free MXene through lewis acidic etching for application as electrode of proton supercapacitors. *J. Alloys Compd.* **2022**, *926*, No. 166903.
(76) Wong, A. J. Y.; Lim, K. R. G.; Seh, Z. W. Fluoride-free synthesis and long-term stabilization of MXenes. *J. Mater. Res.* **2022**, *37* (22), 3988−3997.
(77) Javed, M. S.; Mateen, A.; Ali, S.; Zhang, X.; Hussain, I.; Imran, M.; Shah, S. S. A.; Han, W. The Emergence of 2D MXenes Based Zn-Ion Batteries: Recent Development and Prospects. *Small* **2022**, *18* (26), No. 2201989.
(78) Wang, D.; Zhou, C.; Filatov, A. S.; Cho, W.; Lagunas, F.; Wang, M.; Vaikuntanathan, S.; Liu, C.; Klie, R. F.; Talapin, D. V. Direct synthesis and chemical vapor deposition of 2D carbide and nitride MXenes. *Science* **2023**, *379* (6638), 1242−1247.
(79) Buke, G. C.; Caylan, O. R.; Ogurtani, O. T. Growth Mechanism of 2D Mo2C on Cu via CVD. *Cryst. Growth Des.* **2023**, *23* (8), 5462−5468.
(80) Choi, J.; Oh, M. S.; Cho, A.; Ryu, J.; Kim, Y.-J.; Kang, H.; Cho, S.-Y.; Im, S. G.; Kim, S. J.; Jung, H.-T. Simple Approach to Enhance Long-Term Environmental Stability of MXene Using Initiated Chemical Vapor Deposition Surface Coating. *ACS Nano* **2023**, *17* (11), 10898−10905.
(81) Dadashi Firouzjaei, M.; Nemani, S. K.; Sadrzadeh, M.; Wujcik, E. K.; Elliott, M.; Anasori, B. Life-Cycle Assessment of Ti3C2Tx MXene Synthesis. *Adv. Mater.* **2023**, *35* (31), No. 2300422.
(82) Zhou, J.; Lin, S.; Huang, Y.; Tong, P.; Zhao, B.; Zhu, X.; Sun, Y. Synthesis and lithium ion storage performance of two-dimensional V4C3MXene. *Chemical Engineering Journal* **2019**, *373*, 203−212.
(83) Zhou, J.; Zha, X.; Chen, F. Y.; Ye, Q.; Eklund, P.; Du, S.; Huang, Q. A Two-Dimensional Zirconium Carbide by Selective Etching of Al3C3 from Nanolaminated Zr3Al3C5. *Angew. Chem., Int. Ed.* **2016**, *55* (16), 5008−5013.
(84) Meshkian, R.; Dahlqvist, M.; Lu, J.; Wickman, B.; Halim, J.; Thörnberg, J.; Tao, Q.; Li, S.; Intikhab, S.; Snyder, J.; et al. W-Based Atomic Laminates and Their 2D Derivative W1.33C MXene with Vacancy Ordering. *Adv. Mater.* **2018**, *30* (21), No. 1706409.
(85) Naguib, M.; Halim, J.; Lu, J.; Cook, K. M.; Hultman, L.; Gogotsi, Y.; Barsoum, M. W. New Two-Dimensional Niobium and Vanadium Carbides as Promising Materials for Li-Ion Batteries. *J. Am. Chem. Soc.* **2013**, *135* (43), 15966−15969.
(86) Tran, M. H.; Schäfer, T.; Shahraei, A.; Dürrschnabel, M.; Molina-Luna, L.; Kramm, U. I.; Birkel, C. S. Adding a New Member to the MXene Family: Synthesis, Structure, and Electrocatalytic Activity for the Hydrogen Evolution Reaction of V4C3Tx. *ACS Applied Energy Materials* **2018**, *1* (8), 3908−3914.
(87) Meshkian, R.; Tao, Q.; Dahlqvist, M.; Lu, J.; Hultman, L.; Rosen, J. Theoretical stability and materials synthesis of a chemically ordered MAX phase, Mo2ScAlC2, and its two-dimensional derivate Mo2ScC2MXene. *Acta Mater.* **2017**, *125*, 476−480.
(88) Meshkian, R.; Lind, H.; Halim, J.; El Ghazaly, A.; Thörnberg, J.; Tao, Q.; Dahlqvist, M.; Palisaitis, J.; Persson, P. O. Å.; Rosen, J. Theoretical Analysis, Synthesis, and Characterization of 2D W1.33C (MXene) with Ordered Vacancies. *ACS Applied Nano Materials* **2019**, *2* (10), 6209−6219.
(89) Naguib, M.; Mashtalir, O.; Carle, J.; Presser, V.; Lu, J.; Hultman, L.; Gogotsi, Y.; Barsoum, M. W. Two-Dimensional Transition Metal Carbides. *ACS Nano* **2012**, *6* (2), 1322−1331.
(90) Lin, H.; Wang, Y.; Gao, S.; Chen, Y.; Shi, J. Theranostic 2D Tantalum Carbide (MXene). *Adv. Mater.* **2018**, *30* (4), No. 1703284.
(91) Wang, D.; Si, J.; Lin, S.; Zhang, R.; Huang, Y.; Yang, J.; Lu, W.; Zhu, X.; Sun, Y. Achieving Macroscopic V4C3Tx MXene by Selectively Etching Al from V4AlC3 Single Crystals. *Inorg. Chem.* **2020**, *59* (5), 3239−3248.
(92) Cockreham, C. B.; Goncharov, V. G.; Hammond-Pereira, E.; Reece, M. E.; Strzelecki, A. C.; Xu, W.; Saunders, S. R.; Xu, H.; Guo, X.; Wu, D. Energetic Stability and Interfacial Complexity of Ti3C2Tx MXenes Synthesized with HF/HCl and CoF2/HCl as Etching Agents. *ACS Appl. Mater. Interfaces* **2022**, *14* (36), 41542−41554.
(93) Liu, F.; Zhou, J.; Wang, S.; Wang, B.; Shen, C.; Wang, L.; Hu, Q.; Huang, Q.; Zhou, A. Preparation of High-Purity V2C MXene and Electrochemical Properties as Li-Ion Batteries. *J. Electrochem. Soc.* **2017**, *164* (4), A709.
(94) Yan, Y.; Han, H.; Dai, Y.; Zhu, H.; Liu, W.; Tang, X.; Gan, W.; Li, H. Nb2CTx MXene Nanosheets for Dye Adsorption. *ACS Applied Nano Materials* **2021**, *4* (11), 11763−11769.
(95) Seredych, M.; Shuck, C. E.; Pinto, D.; Alhabeb, M.; Precetti, E.; Deysher, G.; Anasori, B.; Kurra, N.; Gogotsi, Y. High-Temperature Behavior and Surface Chemistry of Carbide MXenes Studied by Thermal Analysis. *Chem. Mater.* **2019**, *31* (9), 3324−3332.
(96) Wang, S.; Liu, Y.; Liu, Y.; Hu, W. Effect of HF etching on titanium carbide (Ti3C2Tx) microstructure and its capacitive properties. *Chemical Engineering Journal* **2023**, *452*, No. 139512.
(97) Thirumal, V.; Yuvakkumar, R.; Kumar, P. S.; Ravi, G.; Keerthana, S. P.; Velauthapillai, D. Facile single-step synthesis of MXene@CNTs hybrid nanocomposite by CVD method to remove hazardous pollutants. *Chemosphere* **2022**, *286*, No. 131733.
(98) Yang, C.; Jiang, Q.; Li, W.; He, H.; Yang, L.; Lu, Z.; Huang, H. Ultrafine Pt Nanoparticle-Decorated 3D Hybrid Architectures Built from Reduced Graphene Oxide and MXene Nanosheets for Methanol Oxidation. *Chem. Mater.* **2019**, *31* (22), 9277−9287.
(99) Yang, C.; Jiang, Q.; Huang, H.; He, H.; Yang, L.; Li, W. Polyelectrolyte-Induced Stereoassembly of Grain Boundary-Enriched Platinum Nanoworms on Ti3C2Tx MXene Nanosheets for Efficient Methanol Oxidation. *ACS Appl. Mater. Interfaces* **2020**, *12* (21), 23822−23830.
(100) Yang, B.; Liu, B.; Chen, J.; Ding, Y.; Sun, Y.; Tang, Y.; Yan, X. Realizing high-performance lithium ion hybrid capacitor with a 3D MXene-carbon nanotube composite anode. *Chemical Engineering Journal* **2022**, *429*, No. 132392.
(101) Kumar, S.; Rehman, M. A.; Lee, S.; Kim, M.; Hong, H.; Park, J.-Y.; Seo, Y. Supercapacitors based on Ti3C2Tx MXene extracted from supernatant and current collectors passivated by CVD-graphene. *Sci. Rep.* **2021**, *11* (1), 649.
(102) Wang, D.; Zhang, D.; Li, P.; Yang, Z.; Mi, Q.; Yu, L. Electrospinning of Flexible Poly(vinyl alcohol)/MXene Nanofiber-Based Humidity Sensor Self-Powered by Monolayer Molybdenum Diselenide Piezoelectric Nanogenerator. *Nano-Micro Letters* **2021**, *13* (1), 57.

(103) Wang, M.; Qin, B.; Xu, F.; Yang, W.; Liu, Z.; Zhang, Y.; Fan, H. Hetero-structural and hetero-interfacial engineering of MXene@ Bi2S3/Mo7S8 hybrid for advanced sodium/potassium-ion batteries. *J. Colloid Interface Sci.* **2023**, *650*, 446−455.

(104) Xia, Z.; Chen, X.; Ci, H.; Fan, Z.; Yi, Y.; Yin, W.; Wei, N.; Cai, J.; Zhang, Y.; Sun, J. Designing N-doped graphene/ReSe2/Ti3C2MXene heterostructure frameworks as promising anodes for high-rate potassium-ion batteries. *Journal of Energy Chemistry* **2021**, *53*, 155−162.

(105) Yue, Y.; Wang, Y.; Xu, X.; Wang, C.; Yao, Z.; Liu, D. In-situ growth of bamboo-shaped carbon nanotubes and helical carbon nanofibers on Ti3C2Tx MXene at ultra-low temperature for enhanced electromagnetic wave absorption properties. *Ceram. Int.* **2022**, *48* (5), 6338−6346.

(106) Li, X.; Yin, S.; Cai, L.; Wang, Z.; Zeng, C.; Jiang, H.; Cheng, J.; Lu, W. Sea-urchin-like NiCo2S4 modified MXene hybrids with enhanced microwave absorption performance. *Chemical Engineering Journal* **2023**, *454*, No. 140127.

(107) Li, H.; Li, X.; Liang, J.; Chen, Y. Hydrous RuO2-Decorated MXene Coordinating with Silver Nanowire Inks Enabling Fully Printed Micro-Supercapacitors with Extraordinary Volumetric Performance. *Adv. Energy Mater.* **2019**, *9* (15), No. 1803987.

(108) Jiang, H.; Wang, Z.; Yang, Q.; Hanif, M.; Wang, Z.; Dong, L.; Dong, M. A novel MnO2/Ti3C2Tx MXene nanocomposite as high performance electrode materials for flexible supercapacitors. *Electrochim. Acta* **2018**, *290*, 695−703.

(109) Adepu, V.; Kunchur, A.; Kolli, C. S. R.; Siddhartha, S.; Mattela, V.; Sahatiya, P. High-Performance Visible Light Photodetector Based on 1D SnO2 Nanofibers with a Ti3C2Tx (MXene) Electron Transport Layer. *ACS Applied Nano Materials* **2022**, *5* (5), 6852−6863.

(110) Purbayanto, M. A. K.; Bury, D.; Chandel, M.; Shahrak, Z. D.; Mochalin, V. N.; Wójcik, A.; Moszczyńska, D.; Wojciechowska, A.; Tabassum, A.; Naguib, M.; et al. Ambient Processed rGO/Ti3CNTx MXene Thin Film with High Oxidation Stability, Photosensitivity, and Self-Cleaning Potential. *ACS Appl. Mater. Interfaces* **2023**, *15* (37), 44075−44086.

(111) Hilal, M.; Yang, W.; Hwang, Y.; Xie, W. Tailoring MXene Thickness and Functionalization for Enhanced Room-Temperature Trace NO2 Sensing. *Nano-Micro Letters* **2024**, *16* (1), 84.

(112) Chu, Y. Z.; Hoover, M.; Ward, P.; Lau, K. C. First-principles study of MXene properties with varying hydrofluoric acid concentration. *iScience* **2024**, *27* (2), No. 108784.

(113) Halim, J.; Kota, S.; Lukatskaya, M. R.; Naguib, M.; Zhao, M.-Q.; Moon, E. J.; Pitock, J.; Nanda, J.; May, S. J.; Gogotsi, Y.; et al. Synthesis and Characterization of 2D Molybdenum Carbide (MXene). *Adv. Funct. Mater.* **2016**, *26* (18), 3118−3127.

(114) Soundiraraju, B.; George, B. K. Two-Dimensional Titanium Nitride (Ti2N) MXene: Synthesis, Characterization, and Potential Application as Surface-Enhanced Raman Scattering Substrate. *ACS Nano* **2017**, *11* (9), 8892−8900.

(115) Alhabeb, M.; Maleski, K.; Mathis, T. S.; Sarycheva, A.; Hatter, C. B.; Uzun, S.; Levitt, A.; Gogotsi, Y. Selective Etching of Silicon from Ti3SiC2 (MAX) To Obtain 2D Titanium Carbide (MXene). *Angew. Chem., Int. Ed.* **2018**, *57* (19), 5444−5448.

(116) Peng, C.; Wei, P.; Chen, X.; Zhang, Y.; Zhu, F.; Cao, Y.; Wang, H.; Yu, H.; Peng, F. A hydrothermal etching route to synthesis of 2D MXene (Ti3C2, Nb2C): Enhanced exfoliation and improved adsorption performance. *Ceram. Int.* **2018**, *44* (15), 18886−18893.

(117) Zhu, K.; Jin, Y.; Du, F.; Gao, S.; Gao, Z.; Meng, X.; Chen, G.; Wei, Y.; Gao, Y. Synthesis of Ti2CTx MXene as electrode materials for symmetric supercapacitor with capable volumetric capacitance. *Journal of Energy Chemistry* **2019**, *31*, 11−18.

(118) Michael, J.; Qifeng, Z.; Danling, W. Titanium carbide MXene: Synthesis, electrical and optical properties and their applications in sensors and energy storage devices. *Nanomater. Nanotechnol.* **2019**, *9*, No. 184798041882447.

(119) Li, X.; Liu, M.; Fang, Y.; Wu, Z.; Dong, J.; Zhao, X.; Teng, C. Flexible and efficient MXene/PANI/aramid fabrics with high interface durability for wearable electromagnetic wave shielding. *Composites Communications* **2024**, *45*, No. 101776.

(120) Hong, H.; Kim, H. Y.; Cho, W. I.; Song, H. C.; Ham, H. C.; Chae, K.; Marques Mota, F.; Kim, J. Y.; Kim, D. H. Surface-functionalized three-dimensional MXene supports to boost the hydrogen evolution activity of Pt catalysts in alkaline media. *Journal of Materials Chemistry A* **2023**, *11* (10), 5328−5336.

(121) Guo, Y.; Zhang, X.; Jin, S.; Xia, Q.; Chang, Y.; Wang, L.; Zhou, A. Synthesis of Mo2C MXene with high electrochemical performance by alkali hydrothermal etching. *Journal of Advanced Ceramics* **2023**, *12* (10), 1889−1901.

(122) Hasani Khaneghahi, B.; Dehghan Abkenar, S.; Gilnejad, J.; Ganjali, M. R.; Hosseini, M. Application of Ti3C2(OH)2 MXene Nanosheets as a Potential Adsorbent and Photocatalyst for Degradation of Organic Dye in Aqueous Media. *Pollution* **2023**, *9* (2), 782−794.

(123) Hakim, M. W.; Ali, I.; Fatima, S.; Li, H.; Jafri, S. H. M.; Rizwan, S. Enhanced Electrochemical Performance of MWCNT-Assisted Molybdenum−Titanium Carbide MXene as a Potential Electrode Material for Energy Storage Application. *ACS Omega* **2024**, *9*, 8763.

(124) Khan, U.; Gao, B.; Kong, L. B.; Chen, Z.; Que, W. Green synthesis of fluorine-free MXene via hydrothermal process: A sustainable approach for proton supercapacitor electrodes. *Electrochim. Acta* **2024**, *475*, No. 143651.

(125) Deysher, G.; Shuck, C. E.; Hantanasirisakul, K.; Frey, N. C.; Foucher, A. C.; Maleski, K.; Sarycheva, A.; Shenoy, V. B.; Stach, E. A.; Anasori, B.; et al. Synthesis of Mo4VAlC4MAX Phase and Two-Dimensional Mo4VC4MXene with Five Atomic Layers of Transition Metals. *ACS Nano* **2020**, *14* (1), 204−217.

(126) Zou, G.; Zhang, Z.; Guo, J.; Liu, B.; Zhang, Q.; Fernandez, C.; Peng, Q. Synthesis of MXene/Ag Composites for Extraordinary Long Cycle Lifetime Lithium Storage at High Rates. *ACS Appl. Mater. Interfaces* **2016**, *8* (34), 22280−22286.

(127) Zhang, Z.; Li, H.; Zou, G.; Fernandez, C.; Liu, B.; Zhang, Q.; Hu, J.; Peng, Q. Self-Reduction Synthesis of New MXene/Ag Composites with Unexpected Electrocatalytic Activity. *ACS Sustainable Chem. Eng.* **2016**, *4* (12), 6763−6771.

(128) Feng, A.; Yu, Y.; Wang, Y.; Jiang, F.; Yu, Y.; Mi, L.; Song, L. Two-dimensional MXene Ti3C2 produced by exfoliation of Ti3AlC2. *Materials & Design* **2017**, *114*, 161−166.

(129) Cockreham, C. B.; Zhang, X.; Li, H.; Hammond-Pereira, E.; Sun, J.; Saunders, S. R.; Wang, Y.; Xu, H.; Wu, D. Inhibition of AlF3·3H2O Impurity Formation in Ti3C2Tx MXene Synthesis under a Unique CoFx/HCl Etching Environment. *ACS Applied Energy Materials* **2019**, *2* (11), 8145−8152.

(130) Kumar, D. R.; Karthik, R.; Hasan, M.; Sayed, M. S.; Shim, J.-J. Mo-MXene-filled gel polymer electrolyte for high-performance quasi-solid-state zinc metal batteries. *Chemical Engineering Journal* **2023**, *473*, No. 145207.

(131) Li, X.; Li, M.; Yang, Q.; Liang, G.; Huang, Z.; Ma, L.; Wang, D.; Mo, F.; Dong, B.; Huang, Q.; et al. In Situ Electrochemical Synthesis of MXenes without Acid/Alkali Usage in/for an Aqueous Zinc Ion Battery. *Adv. Energy Mater.* **2020**, *10* (36), No. 2001791.

(132) Yang, S.; Zhang, P.; Wang, F.; Ricciardulli, A. G.; Lohe, M. R.; Blom, P. W. M.; Feng, X. Fluoride-Free Synthesis of Two-Dimensional Titanium Carbide (MXene) Using A Binary Aqueous System. *Angew. Chem., Int. Ed.* **2018**, *57* (47), 15491−15495.

(133) Yin, T.; Li, Y.; Wang, R.; Al-Hartomy, O. A.; Al-Ghamdi, A.; Wageh, S.; Luo, X.; Tang, X.; Zhang, H. Synthesis of Ti3C2Fx MXene with controllable fluorination by electrochemical etching for lithium-ion batteries applications. *Ceram. Int.* **2021**, *47* (20), 28642−28649.

(134) Lukatskaya, M. R.; Halim, J.; Dyatkin, B.; Naguib, M.; Buranova, Y. S.; Barsoum, M. W.; Gogotsi, Y. Room-Temperature Carbide-Derived Carbon Synthesis by Electrochemical Etching of MAX Phases. *Angew. Chem., Int. Ed.* **2014**, *53* (19), 4877−4880.

(135) Pang, S.-Y.; Wong, Y.-T.; Yuan, S.; Liu, Y.; Tsang, M.-K.; Yang, Z.; Huang, H.; Wong, W.-T.; Hao, J. Universal Strategy for HF-Free Facile and Rapid Synthesis of Two-dimensional MXenes as Multifunctional Energy Materials. *J. Am. Chem. Soc.* **2019**, *141* (24), 9610−9616.

(136) Cao, Y.; Guo, C.; Zou, Y. Rapid synthesis of MXenes at room temperature. *Mater. Sci. Technol.* **2019**, *35* (15), 1904−1907.
(137) Zhao, L.; Wang, Z.; Li, Y.; Wang, S.; Wang, L.; Qi, Z.; Ge, Q.; Liu, X.; Zhang, J. Z. Designed synthesis of chlorine and nitrogen co-doped Ti3C2MXene quantum dots and their outstanding hydroxyl radical scavenging properties. *Journal of Materials Science & Technology* **2021**, *78*, 30−37.
(138) Mai, Y. J.; Li, Y. G.; Li, S. L.; Zhang, L. Y.; Liu, C. S.; Jie, X. H. Self-lubricating Ti3C2 nanosheets/copper composite coatings. *J. Alloys Compd.* **2019**, *770*, 1−5.
(139) Nouseen, S.; Ghosh, K.; Pumera, M. 3D printing of MAX/PLA filament: Electrochemical in-situ etching for enhanced energy conversion and storage. *Electrochem. Commun.* **2024**, *160*, No. 107652.
(140) Yao, Y.; Han, Y.; Wang, Z.; Li, Z.; Zhu, Z. Controlled etching of MXene for highly selective triethylamine detection at room temperature. *Sens. Actuators, B* **2024**, *402*, No. 135078.
(141) Hu, J.; Liang, C.; Li, J.; Lin, C.; Liang, Y.; Wang, H.; Li, X.; Wang, Q.; Dong, D. Lewis acidic molten salts etching route driven construction of double-layered MXene-Fe/carbon nanotube/silicone rubber composites for high-performance microwave absorption. *Carbon* **2023**, *204*, 136−146.
(142) Zhou, H.; Tian, J.; Wang, R.; Zhan, D.; Liu, P.; Chen, R.; Huang, Y.; Liu, Z.; Han, C. Lewis acid molten salts prepared Ti3C2Cl2MXenes assembling with g-C3N4 nanosheets for enhanced photocatalytic H2 evolution. *Ceram. Int.* **2023**, *49* (8), 13042−13049.
(143) Liu, X.; Li, Y.; Ding, H.; Chen, L.; Du, S.; Chai, Z.; Huang, Q. Topotactic transition of Ti4AlN3MAX phase in Lewis acid molten salt. *Journal of Materiomics* **2023**, *9* (6), 1032−1038.
(144) Liu, L.; Raymundo-Piñero, E.; Taberna, P.-L.; Simon, P. Electrochemical characterization of Ti3C2Tx MXene prepared via a molten salt etching route in an acetonitrile-based electrolyte. *Electrochem. Commun.* **2023**, *148*, No. 107453.
(145) Zheng, W.; Yang, Z.; Chen, J.; He, W.; Qin, R.; Zu, H.; Qu, W.; Yang, J.; Leng, L.; Li, H. Copper selenide anchored on Ti3C2MXene via Lewis acidic etching route for efficient removal of gaseous elemental mercury. *Fuel* **2024**, *356*, No. 129636.
(146) Wang, Y.; Gu, H.; Lu, Y.; Zhang, W.; Li, Z. The synergistic effect of Lewis acidic etching V4C3(MXene)@CuSe2/CoSe2 as an advanced cathode material for aluminum batteries. *Journal of Materials Science & Technology* **2024**, *177*, 205−213.
(147) Gong, S.; Liu, H.; Zhao, F.; Zhang, Y.; Xu, H.; Li, M.; Qi, J.; Wang, H.; Li, C.; Peng, W.; et al. Vertically Aligned Bismuthene Nanosheets on MXene for High-Performance Capacitive Deionization. *ACS Nano* **2023**, *17* (5), 4843−4853.
(148) Liu, L.; Zschiesche, H.; Antonietti, M.; Daffos, B.; Tarakina, N. V.; Gibilaro, M.; Chamelot, P.; Massot, L.; Duployer, B.; Taberna, P.-L.; et al. Tuning the Surface Chemistry of MXene to Improve Energy Storage: Example of Nitrification by Salt Melt. *Adv. Energy Mater.* **2023**, *13* (2), No. 2202709.
(149) Chen, J.; Jin, Q.; Li, Y.; Shao, H.; Liu, P.; Liu, Y.; Taberna, P.-L.; Huang, Q.; Lin, Z.; Simon, P. Molten Salt-Shielded Synthesis (MS3) of MXenes in Air. *ENERGY & ENVIRONMENTAL MATERIALS* **2023**, *6* (2), No. e12328.
(150) Tang, Q.; Xiong, P.; Wang, H.; Wu, Z. Boosted CO2 photoreduction performance on Ru-Ti3CN MXene-TiO2 photocatalyst synthesized by non-HF Lewis acidic etching method. *J. Colloid Interface Sci.* **2022**, *619*, 179−187.
(151) Wu, Z.; Zhu, S.; Bai, X.; Liang, M.; Zhang, X.; Zhao, N.; He, C. One-step in-situ synthesis of Sn-nanoconfined Ti3C2Tx MXene composites for Li-ion battery anode. *Electrochim. Acta* **2022**, *407*, No. 139916.
(152) Wang, Y.; Lv, W.; Wu, G.; Zhang, W.; Li, Z. Lewis metal salt synthesis of V2C (MXene) composite nickel diselenide as a high-performance cathode material for secondary aluminum batteries. *Appl. Surf. Sci.* **2023**, *637*, No. 157911.
(153) Ren, F.; Lu, Z.; Liu, X.; Wang, T.; Huang, X.; Dou, J.; Wu, D.; Yu, J.; Chen, X. Lewis acid-etched MXene self-assembled with reduced graphene oxide for symmetrical supercapacitors with liquid/ solid electrolytes. *J. Alloys Compd.* **2024**, *978*, No. 173480.
(154) Cui, Z.; Zhao, P.; Wang, H.; Li, C.; Peng, W.; Fan, X.; Liu, J. Molten salts etching strategy construct alloy/MXene heterostructures for efficient ammonia synthesis and energy supply via Zn-nitrite battery. *Applied Catalysis B: Environment and Energy* **2024**, *348*, No. 123862.
(155) Arole, K.; Blivin, J. W.; Saha, S.; Holta, D. E.; Zhao, X.; Sarmah, A.; Cao, H.; Radovic, M.; Lutkenhaus, J. L.; Green, M. J. Water-dispersible Ti3C2Tz MXene nanosheets by molten salt etching. *iScience* **2021**, *24* (12), No. 103403.
(156) Wu, M.; Wang, B.; Hu, Q.; Wang, L.; Zhou, A. The Synthesis Process and Thermal Stability of V2C MXene. *Materials* **2018**, *11* (11), 2112.
(157) Lokhande, P. E.; Pakdel, A.; Pathan, H. M.; Kumar, D.; Vo, D.-V. N.; Al-Gheethi, A.; Sharma, A.; Goel, S.; Singh, P. P.; Lee, B.-K. Prospects of MXenes in energy storage applications. *Chemosphere* **2022**, *297*, No. 134225.
(158) Fatheema, J.; Akinwande, D.; Rizwan, S. 10 - Two-dimensional transition metal carbide (MXene) for enhanced energy storage. In *Metal Oxide-Carbon Hybrid Materials*; Chaudhry, M. A., Hussain, R., Butt, F. K., Eds.; Elsevier, 2022; pp 255−283.
(159) Khazaei, M.; Ranjbar, A.; Arai, M.; Sasaki, T.; Yunoki, S. Electronic properties and applications of MXenes: a theoretical review. *Journal of Materials Chemistry C* **2017**, *5* (10), 2488−2503.
(160) Sarycheva, A.; Gogotsi, Y. Raman Spectroscopy Analysis of the Structure and Surface Chemistry of Ti3C2Tx MXene. *Chem. Mater.* **2020**, *32* (8), 3480−3488.
(161) Ronchi, R. M.; Arantes, J. T.; Santos, S. F. Synthesis, structure, properties and applications of MXenes: Current status and perspectives. *Ceram. Int.* **2019**, *45* (15), 18167−18188.
(162) Liu, Y.; Xiao, H.; Goddard, W. A., III Schottky-Barrier-Free Contacts with Two-Dimensional Semiconductors by Surface-Engineered MXenes. *J. Am. Chem. Soc.* **2016**, *138* (49), 15853−15856.
(163) Luo, J.; Tao, X. Interfacial structure design of MXene-based nanomaterials for supercapacitors and batteries. In *Encyclopedia of Nanomaterials*, 1st ed.; Yin, Y., Lu, Y., Xia, Y., Eds.; Elsevier, 2023; pp 558−577.
(164) (a) Wang, L.; Han, M.; Shuck, C. E.; Wang, X.; Gogotsi, Y. Adjustable electrochemical properties of solid-solution MXenes. *Nano Energy* **2021**, *88*, No. 106308. (b) Hong, W.; Wyatt, B. C.; Nemani, S. K.; Anasori, B. Double transition-metal MXenes: Atomistic design of two-dimensional carbides and nitrides. *MRS Bull.* **2020**, *45* (10), 850−861. (c) Hu, Y.; Fan, X. L.; Guo, W. J.; An, Y. R.; Luo, Z. F.; Kong, J. Ordered double-M elements MXenes TiMC: Large in-plane stiffness and ferromagnetism. *J. Magn. Magn. Mater.* **2019**, *486*, No. 165280. (d) Lind, H.; Wickman, B.; Halim, J.; Montserrat-Sisó, G.; Hellman, A.; Rosen, J. Hydrogen Evolution Reaction for Vacancy-Ordered i-MXenes and the Impact of Proton Absorption into the Vacancies. *Advanced Sustainable Systems* **2021**, *5* (2), No. 2000158. (e) Halim, J.; Palisaitis, J.; Lu, J.; Thörnberg, J.; Moon, E. J.; Precner, M.; Eklund, P.; Persson, P. O. Å.; Barsoum, M. W.; Rosen, J. Synthesis of Two-Dimensional Nb1.33C (MXene) with Randomly Distributed Vacancies by Etching of the Quaternary Solid Solution (Nb2/3Sc1/3)2AlC MAX Phase. *ACS Applied Nano Materials* **2018**, *1* (6), 2455−2460.
(165) Liu, Z.; Wu, E.; Wang, J.; Qian, Y.; Xiang, H.; Li, X.; Jin, Q.; Sun, G.; Chen, X.; Wang, J.; et al. Crystal structure and formation mechanism of (Cr2/3Ti1/3)3AlC2MAX phase. *Acta Mater.* **2014**, *73*, 186−193.
(166) Li, Y.; Vallem, S.; Bae, J. MXene-based composites for high-performance and fire-safe lithium-ion battery. *Curr. Appl. Phys.* **2023**, *53*, 142−164.
(167) Guo, Y.; Zhou, X.; Wang, D.; Xu, X.; Xu, Q. Nanomechanical Properties of Ti3C2Mxene. *Langmuir* **2019**, *35* (45), 14481−14485.
(168) Anasori, B.; Gogotsi, Y. Introduction to 2D transition metal carbides and nitrides (MXenes). *2D Metal Carbides and Nitrides (MXenes) Structure, Properties and Applications* **2019**, 3−12.
(169) Berdiyorov, G. Optical properties of functionalized Ti3C2T2 (T= F, O, OH) MXene: First-principles calculations. *AIP Adv.* **2016**, *6* (5), 055105.
(170) Halim, J.; Persson, I.; Moon, E. J.; Kühne, P.; Darakchieva, V.; Persson, P. O. Å.; Eklund, P.; Rosen, J.; Barsoum, M. W. Electronic and

optical characterization of 2D Ti2C and Nb2C (MXene) thin films. *J. Phys.: Condens. Matter* **2019**, *31* (16), No. 165301.
(171) Li, R.; Zhang, L.; Shi, L.; Wang, P. MXene Ti3C2: an effective 2D light-to-heat conversion material. *ACS Nano* **2017**, *11* (4), 3752−3759.
(172) Jiang, X.; Liu, S.; Liang, W.; Luo, S.; He, Z.; Ge, Y.; Wang, H.; Cao, R.; Zhang, F.; Wen, Q.; et al. Broadband nonlinear photonics in few-layer MXene Ti3C2Tx (T= F, O, or OH). *Laser Photon. Rev.* **2018**, *12* (2), No. 1700229.
(173) Papadopoulou, K. A.; Chroneos, A.; Parfitt, D.; Christopoulos, S.-R. G. A perspective on MXenes: Their synthesis, properties, and recent applications. *J. Appl. Phys.* **2020**, *128* (17), 170902.
(174) Hantanasirisakul, K.; Gogotsi, Y. Electronic and optical properties of 2D transition metal carbides and nitrides (MXenes). *Adv. Mater.* **2018**, *30* (52), No. 1804779.
(175) Gao, L.; Chen, H.; Kuklin, A. V.; Wageh, S.; Al-Ghamdi, A. A.; Ågren, H.; Zhang, H. Optical Properties of Few-Layer Ti3CN MXene: From Experimental Observations to Theoretical Calculations. *ACS Nano* **2022**, *16* (2), 3059−3069.
(176) Muhammed, M. M.; Mokkath, J. H. Surface termination dependent optical characteristics of MXene nanoflakes. *Materials Today Chemistry* **2023**, *29*, No. 101447.
(177) Wang, X.-Y.; Liao, S.-Y.; Huang, H.-P.; Wang, Q.-F.; Shi, Y.-Y.; Zhu, P.-L.; Hu, Y.-G.; Sun, R.; Wan, Y.-J. Enhancing the Chemical Stability of MXene Through Synergy of Hydrogen Bond and Coordination Bond in Aqueous Solution. *Small Methods* **2023**, *7* (4), No. 2201694.
(178) Zhang, Y.; Zha, X.-H.; Luo, K.; Qiu, N.; Zhou, Y.; He, J.; Chai, Z.; Huang, Z.; Huang, Q.; Liang, Y.; et al. Tuning the Electrical Conductivity of Ti2CO2MXene by Varying the Layer Thickness and Applying Strains. *J. Phys. Chem. C* **2019**, *123* (11), 6802−6811.
(179) Liu, M.-Z.; Li, X.-H.; Yan, H.-T.; Zhang, R.-Z.; Cui, H.-L. Influence of N-doped concentration on the electronic properties and quantum capacitance of Hf2CO2MXene. *Vacuum* **2023**, *210*, No. 111826.
(180) Sanjeev; Singh, M.; Kumar, R.; Srivastava, S.; Tankeshwar, K. Non-trivial topological crossover in functionalized AlBi monolayer. *Chem. Phys. Lett.* **2023**, *816*, No. 140388.
(181) Zhao, S.; Kang, W.; Xue, J. Manipulation of electronic and magnetic properties of M2C (M= Hf, Nb, Sc, Ta, Ti, V, Zr) monolayer by applying mechanical strains. *Appl. Phys. Lett.* **2014**, *104* (13), 133106.
(182) Gao, G.; Ding, G.; Li, J.; Yao, K.; Wu, M.; Qian, M. Monolayer MXenes: promising half-metals and spin gapless semiconductors. *Nanoscale* **2016**, *8* (16), 8986−8994.
(183) Si, C.; Zhou, J.; Sun, Z. Half-Metallic Ferromagnetism and Surface Functionalization-Induced Metal−Insulator Transition in Graphene-like Two-Dimensional Cr2C Crystals. *ACS Appl. Mater. Interfaces* **2015**, *7* (31), 17510−17515.
(184) Yang, J.; Luo, X.; Zhang, S.; Chen, L. Investigation of magnetic and electronic properties of transition metal doped Sc 2 CT 2 (T= O, OH or F) using a first principles study. *Phys. Chem. Chem. Phys.* **2016**, *18* (18), 12914−12919.
(185) Ao, L.; Pham, A.; Zu, X. T.; Li, S. Engineering the electronic and magnetic properties of Sc2CF2MXene material through vacancy doping and lattice straining. *Mater. Sci. Forum* **2017**, *900*, 61−64.
(186) Yue, Y. Fe2C monolayer: An intrinsic ferromagnetic MXene. *J. Magn. Magn. Mater.* **2017**, *434*, 164−168.
(187) Bandyopadhyay, A.; Ghosh, D.; Pati, S. K. Effects of point defects on the magnetoelectronic structures of MXenes from first principles. *Phys. Chem. Chem. Phys.* **2018**, *20* (6), 4012−4019.
(188) Zhao, S.; Kang, W.; Xue, J. Manipulation of electronic and magnetic properties of M2C (M = Hf, Nb, Sc, Ta, Ti, V, Zr) monolayer by applying mechanical strains. *Appl. Phys. Lett.* **2014**, *104* (13), 133106 DOI: 10.1063/1.4870515.
(189) Paul, P.; Chakraborty, P.; Das, T.; Nafday, D.; Saha-Dasgupta, T. Properties at the interface of graphene and ${\mathrm{Ti}}_{2}\mathrm{C}$ MXene. *Phys. Rev. B* **2017**, *96* (3), No. 035435.
(190) (a) Iqbal, M.; Fatheema, J.; Noor, Q.; Rani, M.; Mumtaz, M.; Zheng, R.-K.; Khan, S. A.; Rizwan, S. Co-existence of magnetic phases in two-dimensional MXene. *Materials Today Chemistry* **2020**, *16*, No. 100271. (b) Zhou, Y.; Yu, M.; Liang, H.; Chen, J.; Xu, L.; Niu, J. Novel dual-effective Z-scheme heterojunction with g-C3N4, Ti3C2M-Xene and black phosphorus for improving visible light-induced degradation of ciprofloxacin. *Applied Catalysis B: Environmental* **2021**, *291*, No. 120105.
(191) Zhang, Y.; Li, F. Robust half-metallic ferromagnetism in Cr3C2MXene. *J. Magn. Magn. Mater.* **2017**, *433*, 222−226.
(192) Hu, Y.; Liu, X. Y.; Shen, Z. H.; Luo, Z. F.; Chen, Z. G.; Fan, X. L. High Curie temperature and carrier mobility of novel Fe, Co and Ni carbide MXenes. *Nanoscale* **2020**, *12* (21), 11627−11637.
(193) Ketolainen, T.; Karlický, F. Optical gaps and excitons in semiconducting transition metal carbides (MXenes). *Journal of Materials Chemistry C* **2022**, *10* (10), 3919−3928.
(194) Li, Y.-L.; Lv, P. First-principles study on the electric field manipulation of the magnetic property and the electronic structures for monolayer Fe2C MXene. *Phys. Lett. A* **2021**, *386*, No. 126960.
(195) Wang, P.; Liu, Q.; Liu, N.; Kuang, M.; Yang, T.; Wang, B.; Ju, M.; Yuan, H.; Jiang, X.; Zhao, J. Electric Field-Controlled Magneto-Optical Kerr Effect in A-Type Antiferromagnetic Fe2CX2 (X = F, Cl) and Its Janus Monolayer. *ACS Appl. Mater. Interfaces* **2023**, *15* (45), 52767−52775.
(196) Zhang, X.; He, T.; Meng, W.; Jin, L.; Li, Y.; Dai, X.; Liu, G. Mn2C Monolayer: Hydrogenation/Oxygenation-Induced Strong Ferromagnetism and Potential Applications. *J. Phys. Chem. C* **2019**, *123* (26), 16388−16392.
(197) Kumar, H.; Frey, N. C.; Dong, L.; Anasori, B.; Gogotsi, Y.; Shenoy, V. B. Tunable Magnetism and Transport Properties in Nitride MXenes. *ACS Nano* **2017**, *11* (8), 7648−7655.
(198) Lian-Yan, W.; Qian, Y.; Cheng-Cai, H.; Ling-Ling, H.; Yang, W.; Deng-Feng, L.; Jun, L. Tunable magnetic and electronic properties of two intrinsic half-metallic MXene monolayers Sc2Na2CNC and Sc2K2CNC. *Vacuum* **2024**, *219*, No. 112707.
(199) Li, Y.-L.; Lv, P. The tuning on the magnetism and the electronic structures of monolayer Ti2N MXene by electric field. *Physica B: Condensed Matter* **2021**, *618*, No. 413183.
(200) Zhong, S.; Xu, B.; Cui, A.; Li, S.; Liao, S.; Wang, G.; Liu, G.; Sun, B. Robust Net Magnetic Moment in Janus V-Based Nitride MXenes: Insight from First-Principles Calculations. *ACS Omega* **2020**, *5* (1), 864−870.
(201) Zhang, Y.; Cui, Z.; Sa, B.; Miao, N.; Zhou, J.; Sun, Z. Computational design of double transition metal MXenes with intrinsic magnetic properties. *Nanoscale Horizons* **2022**, *7* (3), 276−287.
(202) Özcan, S.; Biel, B. Exploring a novel class of Janus MXenes by first principles calculations: structural, electronic and magnetic properties of Sc2CXT, X = O, F, OH; T = C, S, N. *Phys. Chem. Chem. Phys.* **2023**, *25* (3), 1881−1888.
(203) Li, P.; Wu, C.; Peng, C.; Yang, M.; Xun, W. Multifield tunable valley splitting in two-dimensional MXene ${\mathrm{Cr}}_{2}\mathrm{COOH}$. *Phys. Rev. B* **2023**, *108* (19), No. 195424.
(204) Jun, L.; Cheng-Cai, H.; Yang, W.; qian, Y.; Lian-Yan, W.; Deng-Feng, L. A promising robust intrinsic half-metallic MXene nanosheet Cr2CuC2 with high Curie temperature. *Physica E: Low-dimensional Systems and Nanostructures* **2022**, *143*, No. 115276.
(205) Yao, Q.; Wang, L.-Y.; Huang, C.-C.; Huang, H.-Y.; Wang, Y.; Li, D.-F.; Liu, J. A Promising Intrinsic Half-Metallic MXene Nanosheet Sc2Li2N3: the First-Principles Study. *Journal of Superconductivity and Novel Magnetism* **2022**, *35* (12), 3727−3734.
(206) Cheng-Cai, H.; Yang, W.; Qian, Y.; Deng-Feng, L.; Jun, L. MXene monolayer Mn2ZnN2: a promising robust intrinsic half-metallic nanosheet. *J. Phys.: Condens. Matter* **2022**, *34* (10), No. 105301.
(207) Yang, W.; Lian-Yan, W.; Cheng-Cai, H.; qian, Y.; Deng-Feng, L.; Jun, L. A Promising Half-Metallic MXene Monolayer Ti2ZnC2 Induced by the Charge States. *Journal of Superconductivity and Novel Magnetism* **2022**, *35* (7), 2127−2134.

(208) Zhang, R.-Z.; Cui, X.-H.; Cui, H.-L.; Li, X.-H. First-principles study of structural, electronic and magnetic properties of transition metal doped Sc2CF2MXene. *Appl. Surf. Sci.* **2022**, *581*, No. 152360.
(209) Balcı, E.; Akkuş, Ü. Ö.; Berber, S. Band gap modification in doped MXene: Sc2CF2. *Journal of Materials Chemistry C* **2017**, *5* (24), 5956−5961.
(210) Zha, X.-H.; Huang, Q.; He, J.; He, H.; Zhai, J.; Francisco, J. S.; Du, S. The thermal and electrical properties of the promising semiconductor MXene Hf2CO2. *Sci. Rep.* **2016**, *6* (1), No. 27971.
(211) Guo, J.; Sun, Y.; Liu, B.; Zhang, Q.; Peng, Q. Two-dimensional scandium-based carbides (MXene): Band gap modulation and optical properties. *J. Alloys Compd.* **2017**, *712*, 752−759.
(212) Limbu, Y.; Kaphle, G. C.; Karn, A. L.; Shah, N. K.; Paudyal, H.; Paudyal, D. Electronic structure and magnetism of pristine, defected, and strained Ti2N MXene. *J. Magn. Magn. Mater.* **2022**, *563*, No. 169895.
(213) Liu, M.-Z.; Li, X.-H.; Cui, X.-H.; Yan, H.-T.; Zhang, R.-Z.; Cui, H.-L. The influence of different functional groups on quantum capacitance, electronic and optical properties of Hf2C MXene. *Appl. Surf. Sci.* **2022**, *605*, No. 154830.
(214) Frey, N. C.; Bandyopadhyay, A.; Kumar, H.; Anasori, B.; Gogotsi, Y.; Shenoy, V. B. Surface-Engineered MXenes: Electric Field Control of Magnetism and Enhanced Magnetic Anisotropy. *ACS Nano* **2019**, *13* (3), 2831−2839.
(215) Siriwardane, E. M. D.; Karki, P.; Loh, Y. L.; Çakır, D. Strain−Spintronics: Modulating Electronic and Magnetic Properties of Hf2MnC2O2MXene by Uniaxial Strain. *J. Phys. Chem. C* **2019**, *123* (19), 12451−12459.
(216) Li, S.-s.; Hu, S.-j.; Ji, W.-x.; Li, P.; Zhang, K.; Zhang, C.-w.; Yan, S.-s. Emergence of ferrimagnetic half-metallicity in two-dimensional MXene Mo3N2F2. *Appl. Phys. Lett.* **2017**, *111* (20), 202405 DOI: 10.1063/1.4993869.
(217) Yang, J.; Luo, X.; Zhou, X.; Zhang, S.; Liu, J.; Xie, Y.; Lv, L.; Chen, L. Tuning magnetic properties of Cr2M2C3T2 (M = Ti and V) using extensile strain. *Comput. Mater. Sci.* **2017**, *139*, 313−319.
(218) Zha, X.-H.; Ren, J.-C.; Feng, L.; Bai, X.; Luo, K.; Zhang, Y.; He, J.; Huang, Q.; Francisco, J. S.; Du, S. Bipolar magnetic semiconductors among intermediate states during the conversion from Sc2C(OH)2 to Sc2CO2MXene. *Nanoscale* **2018**, *10* (18), 8763−8771.
(219) Mateen, A.; Ansari, M. Z.; Hussain, I.; Eldin, S. M.; Albaqami, M. D.; Bahajjaj, A. A. A.; Javed, M. S.; Peng, K.-Q. Ti2CTx−MXene aerogel based ultra−stable Zn−ion supercapacitor. *Composites Communications* **2023**, *38*, No. 101493.
(220) Ansari, M. Z.; Seo, K.-M.; Kim, S.-H.; Ansari, S. A. Critical Aspects of Various Techniques for Synthesizing Metal Oxides and Fabricating Their Composite-Based Supercapacitor Electrodes: A Review. *Nanomaterials* **2022**, *12*, 1873.
(221) Zhang, Y.; Feng, Z.; Wang, X.; Hu, H.; Wu, M. MXene/carbon composites for electrochemical energy storage and conversion. *Materials Today Sustainability* **2023**, *22*, No. 100350.
(222) Liu, N.; Li, W.; Pasta, M.; Cui, Y. Nanomaterials for electrochemical energy storage. *Frontiers of Physics* **2014**, *9* (3), 323−350.
(223) Qiao, C.; Wu, H.; Xu, X.; Guan, Z.; Ou-Yang, W. Electrical Conductivity Enhancement and Electronic Applications of 2D Ti3C2Tx MXene Materials. *Advanced Materials Interfaces* **2021**, *8* (24), No. 2100903.
(224) Zhang, Q.; Li, W.; Zhao, R.; Tang, P.; Zhao, J.; Wu, G.; Chen, X.; Hu, M.; Yuan, K.; Li, J.; et al. Real-time observation of two distinctive non-thermalized hot electron dynamics at MXene/molecule interfaces. *Nat. Commun.* **2024**, *15* (1), 4406.
(225) Bilibana, M. P. Electrochemical properties of MXenes and applications. *Advanced Sensor and Energy Materials* **2023**, *2* (4), No. 100080.
(226) Liang, K.; Matsumoto, R. A.; Zhao, W.; Osti, N. C.; Popov, I.; Thapaliya, B. P.; Fleischmann, S.; Misra, S.; Prenger, K.; Tyagi, M.; et al. Engineering the Interlayer Spacing by Pre-Intercalation for High Performance Supercapacitor MXene Electrodes in Room Temperature Ionic Liquid. *Adv. Funct. Mater.* **2021**, *31* (33), No. 2104007.
(227) Hussain, I.; Lamiel, C.; Javed, M. S.; Ahmad, M.; Sahoo, S.; Chen, X.; Qin, N.; Iqbal, S.; Gu, S.; Li, Y.; et al. MXene-based heterostructures: Current trend and development in electrochemical energy storage devices. *Prog. Energy Combust. Sci.* **2023**, *97*, No. 101097.
(228) Li, L.; Wen, J.; Zhang, X. Progress of Two-Dimensional Ti3C2Tx in Supercapacitors. *ChemSusChem* **2020**, *13* (6), 1296−1329.
(229) Salim, O.; Mahmoud, K. A.; Pant, K. K.; Joshi, R. K. Introduction to MXenes: synthesis and characteristics. *Materials Today Chemistry* **2019**, *14*, No. 100191.
(230) Zhang, C.; Wang, L.; Lei, W.; Wu, Y.; Li, C.; Khan, M. A.; Ouyang, Y.; Jiao, X.; Ye, H.; Mutahir, S.; et al. Achieving quick charge/discharge rate of 3.0 V s−1 by 2D titanium carbide (MXene) via N-doped carbon intercalation. *Mater. Lett.* **2019**, *234*, 21−25.
(231) Wu, Y.; Yu, Y. 2D material as anode for sodium ion batteries: Recent progress and perspectives. *Energy Storage Materials* **2019**, *16*, 323−343.
(232) Yoo, R.; Pranada, E.; Johnson, D.; Qiao, Z.; Djire, A. Review—The Oxygen Reduction Reaction on MXene-Based Catalysts: Progress and Prospects. *J. Electrochem. Soc.* **2022**, *169* (6), No. 063513.
(233) Rhouati, A.; Berkani, M.; Vasseghian, Y.; Golzadeh, N. MXene-based electrochemical sensors for detection of environmental pollutants: A comprehensive review. *Chemosphere* **2022**, *291*, No. 132921.
(234) Solangi, N. H.; Mubarak, N. M.; Karri, R. R.; Mazari, S. A.; Kailasa, S. K.; Alfantazi, A. Applications of advanced MXene-based composite membranes for sustainable water desalination. *Chemosphere* **2023**, *314*, No. 137643.
(235) Jamil, F.; Ali, H. M.; Janjua, M. M. MXene based advanced materials for thermal energy storage: A recent review. *Journal of Energy Storage* **2021**, *35*, No. 102322.
(236) Aslfattahi, N.; Saidur, R.; Arifutzzaman, A.; Sadri, R.; Bimbo, N.; Sabri, M. F. M.; Maughan, P. A.; Bouscarrat, L.; Dawson, R. J.; Said, S. M.; et al. Experimental investigation of energy storage properties and thermal conductivity of a novel organic phase change material/MXene as A new class of nanocomposites. *Journal of Energy Storage* **2020**, *27*, No. 101115.
(237) Lu, X.; Huang, H.; Zhang, X.; Lin, P.; Huang, J.; Sheng, X.; Zhang, L.; Qu, J.-p. Novel light-driven and electro-driven polyethylene glycol/two-dimensional MXene form-stable phase change material with enhanced thermal conductivity and electrical conductivity for thermal energy storage. *Composites Part B: Engineering* **2019**, *177*, No. 107372.
(238) Cao, Y.; Li, W.; Huang, D.; Zhang, J.; Lin, P.; Zhang, L.; Sheng, X.; Chen, Y.; Lu, X. One-step construction of novel phase change composites supported by a biomass/MXene gel network for efficient thermal energy storage. *Sol. Energy Mater. Sol. Cells* **2022**, *241*, No. 111729.
(239) Mo, S.; Xiao, B.; Mo, B.; Chen, J.; Jia, L.; Wang, Z.; Chen, Y. Improving the Thermal and Photothermal Performances of MXene-Doped Microencapsulated Molten Salts for Medium-Temperature Solar Thermal Energy Storage. *Energy Fuels* **2023**, *37* (10), 7490−7500.
(240) Huang, D.; Wang, Z.; Sheng, X.; Chen, Y. Bio-based MXene hybrid aerogel/paraffin composite phase change materials with superior photo and electrical responses toward solar thermal energy storage. *Sol. Energy Mater. Sol. Cells* **2023**, *251*, No. 112124.
(241) Quan, B.; Wang, J.; Li, Y.; Sui, M.; Xie, H.; Liu, Z.; Wu, H.; Lu, X.; Tong, Y. Cellulose nanofibrous/MXene aerogel encapsulated phase change composites with excellent thermal energy conversion and storage capacity. *Energy* **2023**, *262*, No. 125505.
(242) Gao, Y.; Tang, Z.; Chen, X.; Yan, J.; Jiang, Y.; Xu, J.; Tao, Z.; Wang, L.; Liu, Z.; Wang, G. Magnetically accelerated thermal energy storage within Fe3O4-anchored MXene-based phase change materials. *Aggregate* **2023**, *4* (1), No. e248.
(243) Borysiuk, V. N.; Mochalin, V. N.; Gogotsi, Y. Molecular dynamic study of the mechanical properties of two-dimensional titanium carbides Tin+ 1Cn (MXenes). *Nanotechnology* **2015**, *26* (26), No. 265705.

(244) Lipatov, A.; Lu, H.; Alhabeb, M.; Anasori, B.; Gruverman, A.; Gogotsi, Y.; Sinitskii, A. Elastic properties of 2D Ti3C2Tx MXene monolayers and bilayers. *Sci. Adv.* **2018**, *4*, No. eaat0491.
(245) Wang, H.; Wu, Y.; Yuan, X.; Zeng, G.; Zhou, J.; Wang, X.; Chew, J. W. Clay-inspired MXene-based electrochemical devices and photo-electrocatalyst: state-of-the-art progresses and challenges. *Adv. Mater.* **2018**, *30* (12), No. 1704561.
(246) Zha, X.-H.; Zhou, J.; Zhou, Y.; Huang, Q.; He, J.; Francisco, J. S.; Luo, K.; Du, S. Promising electron mobility and high thermal conductivity in Sc 2 CT 2 (T= F, OH) MXenes. *Nanoscale* **2016**, *8* (11), 6110−6117.
(247) Ling, Z.; Ren, C. E.; Zhao, M.-Q.; Yang, J.; Giammarco, J. M.; Qiu, J.; Barsoum, M. W.; Gogotsi, Y. Flexible and conductive MXene films and nanocomposites with high capacitance. *Proc. Natl. Acad. Sci. U. S. A.* **2014**, *111* (47), 16676−16681.
(248) Wan, Y.-J.; Li, X.-M.; Zhu, P.-L.; Sun, R.; Wong, C.-P.; Liao, W.-H. Lightweight, flexible MXene/polymer film with simultaneously excellent mechanical property and high-performance electromagnetic interference shielding. *Composites Part A: Applied Science and Manufacturing* **2020**, *130*, No. 105764.
(249) Kilikevičius, S.; Kvietkaitė, S.; Žukienė, K.; Omastová, M.; Aniskevich, A.; Zeleniakienė, D. Numerical investigation of the mechanical properties of a novel hybrid polymer composite reinforced with graphene and MXene nanosheets. *Comput. Mater. Sci.* **2020**, *174*, No. 109497.
(250) Yorulmaz, U.; Özden, A.; Perkgöz, N. K.; Ay, F.; Sevik, C. Vibrational and mechanical properties of single layer MXene structures: a first-principles investigation. *Nanotechnology* **2016**, *27* (33), No. 335702.
(251) Guo, Z.; Zhou, J.; Si, C.; Sun, Z. Flexible two-dimensional Tin+1Cn (n= 1, 2 and 3) and their functionalized MXenes predicted by density functional theories. *Phys. Chem. Chem. Phys.* **2015**, *17* (23), 15348−15354.
(252) Grutzmacher, P. G.; Suarez, S.; Tolosa, A.; Gachot, C.; Song, G.; Wang, B.; Presser, V.; Mücklich, F.; Anasori, B.; Rosenkranz, A. Superior wear-resistance of Ti3C2T x multilayer coatings. *ACS Nano* **2021**, *15* (5), 8216−8224.
(253) Zhao, X.; Cao, H.; Coleman, B. J.; Tan, Z.; Echols, I. J.; Pentzer, E. B.; Lutkenhaus, J. L.; Radovic, M.; Green, M. J. The Role of Antioxidant Structure in Mitigating Oxidation in Ti3C2Tx and Ti2CTx MXenes. *Advanced Materials Interfaces* **2022**, *9* (20), No. 2200480.
(254) Fan, B.; Zhao, X.; Zhang, P.; Wei, Y.; Qiao, N.; Yang, B.; Soomro, R. A.; Zhang, R.; Xu, B. Effect of Sodium Dodecyl Sulfate on Stability of MXene Aqueous Dispersion. *Adv. Sci.* **2023**, *10*, No. 2300273.
(255) Ning, Y.; Jian, D.; Liu, S.; Chen, F.; Song, Y.; Li, S.; Liu, B. Designing a Ti3C2Tx MXene with long-term antioxidant stability for high-performance anti-corrosion coatings. *Carbon* **2023**, *202*, 20−30.
(256) Nam, S.; Mahato, M.; Matthews, K.; Lord, R. W.; Lee, Y.; Thangasamy, P.; Ahn, C. W.; Gogotsi, Y.; Oh, I.-K. Bimetal Organic Framework−Ti3C2Tx MXene with Metalloporphyrin Electrocatalyst for Lithium−Oxygen Batteries. *Adv. Funct. Mater.* **2023**, *33* (1), No. 2210702.
(257) Iqbal, A.; Hong, J.; Ko, T. Y.; Koo, C. M. Improving oxidation stability of 2D MXenes: synthesis, storage media, and conditions. *Nano Convergence* **2021**, *8*, 9.
(258) Li, X.; Huang, Z.; Zhi, C. Environmental Stability of MXenes as Energy Storage Materials. *Front. Mater.* **2019**, *6*, No. 312.
(259) Wei, Y.; Xiang, L.; Ou, H.; Li, F.; Zhang, Y.; Qian, Y.; Hao, L.; Diao, J.; Zhang, M.; Zhu, P.; et al. MXene-Based Conductive Organohydrogels with Long-Term Environmental Stability and Multifunctionality. *Adv. Funct. Mater.* **2020**, *30* (48), No. 2005135.
(260) Wang, X.; Wang, X.; Yin, J.; Li, N.; Zhang, Z.; Xu, Y.; Zhang, L.; Qin, Z.; Jiao, T. Mechanically robust, degradable and conductive MXene-composited gelatin organohydrogel with environmental stability and self-adhesiveness for multifunctional sensor. *Composites Part B: Engineering* **2022**, *241*, No. 110052.
(261) Chen, H.; Wen, Y.; Qi, Y.; Zhao, Q.; Qu, L.; Li, C. Pristine Titanium Carbide MXene Films with Environmentally Stable Conductivity and Superior Mechanical Strength. *Adv. Funct. Mater.* **2020**, *30* (5), No. 1906996.
(262) Shekhirev, M.; Ogawa, Y.; Shuck, C. E.; Anayee, M.; Torita, T.; Gogotsi, Y. Delamination of Ti3C2Tx Nanosheets with NaCl and KCl for Improved Environmental Stability of MXene Films. *ACS Applied Nano Materials* **2022**, *5* (11), 16027−16032.
(263) Liu, L.-X.; Chen, W.; Zhang, H.-B.; Ye, L.; Wang, Z.; Zhang, Y.; Min, P.; Yu, Z.-Z. Super-Tough and Environmentally Stable Aramid. Nanofiber@MXene Coaxial Fibers with Outstanding Electromagnetic Interference Shielding Efficiency. *Nano-Micro Letters* **2022**, *14* (1), 111.
(264) Athavale, S.; Micci-Barreca, S.; Arole, K.; Kotasthane, V.; Blivin, J.; Cao, H.; Lutkenhaus, J. L.; Radovic, M.; Green, M. J. Advances in the Chemical Stabilization of MXenes. *Langmuir* **2023**, *39* (3), 918−928.
(265) Borodin, O.; Ren, X.; Vatamanu, J.; von Wald Cresce, A.; Knap, J.; Xu, K. Modeling Insight into Battery Electrolyte Electrochemical Stability and Interfacial Structure. *Acc. Chem. Res.* **2017**, *50* (12), 2886−2894.
(266) Borodin, O. Challenges with prediction of battery electrolyte electrochemical stability window and guiding the electrode − electrolyte stabilization. *Current Opinion in Electrochemistry* **2019**, *13*, 86−93.
(267) Lukatskaya, M. R.; Mashtalir, O.; Ren, C. E.; Dall'Agnese, Y.; Rozier, P.; Taberna, P. L.; Naguib, M.; Simon, P.; Barsoum, M. W.; Gogotsi, Y. Cation Intercalation and High Volumetric Capacitance of Two-Dimensional Titanium Carbide. *Science* **2013**, *341*, 1502−1505.
(268) Yaqoob, T.; Rani, M.; Mahmood, A.; Shafique, R.; Khan, S.; Janjua, N. K.; Shah, A. A.; Ahmad, A.; Al-Kahtani, A. A. MXene/Ag2CrO4 Nanocomposite as Supercapacitors Electrode. *Materials* **2021**, *14*, 6008.
(269) Ghidiu, M.; Lukatskaya, M. R.; Zhao, M.-Q.; Gogotsi, Y.; Barsoum, M. W. Conductive two-dimensional titanium carbide 'clay'with high volumetric capacitance. *Nature* **2014**, *516*, 78−81.
(270) Yang, C.; Tang, Y.; Tian, Y.; Luo, Y.; Faraz Ud Din, M.; Yin, X.; Que, W. Flexible Nitrogen-Doped 2D Titanium Carbides (MXene) Films Constructed by an Ex Situ Solvothermal Method with Extraordinary Volumetric Capacitance. *Adv. Energy Mater.* **2018**, *8* (31), No. 1802087.
(271) VahidMohammadi, A.; Mojtabavi, M.; Caffrey, N. M.; Wanunu, M.; Beidaghi, M. Assembling 2D MXenes into Highly Stable Pseudocapacitive Electrodes with High Power and Energy Densities. *Adv. Mater.* **2019**, *31* (8), No. 1806931.
(272) Shan, Q.; Mu, X.; Alhabeb, M.; Shuck, C. E.; Pang, D.; Zhao, X.; Chu, X.-F.; Wei, Y.; Du, F.; Chen, G.; et al. Two-dimensional vanadium carbide (V2C) MXene as electrode for supercapacitors with aqueous electrolytes. *Electrochem. Commun.* **2018**, *96*, 103−107.
(273) Wustoni, S.; Saleh, A.; El-Demellawi, J. K.; Koklu, A.; Hama, A.; Druet, V.; Wehbe, N.; Zhang, Y.; Inal, S. MXene improves the stability and electrochemical performance of electropolymerized PEDOT films. *APL Materials* **2020**, *8* (12), No. 121105.
(274) Lin, Z.; Barbara, D.; Taberna, P.-L.; Van Aken, K. L.; Anasori, B.; Gogotsi, Y.; Simon, P. Capacitance of Ti3C2Tx MXene in ionic liquid electrolyte. *J. Power Sources* **2016**, *326*, 575−579.
(275) Zheng, S.; Zhang, C.; Zhou, F.; Dong, Y.; Shi, X.; Nicolosi, V.; Wu, Z.-S.; Bao, X. Ionic liquid pre-intercalated MXene films for ionogel-based flexible micro-supercapacitors with high volumetric energy density. *Journal of Materials Chemistry A* **2019**, *7* (16), 9478−9485.
(276) Dall'Agnese, Y.; Rozier, P.; Taberna, P.-L.; Gogotsi, Y.; Simon, P. Capacitance of two-dimensional titanium carbide (MXene) and MXene/carbon nanotube composites in organic electrolytes. *J. Power Sources* **2016**, *306*, 510−515.
(277) Yadav, S.; Kurra, N. Diffusion kinetics of ionic charge carriers across Ti3C2Tx MXene-aqueous electrochemical interfaces. *Energy Storage Materials* **2024**, *65*, No. 103094.
(278) Sun, Z.; Ahmad, M.; Gao, Z.; Shan, Z.; Xu, L.; Wang, S.; Jin, Y. Highly ionic conductive and mechanically strong MXene/CNF membranes for osmotic energy conversion. *Sustainable Energy & Fuels* **2022**, *6* (2), 299−308.

(279) Dong, Y.; Shi, H.; Wu, Z.-S. Recent Advances and Promise of MXene-Based Nanostructures for High-Performance Metal Ion Batteries. *Adv. Funct. Mater.* **2020**, *30* (47), No. 2000706.
(280) Wang, Y.; Wang, X.; Li, X.; Bai, Y.; Xiao, H.; Liu, Y.; Liu, R.; Yuan, G. Engineering 3D Ion Transport Channels for Flexible MXene Films with Superior Capacitive Performance. *Adv. Funct. Mater.* **2019**, *29* (14), No. 1900326.
(281) Ran, F.; Wang, T.; Chen, S.; Liu, Y.; Shao, L. Constructing expanded ion transport channels in flexible MXene film for pseudocapacitive energy storage. *Appl. Surf. Sci.* **2020**, *511*, No. 145627.
(282) Hui, X.; Zhang, P.; Li, J.; Zhao, D.; Li, Z.; Zhang, Z.; Wang, C.; Wang, R.; Yin, L. In Situ Integrating Highly Ionic Conductive LDH-Array@PVA Gel Electrolyte and MXene/Zn Anode for Dendrite-Free High-Performance Flexible Zn−Air Batteries. *Adv. Energy Mater.* **2022**, *12* (34), No. 2201393.
(283) Xu, S.; Dall'Agnese, Y.; Li, J.; Gogotsi, Y.; Han, W. Thermally Reduced Graphene/MXene Film for Enhanced Li-ion Storage. *Chem.-Eur. J.* **2018**, *24* (69), 18556−18563.
(284) Namvari, M.; Chakrabarti, B. K. Electrophoretic deposition of MXenes and their composites: Toward a scalable approach. *Adv. Colloid Interface Sci.* **2024**, *331*, No. 103208.
(285) Huang, H.; Chu, X.; Su, H.; Zhang, H.; Xie, Y.; Deng, W.; Chen, N.; Liu, F.; Zhang, H.; Gu, B.; et al. Massively manufactured paper-based all-solid-state flexible micro-supercapacitors with sprayable MXene conductive inks. *J. Power Sources* **2019**, *415*, 1−7.
(286) Rubbi, F.; Habib, K.; Saidur, R.; Aslfattahi, N.; Yahya, S. M.; Das, L. Performance optimization of a hybrid PV/T solar system using Soybean oil/MXene nanofluids as A new class of heat transfer fluids. *Sol. Energy* **2020**, *208*, 124−138.
(287) Sreekumar, S.; Pugsley, A.; Chakrabarti, S.; Hewitt, N.; Mondol, J. D.; Shah, N. Experimental investigation on the performance of MXene/C-dot hybrid nanofluid-based photovoltaic/thermal system: An Energy, Exergy, and Enviro-Economic analysis. *Sol. Energy Mater. Sol. Cells* **2024**, *272*, No. 112904.
(288) Awis, N. A.; Ali, S. A.; Mim, M.; Farabi, S. N.; Habib, K. Numerical Heat Transfer Analysis of Evacuated Tube Solar Collector Using MXene/Soyabean Oil Nanofluid. *E3S Web of Conf.* **2024**, *488*, 02005.
(289) Das, L.; Habib, K.; Saidur, R.; Aslfattahi, N.; Yahya, S. M.; Rubbi, F. Improved Thermophysical Properties and Energy Efficiency of Aqueous Ionic Liquid/MXene Nanofluid in a Hybrid PV/T Solar System. *Nanomaterials* **2020**, *10*, 1372.
(290) Samylingam, L.; Aslfattahi, N.; Saidur, R.; Yahya, S. M.; Afzal, A.; Arifutzzaman, A.; Tan, K. H.; Kadirgama, K. Thermal and energy performance improvement of hybrid PV/T system by using olein palm oil with MXene as a new class of heat transfer fluid. *Sol. Energy Mater. Sol. Cells* **2020**, *218*, No. 110754.
(291) Sreekumar, S.; Shah, N.; Mondol, J. D.; Hewitt, N.; Chakrabarti, S. Numerical investigation and feasibility study on MXene/water nanofluid based photovoltaic/thermal system. *Cleaner Energy Systems* **2022**, *2*, No. 100010.
(292) Abdelrazik, A. S.; Tan, K. H.; Aslfattahi, N.; Arifutzzaman, A.; Saidur, R.; Al-Sulaiman, F. A. Optical, stability and energy performance of water-based MXene nanofluids in hybrid PV/thermal solar systems. *Sol. Energy* **2020**, *204*, 32−47.
(293) Aslfattahi, N.; Samylingam, L.; Abdelrazik, A. S.; Arifutzzaman, A.; Saidur, R. MXene based new class of silicone oil nanofluids for the performance improvement of concentrated photovoltaic thermal collector. *Sol. Energy Mater. Sol. Cells* **2020**, *211*, No. 110526.
(294) Shi, J.; Li, X.; Sun, B.; Huang, X.-L.; Ning, X.; Long, Y.-Z.; Zheng, J. Flexible MXene decorative nonwovens with patterned structures for integrated joule heating and strain sensing. *Sensors and Actuators A: Physical* **2023**, *358*, No. 114426.
(295) Lan, C.; Xu, F.; Pan, C.; Hao Guo, Z.; Pu, X. MXene based Janus fabrics with radiative heating towards efficient personal thermal management. *Chemical Engineering Journal* **2023**, *472*, No. 144662.
(296) Xie, J.; Zhang, Y.; Dai, J.; Xie, Z.; Xue, J.; Dai, K.; Zhang, F.; Liu, D.; Cheng, J.; Kang, F.; et al. Multifunctional MoSe2@MXene Heterostructure-Decorated Cellulose Fabric for Wearable Thermal Therapy. *Small* **2023**, *19* (9), No. 2205853.
(297) Ye, L.; Liu, L.-X.; Yin, G.; Liu, Y.; Deng, Z.; Qi, C.-Z.; Zhang, H.-B.; Yu, Z.-Z. Highly conductive, hydrophobic, and acid/alkali-resistant MXene@PVDF hollow core-shell fibers for efficient electromagnetic interference shielding and Joule heating. *Materials Today Physics* **2023**, *35*, No. 101100.
(298) He, G.; Wang, L.; Bao, X.; Lei, Z.; Ning, F.; Li, M.; Zhang, X.; Qu, L. Synergistic flame retardant weft-knitted alginate/viscose fabrics with MXene coating for multifunctional wearable heaters. *Composites Part B: Engineering* **2022**, *232*, No. 109618.
(299) Wang, X.; Lei, Z.; Ma, X.; He, G.; Xu, T.; Tan, J.; Wang, L.; Zhang, X.; Qu, L.; Zhang, X. A lightweight MXene-Coated nonwoven fabric with excellent flame Retardancy, EMI Shielding, and Electro-thermal/Photothermal conversion for wearable heater. *Chemical Engineering Journal* **2022**, *430*, No. 132605.
(300) Li, A.; He, J.; Wang, W.; Cui, C.; Jiang, S.; Jiang, S.; Qin, W.; Cheng, C.; Guo, R. Self-Heating and Hydrophobic Nanofiber Membrane Based on Ti3C2Tx MXene/Ag Nanoparticles/Thermoplastic Polyurethane for Electromagnetic Interference Shielding and Sensing Performance. *Ind. Eng. Chem. Res.* **2022**, *61* (41), 15249−15260.
(301) Sun, X.; Jia, X.; Yang, J.; Wang, S.; Li, Y.; Shao, D.; Song, H. MXenes—An Emerging Class of 2D Materials for Solar Water Desalination: Feasibility and Recent Advances. *Solar RRL* **2022**, *6* (2), No. 2100888.
(302) Zhang, Q.; Yi, G.; Fu, Z.; Yu, H.; Chen, S.; Quan, X. Vertically Aligned Janus MXene-Based Aerogels for Solar Desalination with High Efficiency and Salt Resistance. *ACS Nano* **2019**, *13* (11), 13196−13207.
(303) Saleque, A. M.; Ma, S.; Thakur, A. K.; Saidur, R.; Han, T. K.; Hossain, M. I.; Qarony, W.; Ma, Y.; Sathyamurthy, R.; Tsang, Y. H. MXene/MnO2 nanocomposite coated superior salt-rejecting biodegradable luffa sponge for efficient solar steam generation. *Desalination* **2023**, *554*, No. 116488.
(304) Jiang, G.; Fang, X.; Yu, W.; Xie, H.; Lei, H. Magnetic recyclable Fe3O4@Ti3C2TX nanoparticles for high-efficiency solar membrane distillation. *Desalination* **2023**, *564*, No. 116784.
(305) Sun, J.; Farid, M. U.; Boey, M. W.; Sato, Y.; Chen, G.; An, A. K. MXene-PVA-TiO2-based photothermal-catalytic membrane with high structural stability for efficient desalination and photodegradation. *Chemical Engineering Journal* **2023**, *468*, No. 143744.
(306) Mu, X.; Chen, L.; Qu, N.; Yu, J.; Jiang, X.; Xiao, C.; Luo, X.; Hasi, Q. MXene/polypyrrole coated melamine-foam for efficient interfacial evaporation and photodegradation. *J. Colloid Interface Sci.* **2023**, *636*, 291−304.
(307) Béguin, F.; Raymundo-Piñero, E.; Frackowiak, E. Electrical double-layer capacitors and pseudocapacitors. *Carbons for electrochemical energy storage and conversion systems* **2009**, *20091238*, 329−375.
(308) Yang, J.; Bao, W.; Jaumaux, P.; Zhang, S.; Wang, C.; Wang, G. MXene-Based Composites: Synthesis and Applications in Rechargeable Batteries and Supercapacitors. *Advanced Materials Interfaces* **2019**, *6* (8), No. 1802004.
(309) Wen, Y.; Rufford, T. E.; Chen, X.; Li, N.; Lyu, M.; Dai, L.; Wang, L. Nitrogen-doped Ti3C2Tx MXene electrodes for high-performance supercapacitors. *Nano Energy* **2017**, *38*, 368−376.
(310) Rakhi, R. B.; Ahmed, B.; Anjum, D.; Alshareef, H. N. Direct Chemical Synthesis of MnO2 Nanowhiskers on Transition-Metal Carbide Surfaces for Supercapacitor Applications. *ACS Appl. Mater. Interfaces* **2016**, *8* (29), 18806−18814.
(311) Yang, Q.; Xu, Z.; Fang, B.; Huang, T.; Cai, S.; Chen, H.; Liu, Y.; Gopalsamy, K.; Gao, W.; Gao, C. MXene/graphene hybrid fibers for high performance flexible supercapacitors. *Journal of Materials Chemistry A* **2017**, *5* (42), 22113−22119.
(312) Zhao, C.; Wang, Q.; Zhang, H.; Passerini, S.; Qian, X. Two-Dimensional Titanium Carbide/RGO Composite for High-Performance Supercapacitors. *ACS Appl. Mater. Interfaces* **2016**, *8* (24), 15661−15667.

(313) Tang, X.; Liu, H.; Guo, X.; Wang, S.; Wu, W.; Mondal, A. K.; Wang, C.; Wang, G. A novel lithium-ion hybrid capacitor based on an aerogel-like MXene wrapped Fe 2 O 3 nanosphere anode and a 3D nitrogen sulphur dual-doped porous carbon cathode. *Materials Chemistry Frontiers* **2018**, *2* (10), 1811−1821.
(314) Jiang, Q.; Kurra, N.; Alhabeb, M.; Gogotsi, Y.; Alshareef, H. N. All Pseudocapacitive MXene-RuO2 Asymmetric Supercapacitors. *Adv. Energy Mater.* **2018**, *8* (13), No. 1703043.
(315) Wang, H.; Guan, C.; Wang, X.; Fan, H. J. A High Energy and Power Li-Ion Capacitor Based on a TiO2 Nanobelt Array Anode and a Graphene Hydrogel Cathode. *Small* **2015**, *11* (12), 1470−1477.
(316) Xu, N.; Sun, X.; Zhang, X.; Wang, K.; Ma, Y. A two-step method for preparing Li4Ti5O12−graphene as an anode material for lithium-ion hybrid capacitors. *RSC Adv.* **2015**, *5* (114), 94361−94368.
(317) Zhang, J.; Liu, X.; Wang, J.; Shi, J.; Shi, Z. Different types of pre-lithiated hard carbon as negative electrode material for lithium-ion capacitors. *Electrochim. Acta* **2016**, *187*, 134−142.
(318) Lim, E.; Jo, C.; Kim, H.; Kim, M.-H.; Mun, Y.; Chun, J.; Ye, Y.; Hwang, J.; Ha, K.-S.; Roh, K. C.; et al. Facile Synthesis of Nb2O5@ Carbon Core−Shell Nanocrystals with Controlled Crystalline Structure for High-Power Anodes in Hybrid Supercapacitors. *ACS Nano* **2015**, *9* (7), 7497−7505.
(319) Zhang, F.; Zhang, T.; Yang, X.; Zhang, L.; Leng, K.; Huang, Y.; Chen, Y. A high-performance supercapacitor-battery hybrid energy storage device based on graphene-enhanced electrode materials with ultrahigh energy density. *Energy Environ. Sci.* **2013**, *6* (5), 1623−1632.
(320) Wang, H.; Zhang, Y.; Ang, H.; Zhang, Y.; Tan, H. T.; Zhang, Y.; Guo, Y.; Franklin, J. B.; Wu, X. L.; Srinivasan, M.; et al. A High-Energy Lithium-Ion Capacitor by Integration of a 3D Interconnected Titanium Carbide Nanoparticle Chain Anode with a Pyridine-Derived Porous Nitrogen-Doped Carbon Cathode. *Adv. Funct. Mater.* **2016**, *26* (18), 3082−3093.
(321) Wang, H.; Xu, Z.; Li, Z.; Cui, K.; Ding, J.; Kohandehghan, A.; Tan, X.; Zahiri, B.; Olsen, B. C.; Holt, C. M. B.; et al. Hybrid Device Employing Three-Dimensional Arrays of MnO in Carbon Nanosheets Bridges Battery−Supercapacitor Divide. *Nano Lett.* **2014**, *14* (4), 1987−1994.
(322) Ding, R.; Qi, L.; Wang, H. Porous NiCo2O4 as an anode material for 4.5 V hybrid Li-ion capacitors. *RSC Adv.* **2013**, *3* (31), 12581−12584.
(323) Wang, R.; Lang, J.; Zhang, P.; Lin, Z.; Yan, X. Fast and Large Lithium Storage in 3D Porous VN Nanowires−Graphene Composite as a Superior Anode Toward High-Performance Hybrid Supercapacitors. *Adv. Funct. Mater.* **2015**, *25* (15), 2270−2278.
(324) Tang, Q.; Wang, Y.; Chen, N.; Pu, B.; Qing, Y.; Zhang, M.; Bai, J.; Yang, Y.; Cui, J.; Liu, Y.; et al. Ultra-Efficient Synthesis of Nb4C3Tx MXene via H2O-Assisted Supercritical Etching for Li-Ion Battery. *Small Methods* **2024**, *8* (3), No. 2300836.
(325) Jiang, J.; Wang, Z.; Wang, X.; Wang, S.; Li, S.; Zhuang, Q.; Shao, H. Cubic iron fluoride anchored on Ti3C2Tx MXene as superior anode for high-performance lithium-ion batteries. *J. Power Sources* **2024**, *613*, No. 234850.
(326) Gong, Z.; Jiang, Q.; Bai, W.; Wang, P.; Gao, M.; Cao, D.; Zhou, M.; Sun, Y.; Zhu, K. MXene-loaded sea urchin-like CoP as anode materials for high-performance lithium-ion batteries. *Journal of Energy Storage* **2024**, *88*, No. 111545.
(327) Zhao, J.; Qi, Y.; Yang, Q.; Huang, T.; Wang, H.; Wang, Y.; Niu, Y.; Liu, Y.; Bao, S.; Xu, M. Chessboard structured electrode design for Li-S batteries Based on MXene nanosheets. *Chemical Engineering Journal* **2022**, *429*, No. 131997.
(328) Li, Z.; Wang, X.; Zhang, W.; Yang, S. Two-dimensional Ti3C2@CTAB-Se (MXene) composite cathode material for high-performance rechargeable aluminum batteries. *Chemical Engineering Journal* **2020**, *398*, No. 125679.
(329) Du, Y.; Zhang, B.; Zhang, W.; Jin, H.; Qin, J.; Wan, J.; Zhang, Y.; Wang, Z.; Zhang, J.; Chen, G. Heterostructures assembled from graphitic carbon nitride and Ti3C2Tx MXene as high-capacity cathode for aluminum batteries. *J. Alloys Compd.* **2022**, *896*, No. 162901.
(330) Liu, H.; Wang, H.; Jing, Z.; Wu, K.; Cheng, Y.; Xiao, B. Bare Mo-Based Ordered Double-Transition Metal MXenes as High-Performance Anode Materials for Aluminum-Ion Batteries. *J. Phys. Chem. C* **2020**, *124* (47), 25769−25774.
(331) Sun, R.; Dong, S.; Guo, X.; Xia, P.; Lu, S.; Zhang, Y.; Fan, H. Construction of 2D sandwich-like Na2V6O16·3H2O@MXene heterostructure for advanced aqueous zinc ion batteries. *J. Colloid Interface Sci.* **2024**, *655*, 226−233.
(332) Mao, Y.; Bai, J.; Lin, S.; Wang, P.; Li, W.; Xiao, K.; Wang, S.; Zhu, X.; Zhao, B.; Sun, Y. Two Birds with One Stone: V4C3MXene Synergistically Promoted VS2 Cathode and Zinc Anode for High-Performance Aqueous Zinc-Ion Batteries. *Small* **2024**, *20* (11), No. 2306615.
(333) Luo, J.; Tao, X.; Zhang, J.; Xia, Y.; Huang, H.; Zhang, L.; Gan, Y.; Liang, C.; Zhang, W. Sn4+ Ion Decorated Highly Conductive Ti3C2MXene: Promising Lithium-Ion Anodes with Enhanced Volumetric Capacity and Cyclic Performance. *ACS Nano* **2016**, *10* (2), 2491−2499.
(334) Zhao, L.; Dong, B.; Li, S.; Zhou, L.; Lai, L.; Wang, Z.; Zhao, S.; Han, M.; Gao, K.; Lu, M.; et al. Interdiffusion Reaction-Assisted Hybridization of Two-Dimensional Metal−Organic Frameworks and Ti3C2Tx Nanosheets for Electrocatalytic Oxygen Evolution. *ACS Nano* **2017**, *11* (6), 5800−5807.
(335) Lipton, J.; Röhr, J. A.; Dang, V.; Goad, A.; Maleski, K.; Lavini, F.; Han, M.; Tsai, E. H. R.; Weng, G.-M.; Kong, J.; et al. Scalable, highly conductive, and micropatternable MXene films for enhanced electromagnetic interference shielding. *Matter* **2020**, *3* (2), 546−557.
(336) Kumar, V.; Sharma, N.; Umesh, M.; Sharma, R.; Sharma, M.; Sharma, D.; Sharma, M.; Sondhi, S.; Thomas, J.; Dheeman, D.; et al. Commercialization potential of PET (polyethylene terephthalate) recycled nanomaterials: A review on validation parameters. *Chemosphere* **2024**, *352*, No. 141453.
(337) Yang, H.; Sun, Y.; Peng, M.; Cai, M.; Zhao, B.; Li, D.; Liang, Z.; Jiang, L. Tailoring the Salt Transport Flux of Solar Evaporators for a Highly Effective Salt-Resistant Desalination with High Productivity. *ACS Nano* **2022**, *16* (2), 2511−2520.
(338) Amrillah, T.; Abdullah, C. A.; Hermawan, A.; Sari, F. N.; Alviani, V. N. Towards Greener and More Sustainable Synthesis of MXenes: A Review. *Nanomaterials* **2022**, *12*, 4280.
(339) Xu, X.; Zhang, Y.; Sun, H.; Zhou, J.; Yang, F.; Li, H.; Chen, H.; Chen, Y.; Liu, Z.; Qiu, Z.; et al. Progress and Perspective: MXene and MXene-Based Nanomaterials for High-Performance Energy Storage Devices. *Advanced Electronic Materials* **2021**, *7* (7), No. 2000967.
(340) Saha, S.; Rajbongshi, B. M.; Ramani, V.; Verma, A. Titanium carbide: An emerging electrocatalyst for fuel cell and electrolyser. *Int. J. Hydrogen Energy* **2021**, *46* (24), 12801−12821.
(341) Lu, B.; Zhu, Z.; Ma, B.; Wang, W.; Zhu, R.; Zhang, J. 2D MXene Nanomaterials for Versatile Biomedical Applications: Current Trends and Future Prospects. *Small* **2021**, *17* (46), No. 2100946.
(342) Kwon, O.; Choi, Y.; Kang, J.; Kim, J. H.; Choi, E.; Woo, Y. C.; Kim, D. W. A comprehensive review of MXene-based water-treatment membranes and technologies: Recent progress and perspectives. *Desalination* **2022**, *522*, No. 115448.
(343) Qamar, S.; Fatima, K.; Ullah, N.; Akhter, Z.; Waseem, A.; Sultan, M. Recent progress in use of MXene in perovskite solar cells: for interfacial modification, work-function tuning and additive engineering. *Nanoscale* **2022**, *14* (36), 13018−13039.
(344) Kumar, Y. A.; Raorane, C. J.; Hegazy, H. H.; Ramachandran, T.; Kim, S. C.; Moniruzzaman, M. 2D MXene-based supercapacitors: A promising path towards high-performance energy storage. *Journal of Energy Storage* **2023**, *72*, No. 108433.
(345) Xiong, D.; Li, X.; Bai, Z.; Lu, S. Recent Advances in Layered Ti3C2Tx MXene for Electrochemical Energy Storage. *Small* **2018**, *14* (17), No. 1703419.
(346) Tan, K. H.; Zaed, M. A.; Saidur, R.; Abdullah, N.; Ishak, N. A. I. M.; Cherusseri, J. Strategic Insights for Bulk Production of MXene: A Review. *EDP Sciences* **2024**, *488*, 01003.
(347) Pérez, V.; Moltó, J. L.; Lebrero, R.; Muñoz, R. Ectoine Production from Biogas in Waste Treatment Facilities: A Techno-

Economic and Sensitivity Analysis. *ACS Sustainable Chem. Eng.* **2021**, *9* (51), 17371−17380.
(348) Khalaj, M.; Kamali, M.; Aminabhavi, T. M.; Costa, M. E. V.; Dewil, R.; Appels, L.; Capela, I. Sustainability insights into the synthesis of engineered nanomaterials - Problem formulation and considerations. *Environmental Research* **2023**, *220*, No. 115249.
(349) Fellows, G. K.; Winter, J.; Munzur, A. An Analysis of Industrial Policy Mechanisms to Support Commercial Deployment of Bitumen Partial Upgrading in Alberta. *Energies* **2023**, *16*, 2670.
(350) Xu, X.; Guo, T.; Lanza, M.; Alshareef, H. N. Status and prospects of MXene-based nanoelectronic devices. *Matter* **2023**, *6* (3), 800−837.
(351) AlGhamdi, M. S.; Durugbo, C. M. Business-to-business co-creation management practices for intellectual property value: Insights from Saudi Arabia. *World Patent Information* **2023**, *72*, No. 102180.
(352) Amani, A. M.; Tayebi, L.; Vafa, E.; Abbasi, M.; Vaez, A.; Kamyab, H.; Chelliapan, S.; Azizli, M. J.; Bazargan-Lari, R. On the horizon of greener pathways to travel into a greener future portal: Green MXenes, environment-friendly synthesis, and their innovative applications. *Journal of Cleaner Production* **2024**, *436*, No. 140606.
(353) Jolly, S.; Paranthaman, M. P.; Naguib, M. Synthesis of Ti3C2Tz MXene from low-cost and environmentally friendly precursors. *Materials Today Advances* **2021**, *10*, No. 100139.
(354) Zaed, M. A.; Tan, K. H.; Saidur, R.; Pandey, A. K.; Cherusseri, J. Low-cost synthesis of Ti3C2Tx MXene-based sponge for solar steam generation and clean water production. *Ceram. Int.* **2024**, *50* (16), 27910−27922.
(355) Patel, P. Mighty MXenes: Ready to roll. *C&EN Global Enterprise* **2024**, *102* (9), 26−32.
(356) Patel, P. Mighty MXenes are ready for launch. *Chem. Eng. News*, **2024**, *102* (9), 26−32. https://cen.acs.org/materials/2-d-materials/Mighty-MXenes-ready-launch/102/i9.
(357) *Technology readiness assessment guide*; U.S. Department of Energy: Washington, D.C., 2011. https://www.directives.doe.gov/directives-documents/400-series/0413.3-EGuide-04a/%40%40images/file.

https://doi.org/10.1021/acsomega.4c04849
ACS Omega 2024, 9, 32350−32393